From: Zbigniew Florjańczyk
Warsaw University of Technology, Faculty of Chemistry
00-664 Warszawa, ul. Noakowskiego 3, Poland
Tel.: (+4822) 660-7303; fax: (+4822) 660-7279;
e-mail: nolang@ch.pw.edu.pl; evala@ch.pw.edu.pl

Date: January 20, 2008

To: Barrett Flake
Department of the Air Force
European Office of Aerospace Research and Development
223/231 Old Marylebone Rd
London, NW1 5TH, England
e-mail: barrett.flake@london.af.mil

Subject: Final report for the period January 21, 2005 – January 20, 2008) concerning the project "Novel, solvent free, single ion conductive polymer electrolytes (Warsaw-2005)" (Contract FA8655-05-1-3014; contractor: Professor Zbigniew Florjańczyk)

Copy to: Lawrence G. Scanlon
Wright Laboratory, Wright – Patterson AFB
Dayton, Ohio 45433-7251
e-mail: lawrence.scanlon@wpafb.af.mil

Bruno Scrosati (bruno.scrosati@uniroma1.it)
Department of Chemistry, University of Rome "La Sapienza"
Piazza Aldo Moro 5, 00185 Rome, Italy

Emanuel Peled (peled@post.tau.ac.il)
Diana Golodnitsky (golod@post.tau.ac.il)
School of Chemistry, Tel Aviv University
Tel Aviv, 69978 Israel

REPORT DOCUMENTATION PAGE

Form Approved OMB No. 0704-0188

Public reporting burden for this collection of information is estimated to average 1 hour per response, including the time for reviewing instructions, searching existing data sources, gathering and maintaining the data needed, and completing and reviewing the collection of information. Send comments regarding this burden estimate or any other aspect of this collection of information, including suggestions for reducing the burden, to Department of Defense, Washington Headquarters Services, Directorate for Information Operations and Reports (0704-0188), 1215 Jefferson Davis Highway, Suite 1204, Arlington, VA 22202-4302. Respondents should be aware that notwithstanding any other provision of law, no person shall be subject to any penalty for failing to comply with a collection of information if it does not display a currently valid OMB control number. **PLEASE DO NOT RETURN YOUR FORM TO THE ABOVE ADDRESS.**

1. REPORT DATE *(DD-MM-YYYY)* 14-03-2008	2. REPORT TYPE Final Report	3. DATES COVERED *(From – To)* 14 January 2005 - 09-Oct-08

4. TITLE AND SUBTITLE Novel, Solvent-Free, Single Ion-Conductive Polymer Electrolytes	5a. CONTRACT NUMBER FA8655-05-1-3014
	5b. GRANT NUMBER
	5c. PROGRAM ELEMENT NUMBER
6. AUTHOR(S) Professor Zbigniew Florjanczyk	5d. PROJECT NUMBER
	5d. TASK NUMBER
	5e. WORK UNIT NUMBER

7. PERFORMING ORGANIZATION NAME(S) AND ADDRESS(ES) Warsaw University of Technology ul. Noakowskiego 3 Warsaw PL-00 664 Poland	8. PERFORMING ORGANIZATION REPORT NUMBER N/A

9. SPONSORING/MONITORING AGENCY NAME(S) AND ADDRESS(ES) EOARD Unit 4515 BOX 14 APO AE 09421	10. SPONSOR/MONITOR'S ACRONYM(S)
	11. SPONSOR/MONITOR'S REPORT NUMBER(S) Grant 05-3014

12. DISTRIBUTION/AVAILABILITY STATEMENT

Approved for public release; distribution is unlimited.

13. SUPPLEMENTARY NOTES

14. ABSTRACT

This project report concerns studies on the synthesis of new polymer electrolytes for application in lithium and lithium-ion batteries, characterized by limited participation of anions in the transport of electrical charge. Studies were carried out additive organoboron compounds and on composite electrolytes with supramolecular anion receptors.

15. SUBJECT TERMS
EOARD, Power, Electrochemistry, Batteries

16. SECURITY CLASSIFICATION OF:			17. LIMITATION OF ABSTRACT UL	18, NUMBER OF PAGES 74	19a. NAME OF RESPONSIBLE PERSON BARRETT A. FLAKE
a. REPORT UNCLAS	b. ABSTRACT UNCLAS	c. THIS PAGE UNCLAS			19b. TELEPHONE NUMBER *(Include area code)* +44 (0)1895 616144

Standard Form 298 (Rev. 8/98)
Prescribed by ANSI Std. Z39-18

Content of report:

Our work concerned studies on the synthesis of new polymer electrolytes for application in lithium and lithium-ion batteries, characterized by limited participation of anions in the transport of electrical charge. Studies were carried out additive organoboron compounds and on composite electrolytes with supramolecular anion receptors.

I. Studies on additive organoboron compounds

In this part of the project studies have been carried out leading to the limitation or elimination of anion mobility in the electron charge conduction involving a lithium salt in polymer electrolytes as a result of complexation with boron trifluoride – a derivative of Lewis acid properties. An increase in the degree of dissociation, decrease in the share of ionic associates and increase in cation mobility was expected as an additional effect of such an interaction. Mono and dibasic phosphorus salts, such lithium diphenylphosphate, lithium diphenylphosphinate, lithium phenylphosphonate and lithium vinylphosphonate. In the further part of studies, the complex salts obtained were used as components of solid electrolytes, in which poly(methyl methacrylate), poly(butyl acrylate) as well as acrylonitrile and butyl acrylate copolymer (poly(AN-*co*-BuA)) were the polymer matrix.

The second group of derivatives used as effective anion traps are trisubstituted boron compounds containing fluorine substituents, which due to a strong induction effect increase the electron deficiency on the boron atom, decisive of its acidic properties and the oligooxyethylene organic substituent (R).

$X^{\ominus}$ anion of the salt

R oxyethylene group
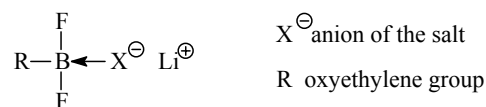
The main stress was put on the synthesis of derivatives comprising oxyethylene groups for application in PEO based electrolytes. The lithium transference number (t_+) values, were determined by the electrochemical method by steady-state technique in collaboration with the Tel-Aviv groups in the lab of Professor Diana Golodnitsky and Professor Emanuel Peled.

The next stage of the project involved studies covered studies on the possibility of introducing sites of Lewis acid properties to a polymer matrix. For this, the reactions of boron trifluoride with polar side groups present in the polyelectrolyte type polymer comprising sulfonic groups as lithium salts were carried out. The polymers obtained were applied as components of polymer electrolytes, of which conducting properties were determined.

I.1. Synthesis and characterization of the complex salts of [(R)$_2$P(O)OLi] with BF$_3$ (R = Ph or PhO)

### I.1.A. Synthesis of the [R$_2$P(O)OLi] and BF$_3$ complexes

In the first reaction step, the lithium salt of phosphorus (V) acid was obtained in the reaction with n-butyllithium, according to the following reaction scheme:
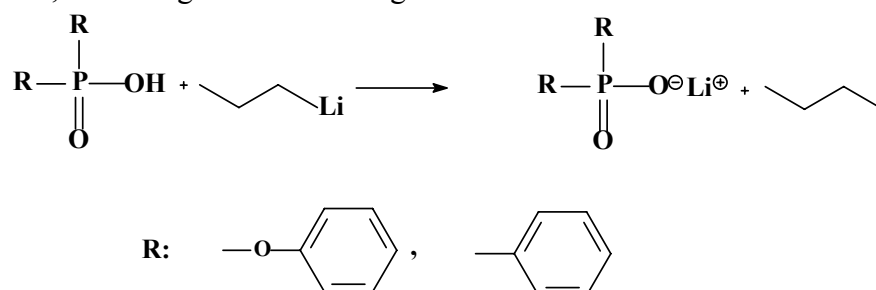
The reaction was carried out in a 100 ml reactor in argon atmosphere. Phosphorus (V) acid [R$_2$P(O)OH] was dissolved in toluene after heating up to 40 °C, and then the solution of n-butyllithium in hexane (2.5 M) in an amount of 1.2 moles with respect to the concentration of acidic groups was added dropwise. The reaction was accompanied by an exothermic effect – the system was cooled in an acetone-dry ice bath. A white precipitate resulted from the reaction, which was washed three times with toluene, and then the product was dried in a vacuum oven at 50 °C.

In the second step the salt obtained was subjected to a reaction with BF_3 etherate:
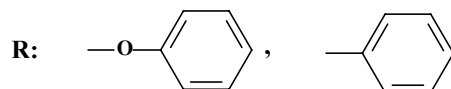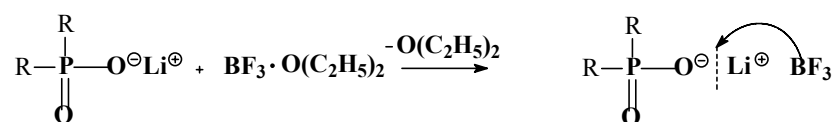
The reaction with BF_3 etherate was carried out in acetonitrile in a nitrogen atmosphere. Since the salt does not dissolve in acetonitrile, the reaction was carried out in a heterogeneous system, in a suspension at vigorous stirring. The BF_3 etherate was added in a five-molar excess with respect to the lithium salt. The reaction heat was collected with a mixture of water and ice to maintain the temperature of the reaction mixture close to room temperature. After reaction completion the solvent and the unreacted complexing agent were distilled off. The product obtained was separated into two fractions by repeated dissolution in acetonitrile and gradual introduction of methylene chloride until a solid precipitated. The precipitate was isolated, and then the second product was isolated from the filtrate after removal of the solvents.

To determine the reaction course and composition of products, an analysis was carried out involving FTIR, ^{1}H NMR, ^{19}F NMR spectroscopy, absorption atomic spectrometry (FAAS) and plasma emission mass spectrometry (ICP-AES) with argon plasma.

I.1.B. Characteristics of the phosphorus (V) acids lithium salts [R₂P(O)OLi] and BF₃ reaction products

In Figure 1 are presented the FTIR spectra of the initial salts $(Ph)_2P(O)OLi$ and $(PhO)_2P(O)OLi$.
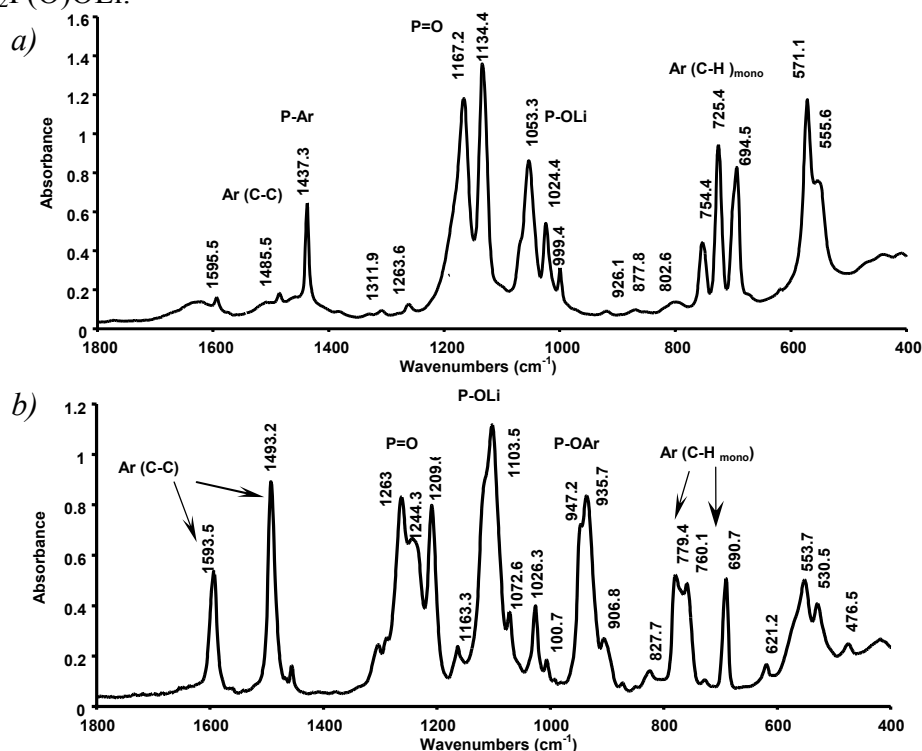
Figure 1. *FTIR spectra of: (a) (Ph)₂P(O)OLi and (b) (PhO)₂P(O)OLi.*

In the spectra we observe the bands of vibrations of groups characteristic of lithium diphenylphosphinate: $\nu_{P-OLi} = 1053.3$ cm^{-1}, 1024.4 cm^{-1} and 999.3 cm^{-1} [Fig 1. (a)] and lithium diphenylphosphate $\nu_{P-OLi} = 1103.5$ cm^{-1} and 1072.6 cm^{-1} [Fig. 1 (b)]. Skeleton bands of phenyl

substituents $\nu_{C=C}$ are present at about 1595 cm^{-1} and 1490 cm^{-1}, and bands of deformation vibrations of monosubstituted phenyl ring γ_{C-H} in the 770-690 cm^{-1} range are visible. Moreover, bands of vibrations of phosphorus and oxygen bonds P=O at 1167.2 cm^{-1} and 1134.4 cm^{-1} of lithium diphenylphosphinate (a) at 1263.6 cm^{-1}, 1244.3 cm^{-1} and 1209.6 cm^{-1} of lithium diphenylphosphate are present in the spectrum.

The solid product (insoluble in methylene chloride) was isolated from the reaction of lithium diphenylphosphinate as well as of lithium diphenylphosphate and boron trifluoride. The FTIR spectrum of this product, which was marked as **AI**, is presented in Figure 2.
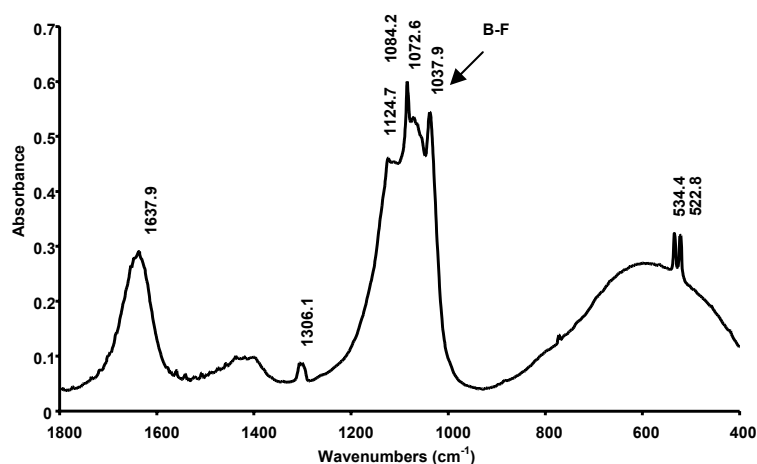

Figure 2. FTIR spectrum of precipitate *AI* resulting from the phosphorus (V) acid lithium salt [(Ph)$_2$P(O)OLi and (PhO)$_2$P(O)OLi] and BF$_3$ reaction**.**

The spectrum obtained is analogous to that of LiBF$_4$, which suggests that this salt is one of the isolated products.

In the fluorine resonance of the **AI** precipitate (Figure 3), signals analogous to those in the ^{19}F NMR spectrum of LiBF$_4$ (Figure 4) are mainly observed. As can be noticed, the isolated reaction product contains additionally fluorine signals of much smaller intensity at about −138 ppm.
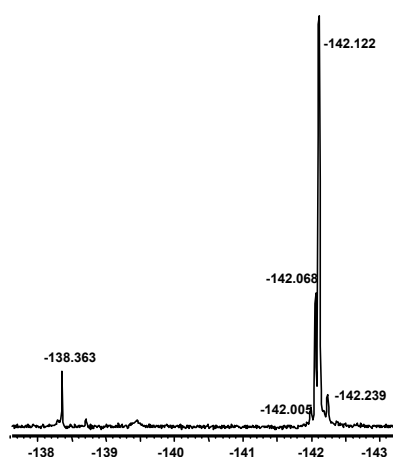

Figure 3. ^{19}F NMR spectrum of precipitate *AI* resulting from the phosphorus (V) acid lithium salt [(Ph)$_2$P(O)OLi and (PhO)$_2$P(O)OLi] and BF$_3$ reaction.
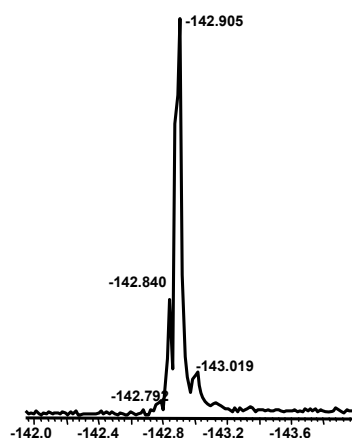
Figure 4. *^{19}F NMR spectrum of $LiBF_4$.*

Precipitate **AI,** which was obtained in both reactions, was additionally subjected to composition analysis by means of mass spectroscopy with plasma induction (ICP-MS).

Elemental analysis of the isolated precipitates gave the following results:

Lithium salt	Element	B	F	Li	P
(Ph)$_2$P(O)OLi		17.14	57.14	0.86	1.43
	Content in wt. %				
(PhO)$_2$P(O)OLi		7.54	44.40	0.44	0.40

Calculated content of elements in $LiBF_4$:

Element	B	F	Li	P
Content in wt. %	11.70	80.85	7.45	-

This analysis seems to be divergent with respect to the expected composition of the product, which according to the spectroscopic analysis seems to be $LiBF_4$. Especially the lithium content is very much lowered. The differences in composition can be explained by the not too exact separation of the products, which is indicated by the presence of phosphorus in the sample. In the case of lithium, the too large intensity of its signal in the spectrum does not permit a quantitative determination of this element. This analysis should be treated qualitatively.

An analysis of the lithium content in the **AI** precipitate carried out by the flame atomic absorption spectrometry FA-AS method showed the presence of 5.5 – 5.7 wt. % of Li (relative error of this analysis is 1%). The result of this analysis shows that $LiBF_4$ is the main component of the precipitates isolated. Assuming that the remaining part does not contain lithium, $LiBF_4$ constitutes 74 – 76.5% of the precipitate.

FTIR spectra of the second isolated fraction, marked as **AII**, are presented in Figure 5. In the case of reaction with lithium diphenylphosphinate this product is a solid, and in reaction with lithium diphenylphosphate the second fraction is a viscous, light-brown liquid, and according to the flame analysis does not contain lithium.
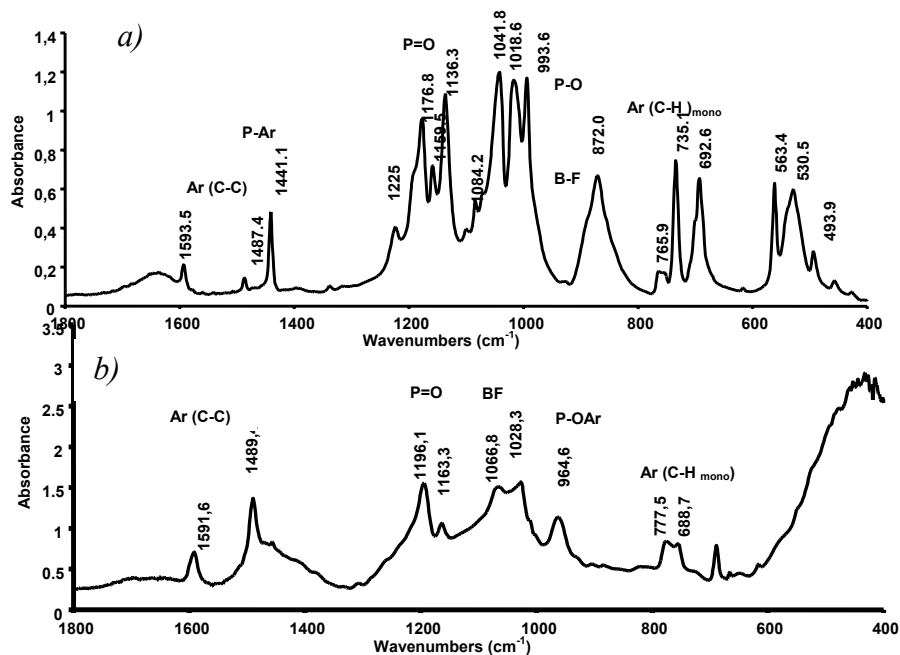
Figure 5. *FTIR spectra of fraction **AII** resulting from the phosphorus (V) acid lithium salt [(Ph)₂P(O)OLi (a) and (PhO)₂P(O)OLi (b)] and BF₃ reaction.*

In the FTIR spectrum of precipitate **AII** obtained from the reaction of $(Ph)_2P(O)OLi$ and BF_3 (a) bands characteristic of the aromatic ring vibrations as well as that of the phosphorus-phenyl ring bond at 1441 cm^{-1} are observed, similarly as for lithium diphenylphosphinate. Two groups of bands in the 1225 – 1136 cm^{-1} and 993 – 1041 cm^{-1} ranges have been attributed to vibrations of P=O and P–O bonds, respectively. A new absorption band appears in the spectrum, which was attributed to vibrations of the B–F bond ($v_{B-F} = 872$ cm^{-1}). In the spectrum of product **AII** obtained from the reaction of $(PhO)_2P(O)OLi$ and BF_3 (b) we do not observe the absorption band assigned to the vibrations of bonds in the POLi group (1103.5 cm^{-1}). The bands at 1028 and 1069 cm^{-1} occur in the region characteristic of B–F bonds. Moreover, absorption bands derived from vibrations of the aromatic ring are distinguished in the spectrum.

From the purification of fraction **AII** obtained in the reaction of $(Ph)_2P(O)OLi$ with BF_3, by means of methylene chloride as solvent, a product of a crystalline structure was obtained. An NMR analysis of fraction **AII**, i.e. the crystalline product of the $(Ph)_2P(O)OLi$ and BF_3 reaction and product obtained form the reaction of $(PhO)_2P(O)OLi$ and BF_3 in the form of a viscous liquid, was carried out.

In the ¹H NMR spectra of fractions **AII** signals characteristic of protons in the aromatic ring are present. Figure 6 presents the spectrum of the product obtained from the reaction of $(Ph)_2P(O)OLi$ with BF_3 with signals in the 7.45 – 7.85 ppm range (a) and the spectrum of product $(PhO)_2P(O)OLi$ with BF_3 (b) where we observe signals of phenolic protons in the 7.1 – 7.5 ppm range.
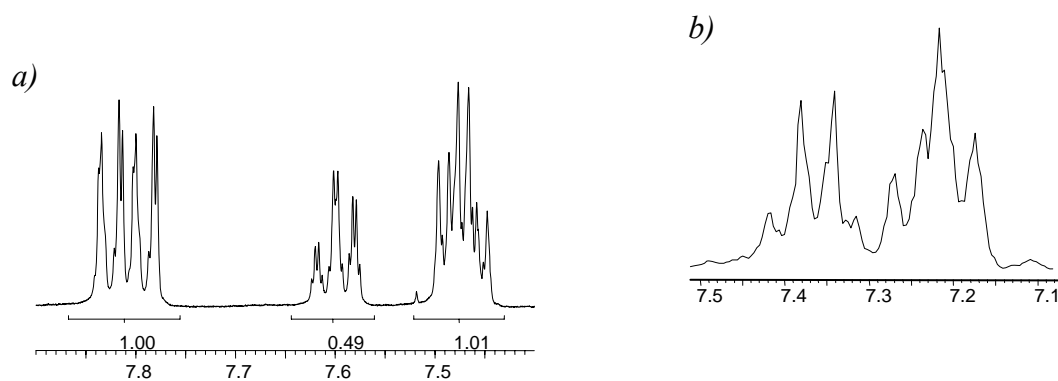
Figure 6. *¹H NMR spectra of fractions **AII** resulting from the reaction of (Ph)₂P(O)OLi (a) and (PhO)₂P(O)OLi (b) with BF₃.*

The ^{19}F NMR spectra recorded in CD_3CN are presented in Figure 7. The crystalline product of the $(Ph)_2P(O)OLi$ with BF_3 reaction shows two triplets in the spectrum, in a very narrow range of shifts, $-144.5 - -144.6$ ppm, characteristic of B−F bonds (a). This indicates a regular structure, in which the fluorine atoms have nearly the same chemical surrounding. In the case of fraction **AII** obtained in the reaction of $(PhO)_2P(O)OLi$ with BF_3, the analyzed post-reaction mixture comprises more than one product involving fluorine. Two basic groups of signals of chemical shifts 136.059 and 146.338 ppm, as well as a number of signals of smaller intensity occurring in the range of the basic signals, are present in the spectrum (b).
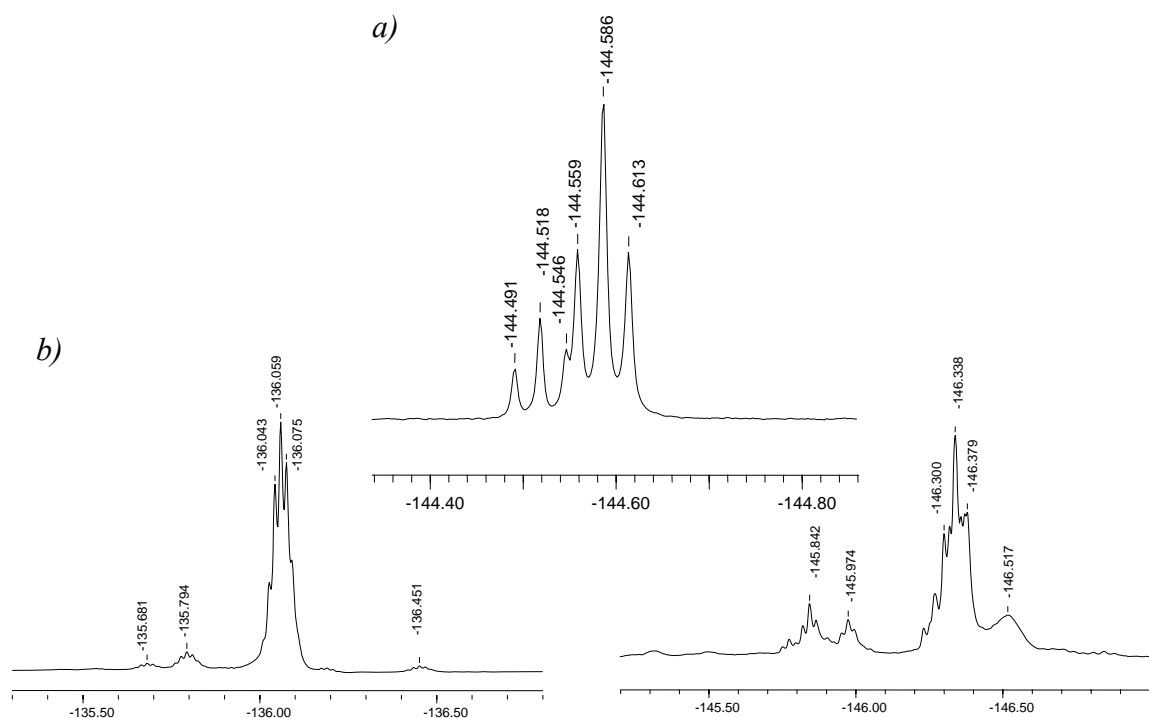
Figure 7. *^{19}F NMR spectra of fractions **AII** resulting from the reaction of (Ph)₂P(O)OLi (a) and (PhO)₂P(O)OLi (b) with BF₃.*

The ^{11}B NMR spectra of product **AII** show one signal characteristic of four coordinative boron. Figure 8 (a) presents a spectrum of the crystal obtained in the reaction of $(Ph)_2P(O)OLi$ with BF_3, in which the boron signal is shifted by -1 ppm. In the spectrum of the product obtained in the reaction of $(PhO)_2P(O)OLi$ with BF_3 (b), this signal is shifted by -1.737 ppm.
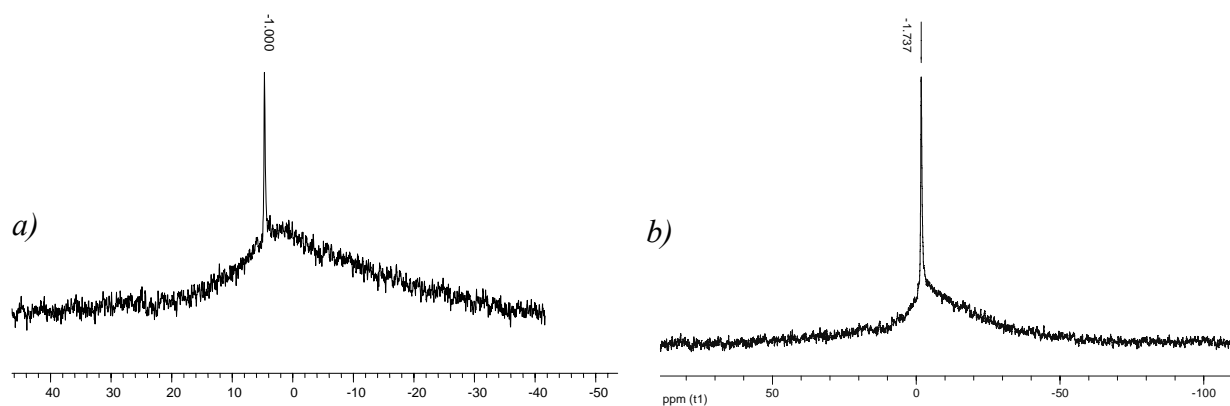
Figure 8. ^{11}B *NMR spectra of fractions* **AII** *resulting from the reaction of (Ph)₂P(O)OLi (a) and (PhO)₂P(O)OLi (b) with BF₃.*

In the phosphorus resonance of the crystalline form of product **AII** resulting from the reaction of (Ph)₂P(O)OLi with BF₃, one splitted signal at about 32 ppm is observed (Figure 9).
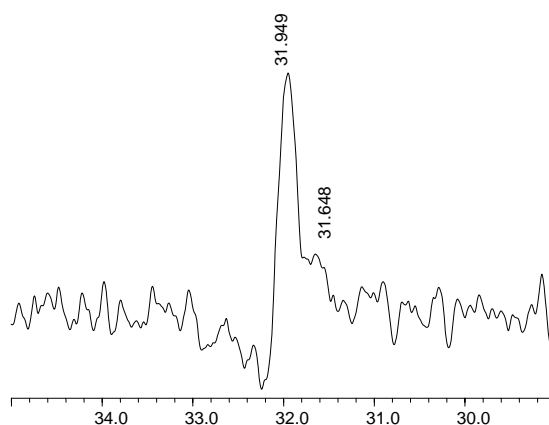
Figure 9. ^{31}P *NMR spectrum of precipitate* **AII** *resulting from the reaction of (Ph)₂P(O)OLi with BF₃.*

In Figure 10 is presented a diagram showing the boron and phosphorus content in samples of **AII**, determined by means of ICP-AES analysis. Fluorine lines, not included in the figure due to the wide scale of the spectrum, are additionally present in the spectrum.

When using LiBF₄ as the standard, the following elemental composition was determined:

Lithium salt	Element	B	F	Li	P
(Ph)₂P(O)OLi		5.45	15.15	0.45	10.9
	Content in wt. %				
(PhO)₂P(O)OLi		3.60	6.06	0.25	12.12
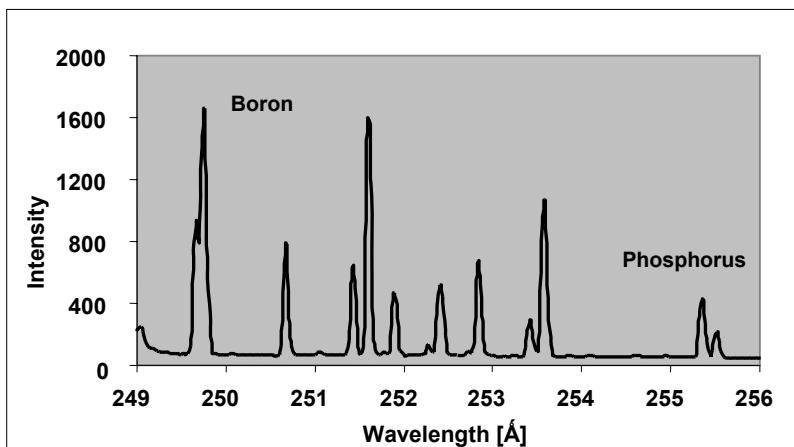
Figure 10. ICP-MS spectrum of precipitate **AII** resulting from the reaction of (Ph)₂P(O)OLi and BF₃.

It can be assumed with great probability that the presence of lithium in this fraction is connected with the not exact separation of fractions and is derived from $LiBF_4$. Then, at the lithium content of 0.45 wt. %, $LiBF_4$ constitutes 6 wt. %.

On the basis of the analysis of products **AII** it can be assumed that in the reaction of phosphorus (V) acids lithium salts $R_2P(O)OLi$ and BF_3 a product not containing lithium is formed, which is an electrically neutral molecule. This product is a derivative of the phosphorus (V) acids containing boron and fluorine.

The calculated amount of elements in the assumed product **AII** obtained in the reaction of $(PhO)_2P(O)OLi$ and BF_3 of the following monomeric or dimeric structures

is:
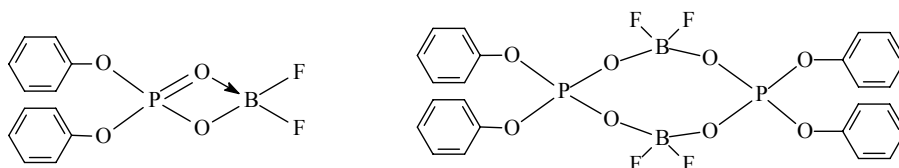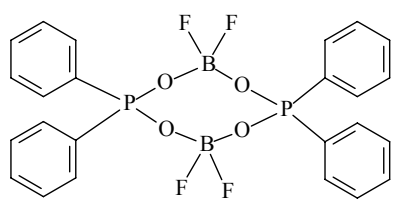
Element	B	F	Li	P
Content in wt. %	3.69	12.75	-	10.40

The presence of lithium in the studied sample and differences in composition indicate a not exact separation of the products. The compound obtained contains considerably less fluorine than shown by the analysis. The dimer shows a better fit of the content of elements, in which less fluorine atoms are present as a result of partial hydrolysis. The stabilization of the molecule results from the formation of an oxygen bridge:
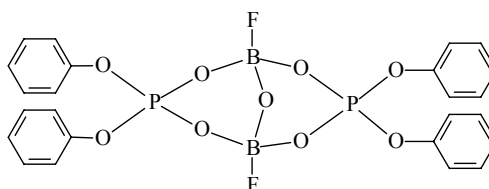
Element	B	F	Li	P
Content in wt. %	3.8	6.6	-	10.8
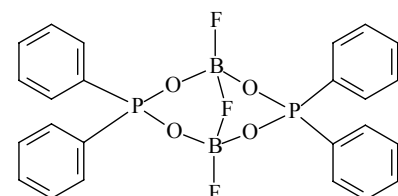
The content of elements at various assumptions of the structure of the compound formed in precipitate **AII** resulting from the reaction of $(Ph)_2P(O)OLi$ and BF_3 was calculated. For the compound of the following structure the calculated content of elements is:

Element	B	F	Li	P
Content in wt. %	4.08 / (4.49)	14.35/ (18.35)	-	11.33 / (10.65)

The values in parenthesis are the content of elements when considering that $LiBF_4$ constitutes 6 wt. % of the precipitate.
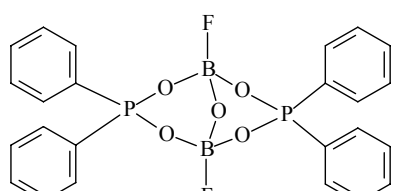
A gradual loss of fluorine leading to a dimer additionally stabilized by a fluoride bridge can probably result from the reaction with moisture:

Such a form of dimer has the following elemental composition:

Element	B	F	Li	P
Content in wt. %	4.23 / (4.67)	11.16 / (15.35)	-	11.75 / (11.04)

The dimeric form of such a compound can be stabilized by an oxygen bridge:

Such a form has the following composition:

Element	B	F	Li	P
content in wt. %.	4.25 / (4.68)	7.49/ (11.90)	-	11.8 / (11.09)

The determined product composition is closest to the theoretical one of the structure of a dimer containing a fluorine bridge.

In the case of the reaction with $(C_6H_5)_2P(O)OLi$, product **AII** was obtained in a crystalline form and was subjected to X-ray analysis. The obtained structure is shown in figure 11.
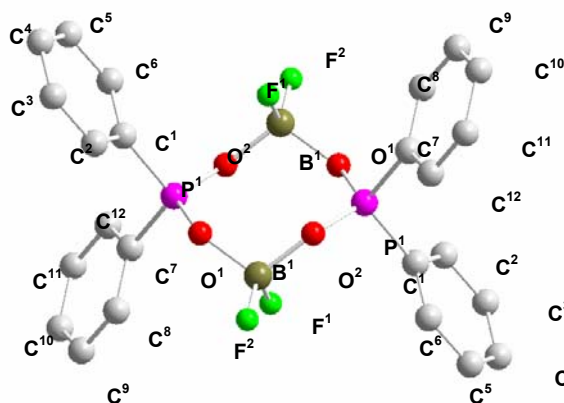
Figure 11. *Crystalline form of organic product resulting from the reaction of (Ph)₂P(O)OLi and BF₃.*

I.2. Characterization of polymer-in-salt electrolytes involving the product of the $(R)_2P(O)OLi$ and BF_3 reaction (R = Ph or PhO)

The electrolytes were prepared comprising $(R)_2P(O)OLi$ complexed with BF_3 (where R = Ph or PhO) with the use of various polymeric matrices: acrylonitrile and butyl acrylate copolymer, poly(methyl methacrylate) and poly(butyl acrylate). The salt was used in an amount of 1.2 moles of Li with respect to the number of moles of the polymer repeating unit. The membranes were obtained by casting from solution in acetonitrile. The electrolytes obtained were characterized by means of thermal analysis (DSC) and impedance spectroscopy.

❖ Matrix of (poly(AN-*co*-BuA 2:1))

The electrolytes comprising poly(AN-*co*-BuA 2:1) and one of the products of $(R)_2P(O)OLi$ complexation with BF_3 bears properties of a flexible membrane.

The results of DSC analysis are presented in Figure 12. The glass transition temperature of $(Ph)_2P(O)OLi/BF_3$ system in the first heating cycle is $T_g = 10.4$ °C. T_g of the poly(AN-*co*-BuA 2:1) matrix is 42.4 °C, and therefore the addition of the studied diphenylphosphinic acid salt causes plastification of the polymer matrix. Moreover, the thermogram shows that the system is completely amorphous. DSC analysis of the electrolyte comprising poly(AN-*co*-ABu 2:1) and the product of $(PhO)_2P(O)OLi$ complexation with BF_3 indicates a considerable decrease in the glass transition temperature (T_g) of the system to −8.8 °C, whereas T_g of the matrix is 42.4 °C. At the same time, the presence of a crystalline phase of melting point $T_m = 104.1$ °C is observed in the first heating cycle [Fig. 12 (*b*)]

Figure 12. Thermogram of the electrolytes comprising $(Ph)_2P(O)OLi + BF_3$ (a) and $(PhO)_2P(O)OLi + BF_3$ (b) and poly(AN-co-BuA).

❖ Matrix of poly(methyl methacrylate) PMMA

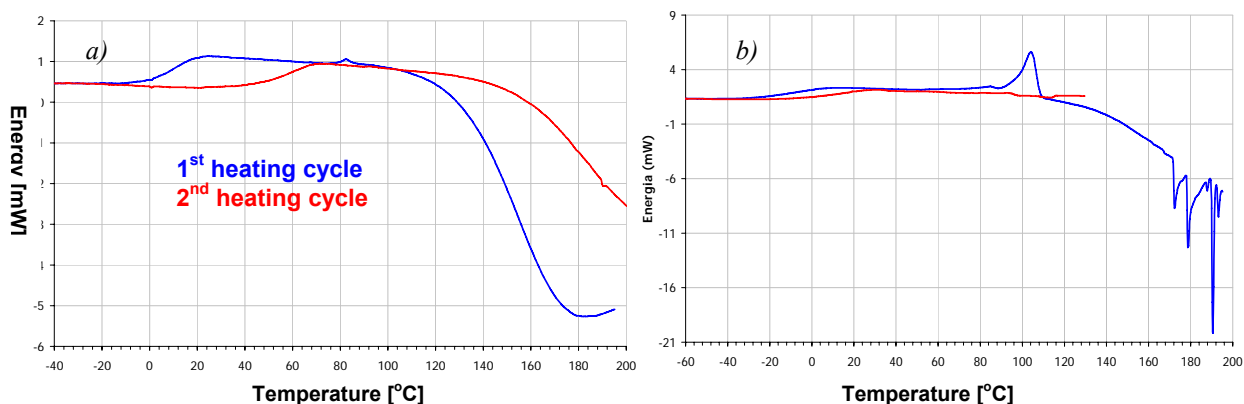The electrolyte obtained from the product of $(Ph)_2P(O)OLi/BF_3$ and PMMA at room temperature is non-homogeneous and brittle. In the first heating cycle it shows T_g of 29.1 °C and a broad melting point peak T_m at 67.4 °C. Therefore, it is noticed that the addition of the complex salt plasticizes the system (T_g of the PMMA matrix is 105 °C). In the second heating cycle the T_g value is repeated and the melting peak practically disappears (Fig. 13 *a*).

When using poly(methyl methacrylate) and $(PhO)_2P(O)OLi/BF_3$ an electrolyte was obtained in the form of a flexible membrane. The addition of a complexing salt caused a considerable decrease in the glass transition temperature to −16.1 °C. In the first heating cycle the presence of a crystalline phase of T_m = 94.5 °C is observed (Fig. 13 *b*).
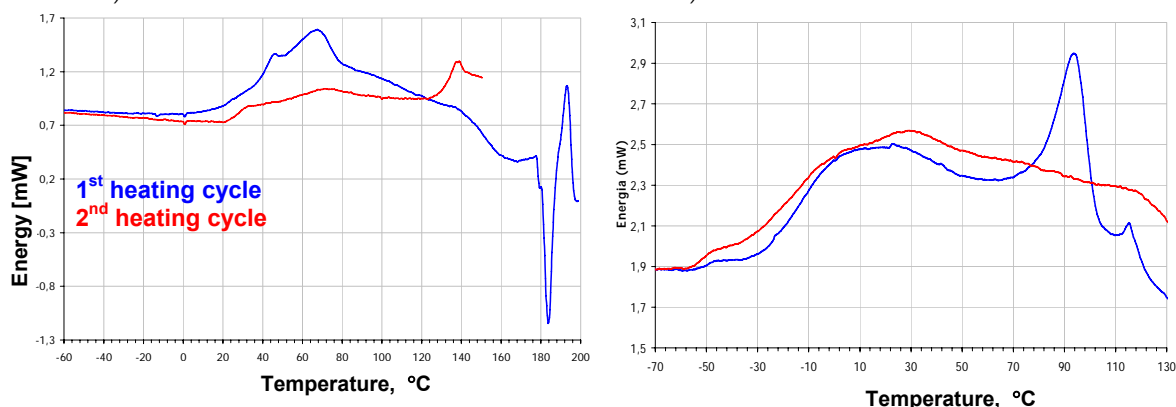
Figure 13. *Thermogram of the electrolytes comprising $(Ph)_2P(O)OLi$ +BF$_3$ (a) and $(PhO)_2P(O)OLi$ +BF$_3$ (b) and poly(methyl methacrylate).*

❖ Matrix of poly(butyl acrylate) PBuA

The electrolyte comprising poly(butyl acrylate) required the use of two solvents: acetonitrile in order to dissolve the salt and chloroform, in which the polymer dissolves. The thermogram of the electrolyte obtained from the product of $(Ph)_2P(O)OLi/BF_3$ and poly(butyl acrylate) is presented in Figure 14 (*a*). In the first heating cycle T_g = −43.1 °C (T_g of the matrix = −55 °C) and a double peak of melting with a maximum at 86.5 °C and 108.7 °C is present. In the second heating cycle T_g is −27.8 °C and the phase of melting point 111.1 °C remains.

The thermal analysis shows that the addition of the product of $(PhO)_2P(O)OLi/BF_3$ to poly(butyl acrylate) causes an increase in its T_g value to −37.7 °C. In both heating cycles the presence of a crystalline phase is observed. In the Ist heating cycle it is 105.1 °C. The thermogram is presented in Figure 14 (*b*).
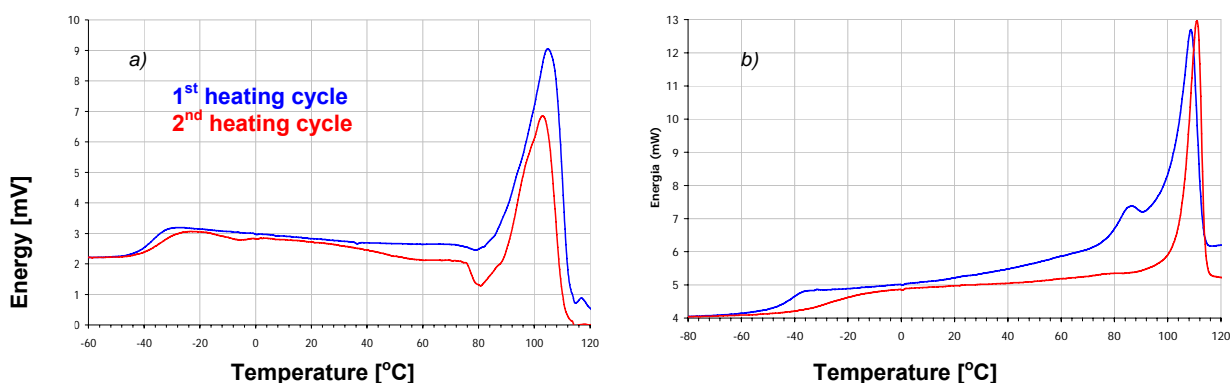

Figure 14. *Thermogram of the electrolytes comprising $(Ph)_2P(O)OLi+BF_3$ (a) and $(PhO)_2P(O)OLi+BF_3$ (b) and poly(butyl acrylate)*

The conductivity of electrolytes comprising the product of the lithium salt of diphenylphosphinic acid and BF_3 reaction as well as various polymeric matrixes is presented in Figure 15 (*a*). As can be noticed, the highest conductivity values (of the order of 10^{-6} - 10^{-4} S·cm^{-1}) are shown by the system involving PMMA as the polymeric matrix. A considerable increase in conductivity takes place in the glass transition temperature range of the system and further occurring melting of the crystalline phase. The lowest conductivity is shown by the system comprising poly(AN-*co*-BuA) (σ = 10^{-9} - 10^{-6} S·cm^{-1}). An increase in conductivity is observed above the glass transition temperature, which was observed in the second heating cycle above 50 °C. A similar course of changes is observed for the electrolytes comprising the product of the lithium salt of diphenylphosphinic acid and BF_3 reaction [Fig. 15 (b)].
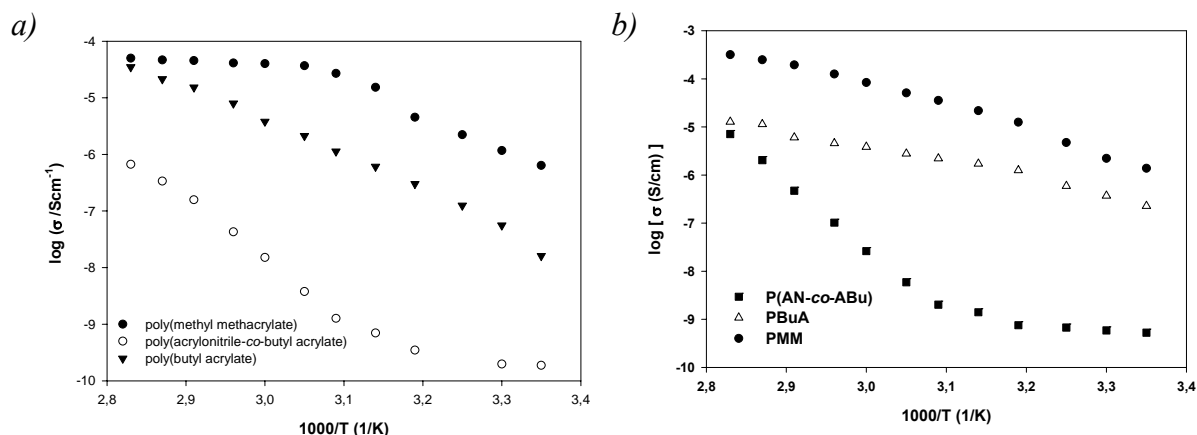
Figure 15. *Conductivity as a function of inverse temperature of the electrolytes comprising the product of the (Ph)₂P(O)OLi+BF₃ (a) or (PhO)₂P(O)OLi+BF₃ reaction (b) and various polymeric matrixes.*

The presented results of studies show that in polymer-in-salt systems characterized by high salt concentrations, considerably weaker conducting properties are exhibited by systems comprising poly(AN-*co*-BuA) as the polymer matrix. Such a behavior can suggest that the matrixes weakly interact with the lithium salt, providing better conditions for ion transport than the matrix comprising acrylonitrile monomeric units. The nitrile groups very clearly interact with positively charged ionic agglomerates, which is observed in the infrared spectrum by a clear shift of the CN group absorption band [Z. Floriańczyk, E. Zygadło-Monikowska, W. Wieczorek, A. Ryszawy, A. Tomaszewska, K. Fredman, D. Golodnitsky, E. Peled, B. Scrosati, *J. Phys. Chem. B* **2004**, *180*, 1407].

An additional experiment in order to check the effect of the phosphorus, boron and fluorine compound formed in the complexation reaction (after removal of LiBF₄) on the electrolyte conductivity involving a typical salt – LiI and poly(AN-*co*-BuA) as the polymer matrix. LiI was used in an amount of 1.2 moles per 1 mole of AN monomeric units (m.u.) in the matrix. The electrolyte obtained is characterized by good mechanical properties and is flexible. In Figure 23 is presented the conductivity of the electrolyte comprising an equimolar amount (with respect to LiI) of the compound, the proposed structure of which is as follows:
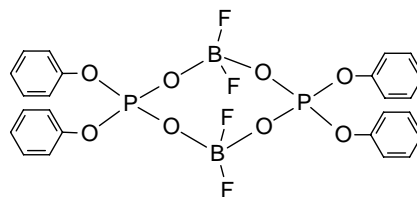
The plot in Figure 16 presents, for comparison, the conductivity of such a same system without addition of the compound formed.
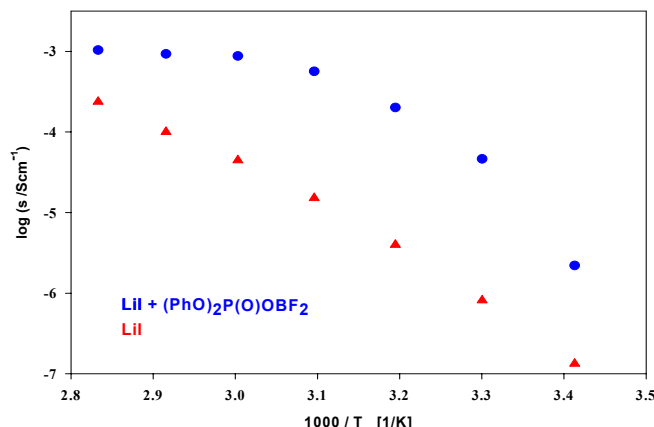
Figure 16. Conductivity of the electrolyte comprising LiI and a liquid product isolated from the reaction of (PhO)$_2$P(O)OLi + BF$_3$ and poly(AN-co-BuA) (2 : 1) as the polymer matrix. Li : AN m.u. in the matrix molar ratio = 1.2 :1.

As can be noticed, the addition of the phosphorus-boron compound to lithium iodide, a salt of relatively good conductivity characteristics, improves this conductivity by an order of magnitude. This means that the boron derivative obtained affects the mobility of the salt ions and it can be expected that due to its acidic character, it interacts with anions.

Synthesis and characterization of the products of phosphonic lithium salts and BF$_3$ reaction

The next part of work is a continuation of studies concerning the synthesis and characteristics of new salts obtained in the reaction of boron trifluoride and lithium derivatives of phosphorus salts. The studies described until now concerned monobasic phosphoric salts. The present part of report describes the results of studies of the BF$_3$ reactions with phosphorus salts containing two basic groups. Two salts: lithium phenylphosphonate and lithium vinylphosphonate were selected for the studies:
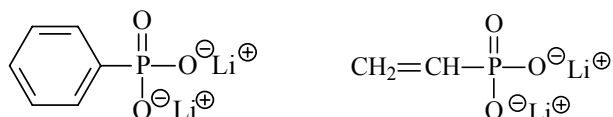
The purpose of these studies was to check the possibility of synthesis of new lithium salts being a combination of phosphorus salts and boron trifluoride. The studies carried out for mono-basic salts show that in the reaction with BF$_3$, in the first reaction step its complex with the salt is formed followed by the isolation of LiBF$_4$ with the formation of a non-ionic product containing a fragment of the phosphorus salt molecule in combination with boron substituted fluorine atoms.
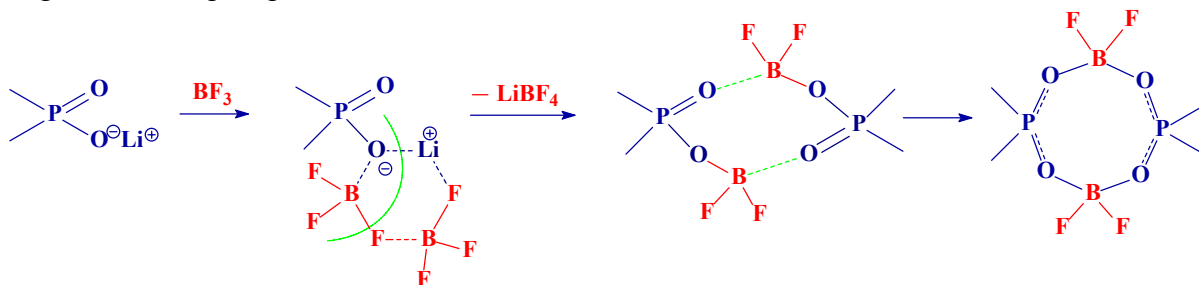
In this part of studies we selected dibasic salts in order to determine whether in this situation, as a result of complexation of the second basic group, the compound remains in the ionic form. The thus formed salt should be characterized by a considerable degree of

delocalization of the negative charge and considerable mobility of the lithium cation. The purpose of the synthesis of these products is to study the possibility of obtaining ionic compounds for application as electric charge carriers in lithium or lithium-ionic batteries.

Lithium phenylphosphonate and lithium vinylphosphonate were obtained in the reaction of phosphonic acid and *n*-butyllithium. The reaction was carried out in methylene chloride.
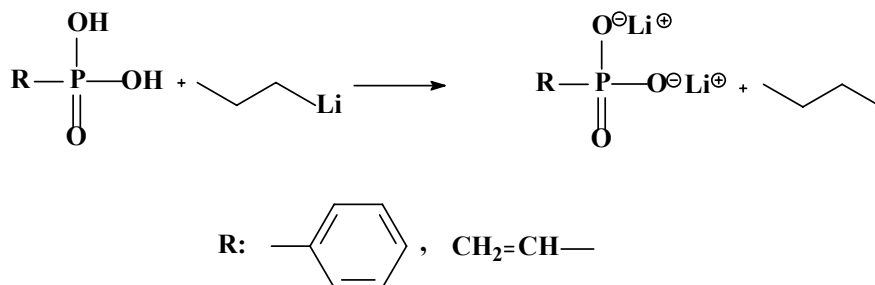
The reaction was carried out in a 100 ml reactor in argon atmosphere. Phosphonic acid was suspended in methylene chloride, and then the solution of *n*-butyllithium in hexane (2.5 M) in an amount of 1.2 moles with respect to the concentration of acidic groups was added dropwise. The reaction was accompanied by an exothermic effect – the system was cooled in an acetone-dry ice bath. A white precipitate resulted from the reaction.

The salts obtained were subjected to reaction with BF_3 etherate. Two products, an inorganic one – white powder and an organic derivative were obtained in all cases. It was found that $LiBF_4$ results from the reaction.

To determine the reaction course and composition of products, an analysis was carried out involving FTIR, ^{1}H, ^{11}B and ^{19}F NMR spectroscopy.

Figure 17 shows the IR spectrum of the organic product of the lithium phenylphosphonate and BF_3 reaction. Vibrations originating from the B–F group (bands at 1052 and 1012 cm^{-1}) and of B–O (bands at 808 and 672 cm^{-1}) are present in the spectrum.
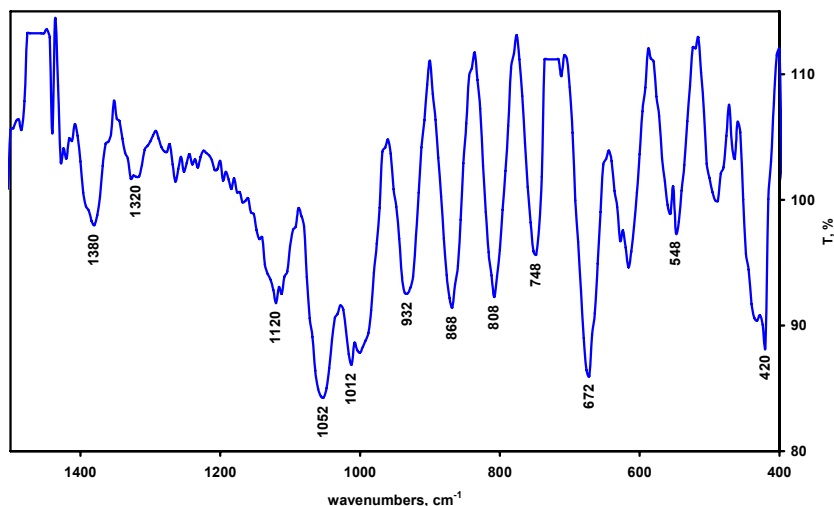
Figure 17. *IR spectrum of the organic product of the lithium phenylphosphonate and BF₃ reaction, obtained in the form of a paste with nujol in a polyethylene bag.*

In the ^{1}H NMR spectrum (Figure 18) a picture of protons of the aromatic ring present in the phosphonate can be observed.
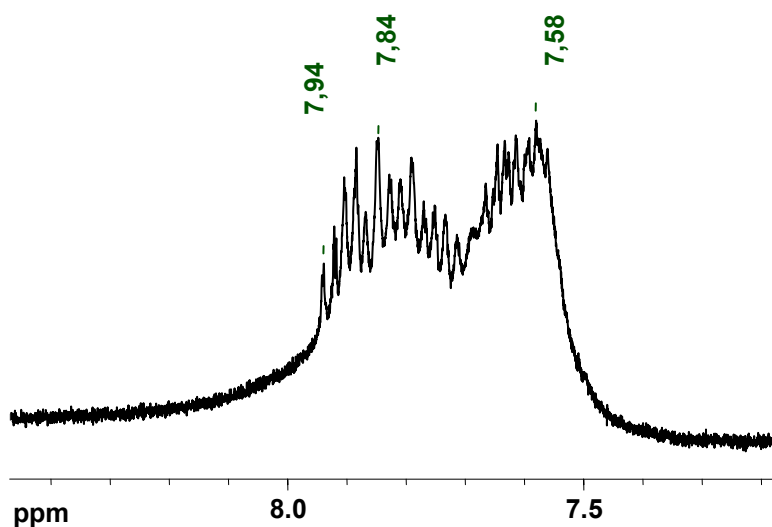
Figure 18. *^1H NMR spectrum (CDCl$_3$) of the organic product of the lithium phenylphosphonate and BF$_3$ reaction.*

In the fluorine resonance (Figure 19) we can see a picture of many signals, indicating a different mode of fluorine substitution at boron. Due to the considerable sensitivity of the signal location depending on the polarity of solution, they cannot be explicitly assigned to any given structure.
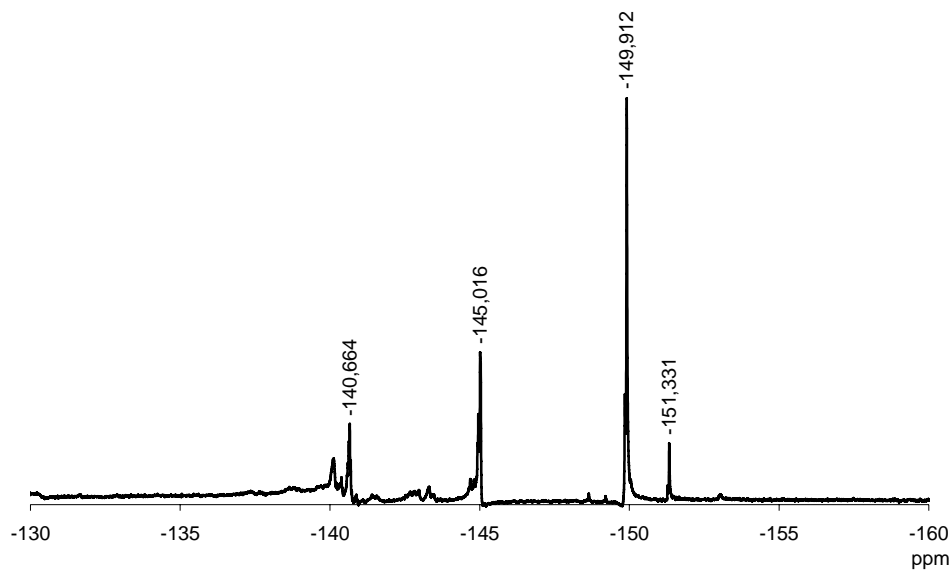
Figure 19. *^{19}F NMR spectrum (CD$_3$CN) of the organic product of the lithium phenylphosphonate and BF$_3$ reaction.*

As can be noticed in the ^{11}B NMR spectrum presented in Figure 20, the boron atoms in the obtained compound show a different chemical shift than that of the earlier studied derivatives obtained from mono-basic salts. Boron in a four-coordinative surrounding in the dimeric product obtained from lithium diphenylphosphinate showed a chemical shift of −1.008 ppm. Two ranges in which boron occurs are present in the spectrum of the analyzed compound: signals of higher intensity of chemical shifts 3.516 and 4.181 ppm as well as the signal of chemical shift 25.055 ppm.
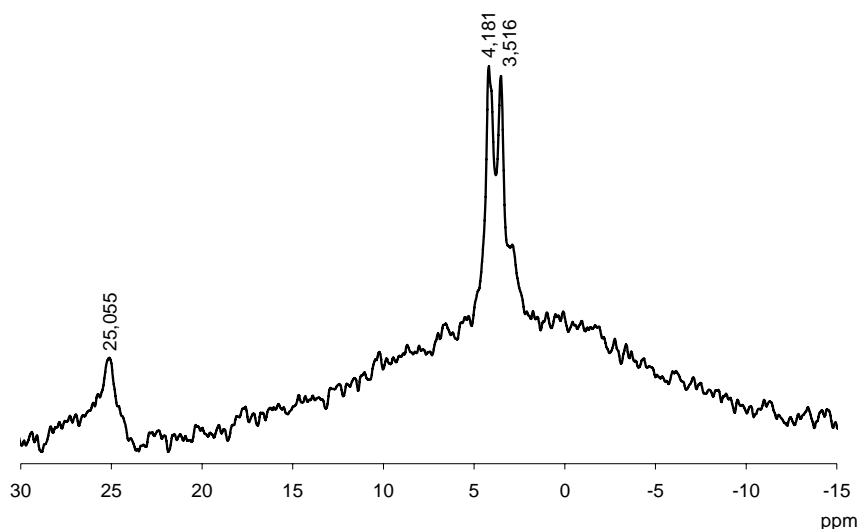
Figure 20. *^{11}B NMR spectrum (CD$_3$CN) of the organic product of the lithium phenylphosphonate and BF$_3$ reaction.*

It can be assumed that the course of reaction with the dibasic salt is more complicated than that in the case of previously studied derivatives. The attack of the Lewis acid on the most basic center in the molecule probably takes place in the first step.
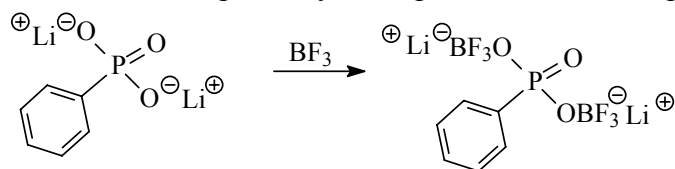
At further reaction steps, a reaction can proceed between the complexed molecules leading to the formation of a cyclic structure and isolation of the LiBF$_4$ salt in the presence of BF$_3$.
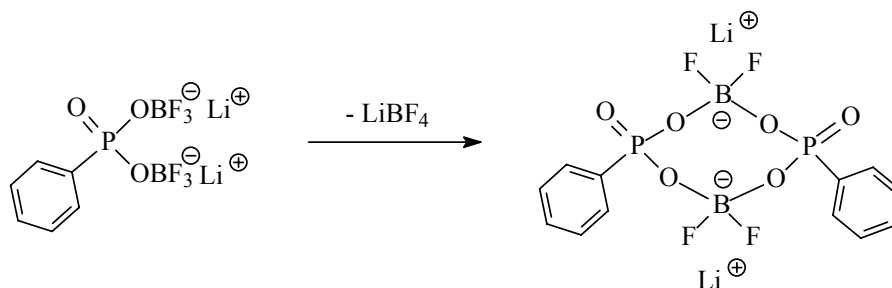
Since nearly all the inorganic part containing lithium ions was separated during the isolation of the product, it can be assumed that consecutive reactions take place leading to the formation of a non-ionic compound. Such reactions can proceed intermolecularly or within one molecule. However, it seems that due to steric reasons this first reaction is more probable. The isolation of the lithium salt can proceed still when carrying out the reaction; when BF$_3$ is present in the system LiBF$_4$ can be formed. If the process occurred after distilling off BF$_3$, LiF would be formed.

However, the determination of the structure of the compound formed is impossible at this stage of studies. It is probable that the signal originating from boron at ca. 25 ppm may be connected with the formation of a structure containing three oxygen atoms bonded with a boron atom and one fluorine atom.
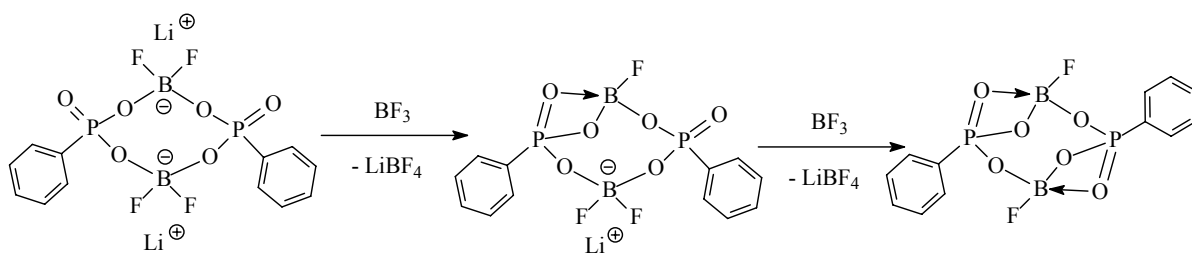
The NMR spectra of the organic phase formed in the reaction involving lithium vinylphosphonate are presented in Figures 21, 22 and 23.
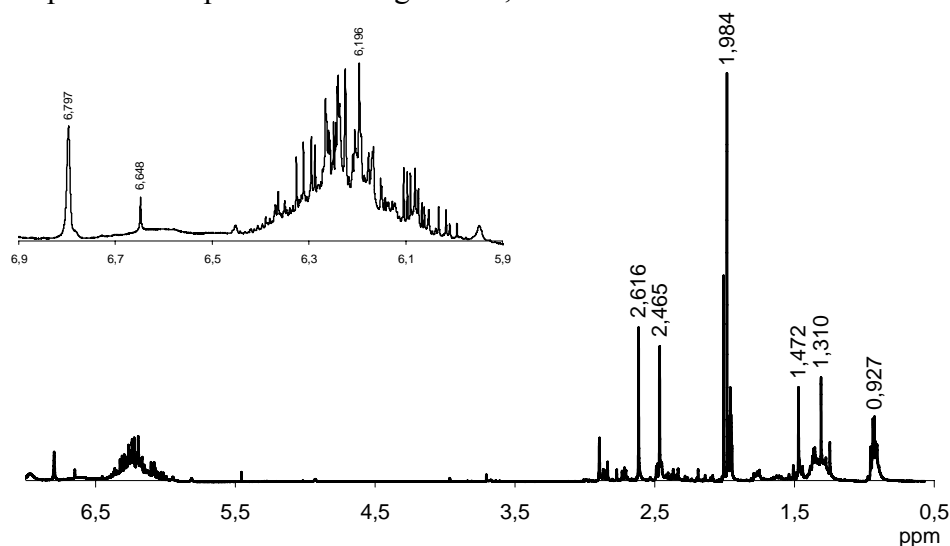
Figure 21. ^1H NMR spectrum (CD$_3$CN) of the lithium vinylphosphonate and BF$_3$ reaction.

The proton spectrum shows the presence in the product of an unsaturated vinyl bond in the 6.0 – 6.4 ppm shift range, and also a certain participation of the product in the polymeric form can be observed, which is indicated by the presence of proton signals of the –CH–CH$_2$– group in the backbone at 0.927 and 1.310 ppm. The other signals are derived from the polymerization inhibitor, hydroquinone, added to the reaction mixture.
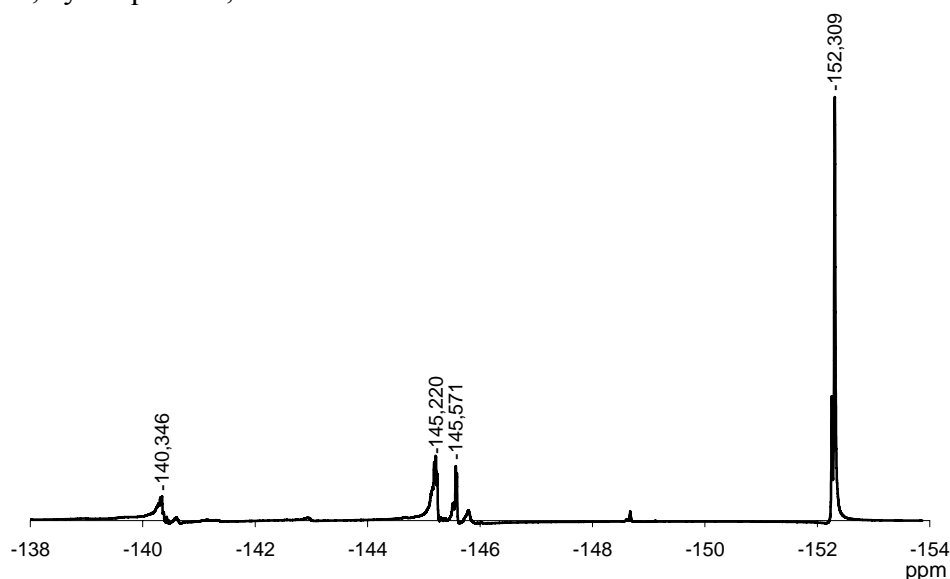
Figure 22. ^{19}F NMR spectrum (CD$_3$CN) of the lithium vinylphosphonate and BF$_3$ reaction.
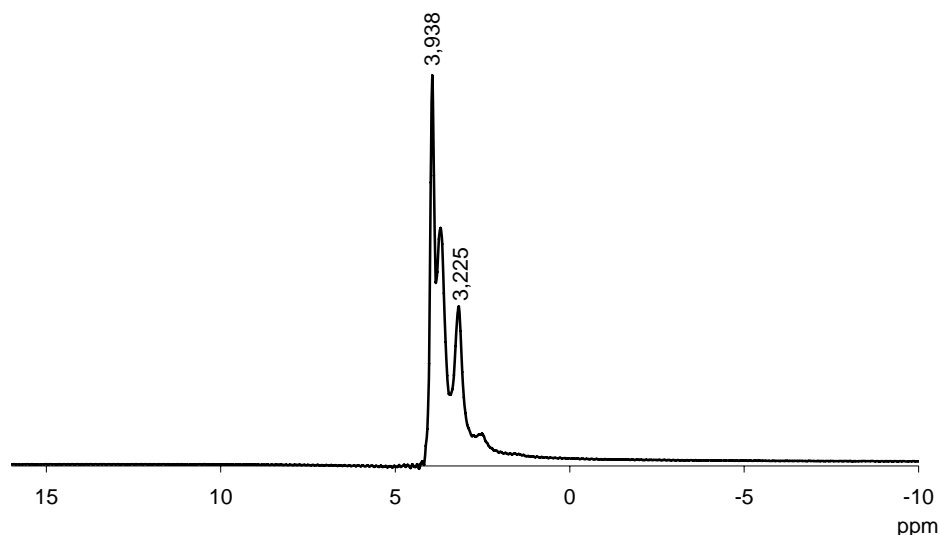
Figure 23. *^{11}B NMR spectrum (CD$_3$CN) of the lithium vinylphosphonate and BF$_3$ reaction.*

^{19}F NMR and ^{11}B NMR spectra of the described product and presented in Figures 22 and 23 show considerable similarity to those earlier described for lithium phenylphosphonate. In the fluorine resonance there are several signals, of which the greatest intensity is shown by the signal at 152.309 ppm, which probably corresponds to the signal at −149.912 ppm in the spectrum of the phenylphosphonate product. This signal can be assigned to fluorine atoms substituted to boron in the structure:
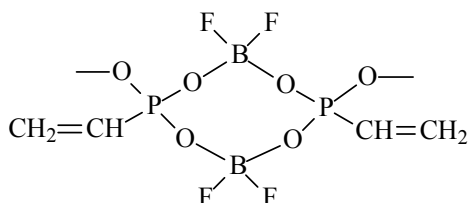
In the ^{11}B NMR spectrum the splitted signal at 3.225 – 3.938 ppm can be assigned to the boron atoms of such a structure. In the fluorine spectrum signals of lower intensity are additionally present at ca. 145 ppm, which may be assigned to the products of further reactions involving the phosphate anion. However, the concentration of these products is small and not visible in the ^{11}B NMR spectrum. It cannot be excluded that in this product a small concentration of lithium ions is present and that unreacted –P–O$^-$ anions remain in the molecule. Exact determination of the structure of products of the BF$_3$ and phosphonic salts reaction requires still further studies.

I.3. New difluoroalkoxyborane compounds as additives for lithium polymer electrolytes

A new class of difluoroalkoxyborane compounds ([R$_n$OBF$_2$]$_2$) containing oligooxyethylene groups of various molecular weight in the form of a methyl monoether ([R$_n$ = CH$_3$(OCH$_2$CH$_2$)$_n$, n = 1, 2, 3, 7) has been obtained in the reaction of BF$_3$ etherate with appropriate glycols. ^{1}H, ^{11}B and ^{19}F NMR spectral analysis of the derivatives obtained was carried out and the properties as Lewis acids of these derivatives have been compared with that of corresponding trialkoxyboranes and boron trifluoride in reaction with pyridine. The strength of the interaction of [R$_2$OBF$_2$]$_2$ with the differing in "hardness" anions of various lithium salts has been analyzed on the basis of NMR spectra. The [R$_n$OBF$_2$]$_2$ obtained were used as additives for polymer electrolytes containing PEO as a polymer matrix and various lithium salts at an

equimolar ratio of the boron compound to salt. The highest ionic conductivities, in the order of $10^{-5}-10^{-4}$ S cm^{-1} at 20–70 °C, were achieved for systems containing LiI and LiN(CF$_3$SO$_2$)$_2$. The lithium transference number (t_+) values, determined by the electrochemical method by steady-state technique for LiF and LiCF$_3$SO$_3$ are in the 0.6 – 0.8 range.

I.3.1. Introduction

Intense studies are being carried out on the utilization of solvent-free polymeric materials as separators in rechargeable lithium batteries [1,2]. Problems connected with the evaporation of low molecular weight solvent and its reactivity towards the anode are thus avoided. However, despite many studies, no SPE has yet been obtained of which the ionic conductivity would be sufficient for practical application. From studies carried out until now it appears that poly(ethylene oxide) (PEO) is characterized by the best properties as a solid solvent for lithium salts. Moreover, a majority of works are concerned with the modification of electrolytes based on PEO, in order to increase the ionic conductivity while maintaining suitable mechanical properties and achieving such operating conditions in which completely or partly the anionic current is eliminated. The motion of anions during operation of the battery causes the formation of polarization layers worsening the battery parameters. Depending on the measurement method and the salt concentration, the lithium transference number values of SPE based on PEO lie in the 0–0.5 range [3]. One of the ideas of achieving this goal consists in the introduction to the electrolyte of an additive, which would increase the ambient temperature ionic conductivity and the lithium ions transference number by interaction with the salt anion. Such an interaction results in the facilitation of the salt dissociation, decrease in the concentration of ion pairs and decrease in the mobility of anions. Examples are reported in the literature of the application of various additives of Lewis acid properties, such as nanometric inorganic fillers, which on the grain surface bear acidic centers interacting with the basic salt anions, which leads to favorable changes in the properties of composite electrolytes, such as increase in conductivity, chemical stability in contact with the lithium electrode and lithium transference number [4–8]. The other method consists in the introduction of so called anion receptors, such as calixarenes [9,10] or calixpyrroles [11], causing a decrease in the share of ion pairs and immobilization of anions, resulting in an increase in the cation transference number. Aluminum [12–14] or boron derivatives of Lewis acid properties capable of complexing salt anions seem to be a very promising group of compounds introduced into SPE. Borate esters containing oligooxyethylene groups of various length were mainly used as boron derivatives, applied as low molecular weight plasticizers [15–18] or incorporated into the polymer linear or crosslinked structure [19–21], for which a considerable increase in ionic conductivity was in many cases achieved. Examples of an increase in the lithium cation transference number (t_+) for SPE containing borate esters have also been described. For trialkoxyborane the highest t_+ value of 0.34 was achieved in the system with LiCF$_3$SO$_3$ [17], and for the crosslinked polymer containing boroxine rings the t_+ value lies in the 0.60–0.88 range [19]. Borane and borate derivatives containing aromatic or aliphatic substituents were also used as boron additives to polymer electrolytes [22–25]. It is assumed that the favorable effect of boron derivatives results from their Lewis acid properties, however, there are no data on the strength of these acids as well as on the strength of interaction with salt anions.

In this report we present the results of studies concerning the synthesis of a new group of boron derivatives comprising two fluorine atoms bonded with boron [R$_n$OBF$_2$]$_2$ and oxyethylene substituents (R$_n$) of various length. On the basis of NMR spectra the effect of interaction of difluoroalkoxyborane, trialkoxyborane and BF$_3$ with a chosen Lewis base – pyridine were compared. The ^{11}B and ^{19}F NMR spectroscopies were used to analyze the interaction of difluoroalkoxyborane and trialkoxyborane with anions of various lithium salts. The obtained

fluorine derivatives of boron $[R_nOBF_2]_2$ were applied as additives to PEO based SPE in order to evaluate their effect on the ionic conductivity and immobilization of salt anions.

I.3.2. Experimental
I.3.2.1. Preparation of boron compounds
I.3.2.1.1. Preparation of difluoroalkoxyborane compounds

Difluoroalkoxyborane compounds were obtained in the reaction of oxyethylene glycols monomethyl ether of various molecular weight (R_nOH , $M_w = 76, 120, 160$ and 350 g mol^{-1}, all from Aldrich) with boron trifluoride in the form of a complex with diethyl ether (BF$_3$ etherate, 98% Aldrich). The most probable course of this reaction is presented in Scheme 1.

$$4\,R_nOH + 4\,BF_3(ether) \longrightarrow 4\,R_nO\overset{\ominus}{B}F_3\overset{\oplus}{H} \xrightarrow{\text{- ether}} [R_nOBF_2]_2 + 2\,HBF_4 + 2\,R_nOH$$

$$R_n = CH_3(OCH_2CH_2)_n \ \text{where n} = 1, 2, 3, 7$$

$\downarrow$ pyridine
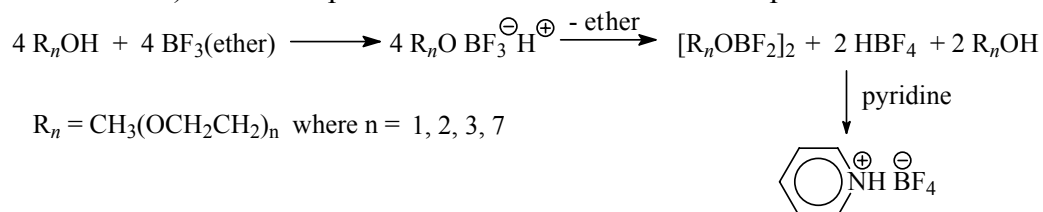
Scheme 1. Preparation of difluoroalkoxyboranes $[R_nOBF_2]_2$ from BF$_3$ etherate and oxyethylene glycols monomethyl ether of various molecular weight.

The reactions of obtaining difluoroalkoxyboranes $[R_nOBF_2]_2$ were carried out in the presence of an equimolar amount of reactants (BF$_3$ etherate and R_nOH) without a solvent, maintaining the reaction mixture temperature close to room temperature. All operations were carried out under the atmosphere of a neutral gas on a vacuum line. After reaction completion the diethyl ether formed in the reaction was removed by distillation under reduced pressure. In the next step pyridine was added and the precipitated tetrafluoroboric hydride of pyridine was separated from the product and glycol mixture; the latter was then distilled off under reduced pressure. In the case of R_nOH containing $n = 3$ or less ethylene oxide monomeric units, the product was purified by distillation under reduced pressure (for $n = 3$, b.p. = 160–180 °C /10^{-4} Torr). In all the cases studied, fluoroalkoxyborane products were viscous liquids. The structure of the products was determined on the basis of ^{1}H, ^{11}B and ^{19}F NMR spectroscopy. An analysis of the spectra indicates a dimeric structure of the difluoroborane derivatives obtained.

I.3.2.1.2. Preparation of trialkoxyborane compounds

The trialkoxyborane derivatives were obtained in the reaction of BF$_3$ etherate with lithium alkoxides of glycols (R_nOH) analogous to those applied in the reaction described in 2.1.1. The alkoxides were obtained in the reaction of oxyethylene glycols with n-butyllithium (BuLi, 2.5 M solution in hexane, Aldrich) using a 1.1 molar excess of BuLi with respect to the hydroxyl groups. The reaction is described by Scheme 2.

$$R_nOH + BuLi \longrightarrow R_nO^{\ominus}Li^{\oplus} + BuH$$

$$3\,R_nO^{\ominus}Li^{\oplus} + 4\,BF_3(ether) \longrightarrow (R_nO)_3B + 3\,Li^{\oplus}BF_4^{\ominus}$$

$$R_n = CH_3(OCH_2CH_2)_n \ \text{where n} = 1, 2, 3, 7$$
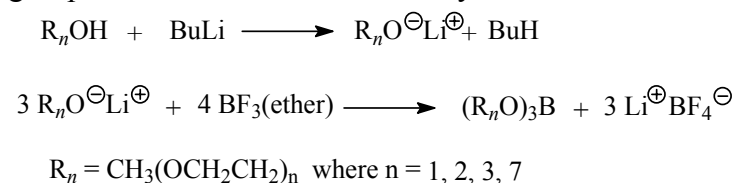
Scheme 2. Preparation of trialkoxyboranes $(R_nO)_3B$ in the reaction of BF$_3$ etherate and lithium monomethyl ether of oxyethylene alkoxides (R_nOLi) of various molecular weight.

Contrary to the reaction involving glycols, in this case trialkoxyborane $(R_nO)_3B$ is formed, and LiBF$_4$ isolates as a side-product. On the basis of boron resonance it was estimated that the

ether fraction may contain from 5 to 10% of the lithium salt in the form of a complex with trialkoxyborane.

I.3.2.1.3. Synthesis of polymer electrolytes containing difluoroalkoxyborane compounds

The electrolytes were obtained according to the standard procedure by film casting of poly(ethylene oxide) (PEO) ($M_w = 5 \times 10^6$ g mol^{-1}, borane compound and lithium salt from a mutual solution in acetonitrile. The mixed components formed a homogeneous solution. All operations connected with the obtaining of electrolytes and performing the measurements were carried out in an atmosphere of dried argon. The solvent was removed under dynamic vacuum in two steps, first for 50 h at a vacuum of 20 Torr and then for 140 h at 10^{-3} Torr at room temperature. In the FTIR spectrum, the signals assigned to acetonitrile completely disappeared after about the first 70 h of such drying. The solvents were dried and distilled in an argon atmosphere prior to use. The electrolytes thus obtained form flexible and homogeneous membranes, with the exception of the system with the LiN(CF$_3$SO$_2$)$_2$ salt, for which the electrolyte was viscous.

I.3.2.2. Thermal analysis

The DSC studies were carried out with a Perkin-Elmer (Pyris-1) analyzer. The measurements were carried out in the −100 to 200 °C temperature range with a heating rate of 20° per minute in hermetically closed aluminum pans. An empty aluminum pan was used as a reference and the samples weights were maintained in the range of 10-15 mg.

I.3.2.3. ^{1}H, ^{11}B and ^{19}F NMR studies

The structures of the borane derivatives and analysis of their mixtures with lithium salts were determined by combining ^{1}H, ^{11}B and ^{19}F NMR spectroscopy. Spectra were recorded on a Varian Mercury 400 spectrometer in CDCl$_3$, CD$_3$CN or dimethoxyethane (DME) with a small amount of DMSO$_{d-6}$ solution at 25 °C. Boron resonance measurements were carried out in quartz tubes. The chemical shifts in ^{19}F NMR spectra were determined with respect to CF$_3$COOH used as an internal standard.

I.3.2.4. Electrochemical measurements

The ionic conductivity of the polymer electrolyte (SPE) membranes was determined by ac impedance spectroscopy between blocking electrodes. The sample was sandwiched between two stainless steel (SS) blocking electrodes with a diameter of 1 cm to form a symmetrical SS/SPE/SS cell and placed in a temperature controlled oven. The impedance tests were carried out in the 1 MHz to 1 Hz frequency range using a Solartron-Schlumberger 1255 impedance analyzer.

For the determination of the lithium ion transference number (t_+) performed in Tel Aviv in the lab of Professor Diana Golodnitsky and Professor Emanuel Peled, the polymer electrolyte symmetrical Li/SPE/Li hermetically sealed 2032 coin cells were assembled and tested with the use of a computer-interfaced Solartron 1260 frequency-response analyzer over the frequency range: 1 MHz–0.1 Hz. The area of the polymer electrolyte sample was 0.96 cm^2. The test temperature range varied from 25 to 100 °C.

The lithium ion transference number (t_+) of polymer electrolytes was determined by a well established steady-state technique introduced by Bruce *et al.* and Scrosati [26,27]. The method is based on the analysis of combined dc and ac runs on the symmetrical cell with non-blocking lithium electrodes. The dc measurements of initial (I_0) and the steady-state (I_{ss}) currents were made by polarizing the test cells at voltage bias of 10 mV. The ac impedance measurements were performed before and after applying a bias, to evaluate the value of the interfacial resistance at

the beginning and at the end of the test, *i.e.*, R_0 and R_{ss}, respectively. Under these conditions, the lithium ion transference number is given by the equation: $t_{Li+} = \dfrac{I_{SS}(\Delta V - I_0 R_0)}{I_0(\Delta V - I_{SS} R_{SS})}$ (1)

The lithium ion transference number of the membrane samples were measured between 55 °C and 90 °C.

I.3.3. Results and discussions
I.3.3.1. NMR characterization of boron compounds

Difluoroalkoxyboranes obtained according to Scheme 1 were characterized by ^{1}H, ^{11}B and ^{19}F NMR spectroscopy. In the ^{1}H NMR spectrum of the product formed in the first reaction stage ($R_n OBF_3{}^- H^+$), a signal characteristic of the acidic hydrogen atoms is present at the chemical shift $\delta_{(CDCl3)}$ 10.89 ppm. Moreover, signals at $\delta_{(CDCl3)}$ 4.01–4.10 (m) of the hydrogen atoms in the $CH_2 OB$ group, which are strongly shifted with respect to that of $R_n OH$ ($\delta_{(CDCl3)}$ $C\underline{H}_2 OH$ 3.50–3.53 ppm (t)) due to the negative induction effect of BF_3, are present. The other protons in the oxyethylene groups give in the spectrum signals in the 3.6–3.8 ppm range in the form of multiplets and the OCH_3 ether group gives a signal $\delta_{(CDCl3)}$ at 3.44–3.46 ppm. In the ^{19}F NMR spectrum this product shows a signal of chemical shift $\delta_{(CDCl3)}$ −158.637 ppm and also one signal in the [11]B spectrum: $\delta_{(CDCl3)}$ −0.638 ppm.

Under the effect of temperature or introduction to the system of a base, such as e.g. pyridine, HBF_4 isolates (with pyridine in the form of $C_5 H_5 NH^+ BF_4{}^-$) and a reaction product is formed containing an alkoxide substituent and two fluorine atoms bonded with the boron atom. In the reaction, simultaneously a molecule of the initial glycol isolates. In the ^{1}H NMR spectrum of the product $[R_n OBF_2]_2$ no signals of acidic protons are present; the $CH_2 OB$ group in the alkoxide substituent shows a picture in the form of a triplet of chemical shift $\delta_{(CDCl3)}$ 3.80–3.83 ppm (t). The chemical shifts of signals of the product in both boron and fluorine resonances depend considerably on the type of solvent. For solutions in $CDCl_3$ the fluorine signal appears at −158.6 ppm, and that of boron at ca. 0.8 ppm (Fig. 25), both in the form of singlets. In acetonitrile the fluorine signal splits showing a quartet of chemical shift in the $\delta_{(CD3CN)}$ −150.45 − −150.54 ppm range, and the boron signal remains a singlet at $\delta_{(CD3CN)}$ 5.8 ppm. In ^{19}F spectra of solutions recorded in DMF (with a several percent share of $DMSO_{d-6}$) a group of signals is observed in the range characteristic for fluorine atoms bonded with the boron atom, which may result from the cleavage of the dimeric form of the compound and its interaction with the solvent. In the ^{11}B NMR spectrum recorded in this solvent one signal is present at $\delta_{(DME)}$ 3.73 ppm (Fig. 26).

In the ^{1}H NMR spectrum of an exemplary trialkoxyborane containing $n = 2$ oxyethylene monomeric units, the signals characteristic of the $CH_2 OB$ group show a chemical shift of $\delta_{(CDCl3)}$ 3.69–3.72 ppm (t), and the remaining CH_2 groups show a picture of three triplets in the $\delta_{(CDCl3)}$ 3.28–3.41 ppm range, and the OCH_3 group shows a signal at $\delta_{(CDCl3)}$ 3.1 ppm. In the ^{11}B NMR spectrum, the trialkoxyboranes signal can be found at $\delta_{(CDCl3)}$ 17.9 ppm in chloroform and at $\delta_{(CD3CN)}$ about 23 ppm in acetonitrile.

I.3.3.2. NMR studies of Lewis acidic properties of trialkoxy and difluoroalkoxyborane compounds

The acidic properties of the obtained two types of derivatives, trialkoxy- and difluoroalkoxyboranes have been compared by complexation reactions with pyridine and various lithium salts. Salts comprising anions of various hardness, such as LiF, LiCl, LiI, $CF_3 SO_3 Li$, $LiClO_4$ and $(CF_3 SO_2)_2 NLi$ were used for the analysis. The strength of interaction of the studied boranes with the mentioned compounds of Lewis base properties was observed by ^{1}H, [11]B and

^{19}F NMR spectroscopy. In the case of lithium salts the measurements were carried out for two types of solutions containing as solvent DME and $CDCl_3$ and for the reaction with pyridine - CD_3CN.
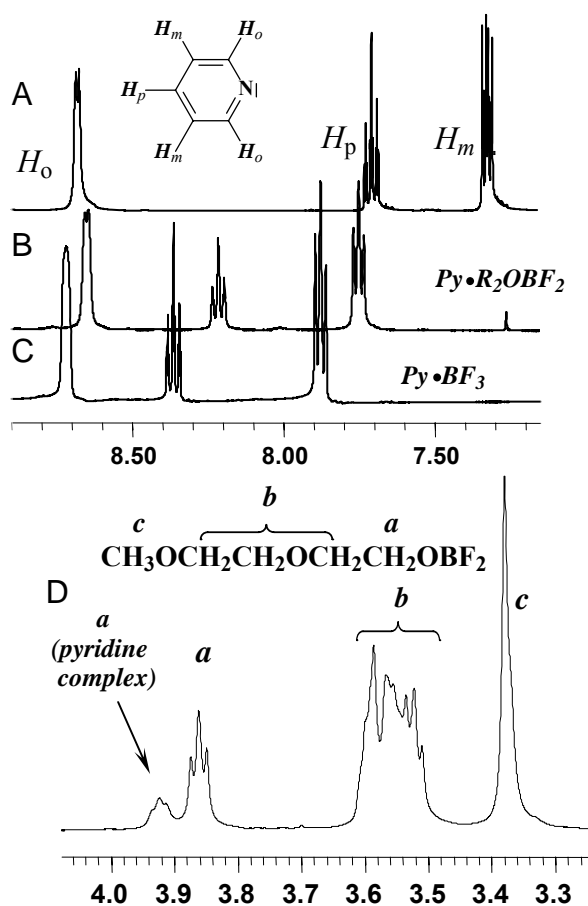
Figure 24. *^{1}H NMR spectra of pyridine (A) and mixture of pyridine with: [R_2OBF_2]$_2$ containing 27% of pyridine (B) and BF$_3$ (1:1) (C) in CD$_3$CN.*

The ^{1}H NMR spectra of solutions of (R$_n$O)$_3$B and pyridine mixtures in CD$_3$CN at an equimolar ratio as well as a twofold excess of pyridine do not show their interaction. The signals characteristic for pyridine ($\delta_{(CD3CN)}$ 7.29−7.33 ppm (t) C$\underline{H}_{metha}$, 7.67−7.72 ppm (t) C$\underline{H}_{para}$, and 8.67, 8.68 ppm (d) C$\underline{H}_{ortho}$) (Fig. 24 A) did not undergo a shift, and also there are no changes in the range of the CH$_2$OB group signals indicating an interaction of (R$_2$O)$_3$B with pyridine. However, in ^{1}H NMR spectra of [R$_2$OBF$_2$]$_2$ with pyridine the changes are considerable. At a small share of pyridine, signals originating form both the complexed and free forms of [R$_2$OBF$_2$]$_2$ can be observed. The spectrum of the [CH$_3$(OCH$_2$CH$_2$)$_2$OBF$_2$]$_2$ (R$_2$OBF$_2$) mixture containing 27% of pyridine is presented in Fig. 24B.

As can be noticed, the position of pyridine signals in the complex changes and these signals occur at $\delta_{(CD3CN)}$ 7.73−7.77 ppm (t) C$\underline{H}_{metha}$, 8.19−8.24 ppm (t) C$\underline{H}_{para}$, and 8.65, 8.66 ppm (d) C$\underline{H}_{ortho}$. In the region characteristic for the alkoxy group, the signal at 3.92 can be assigned to the C$\underline{H}_2$OB group of the difluoroborane derivative complexed form. At an equimolar and excess content of pyridine the spectrum complicates and new signals appear, difficult for interpretation, confirming, however, the strong interaction of the fluoroborane derivative with pyridine. For comparison, in Fig. 24C is presented the ^{1}H NMR spectrum of the BF$_3$ and pyridine complex. In

this spectrum the pyridine signals shift more than in the case of the analyzed difluoroalkoxyborane. These signals occur at 7.86–7.89 ppm (t) C$\underline{H}_{metha}$, 8.34–8.39 ppm (t) C$\underline{H}_{para}$, and 8.72 ppm (d) C$\underline{H}_{ortho}$. Comparing the acidic properties of boron derivatives by the interaction with a Lewis base – pyridine it can be found on the basis of NMR spectra that trialkoxyborane bears very weak acidic properties not observed in NMR, and the analyzed difluoroalkoxyborane shows features of a Lewis acid of weaker strength than that of BF$_3$.
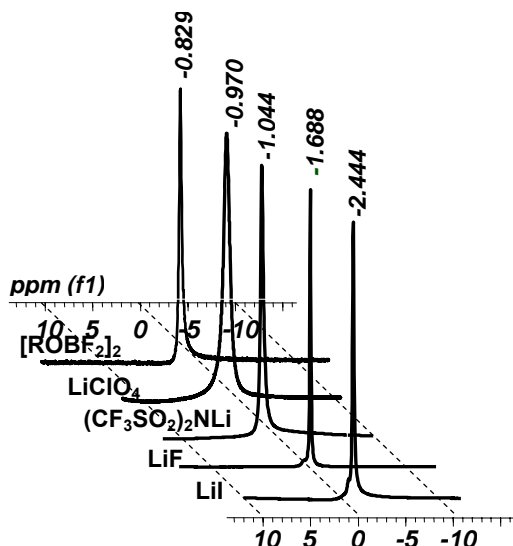
Figure 25. *Influence of various lithium salts addition on the chemical shift of the boron signal in [CH$_3$(OCH$_2$CH$_2$)$_2$OBF$_2$]$_2$ in ^{11}B NMR spectra of equimolar ratio solutions recorded in CDCl$_3$.*

An analysis of the interaction of anions of various lithium salts with the borane compounds obtained was carried out on the basis of ^{11}B and ^{19}F NMR spectra for solutions of mixtures of an equimolar composition. Fig. 25 presents the spectra of solutions of [CH$_3$(OCH$_2$CH$_2$)$_2$OBF$_2$]$_2$ ([R$_2$OBF$_2$]$_2$) mixtures with lithium salts recorded in chloroform. It should be noticed that a majority of the lithium salts studied show a limited solubility in chloroform, and as a result of interaction with the analyzed difluoroalkoxyboranes they achieve considerable solubility in this solvent.

As seen in Fig. 25, in the spectrum of the [R$_2$OBF$_2$]$_2$ solution in CDCl$_3$ a singular signal of boron at −0.829 is present. In the presence of lithium salts this signal undergoes a shift towards the lower field region and this effect depends on the type of the lithium salt anion. As can be noticed, [R$_2$OBF$_2$]$_2$ interacts the strongest with the iodide anion; in the presence of LiI the boron signal shifts by ca. 1.615 ppm to −2.444 ppm. The effect caused by the addition of LiF is much weaker, the chemical shift of boron in the presence of this salt is −1.688 ppm, i.e. the signal shifts by 0.859 ppm. This result is surprising, since it could be expected that the hard fluoride anion should interact stronger with boron. However, the weaker interaction may result in this case from the low polarity of chloroform, in which LiF undergoes dissociation with difficulty, and only in the dissociated form it can compete with the ether basic centers present in the boron compound alkoxy group. It is similar in the case of LiClO$_4$ and LiN(CF$_3$SO$_2$)$_2$; as can be noticed in the spectra, the hard perchlorate anion shows a weaker effect on the boron signal position than the soft imide salt anion.
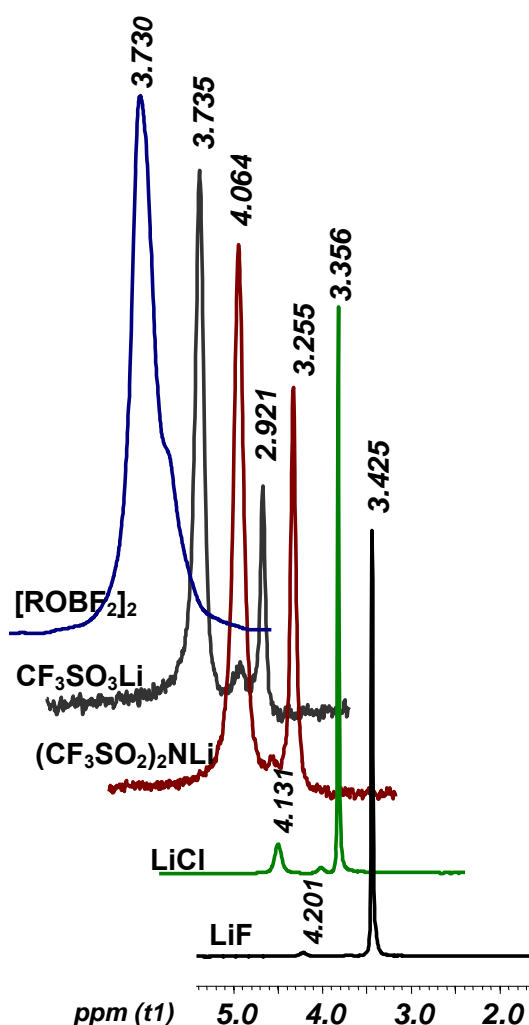
Fig. 26. ^{11}B NMR spectra of complexed and free form of [CH₃(OCH₂CH₂)₂OBF₂]₂ in the mixture with various lithium salts solutions at equimolar ratio, recorded in DME (+10 % of DMSO_{d-6}).

The effect of the solvent on the position of signals in the boron resonance of $[R_2OBF_2]_2$ in the presence of lithium salts was compared using solutions in dimethoxyethane (DME) with 10% $DMSO_{d-6}$. The ^{11}B NMR spectra in this solvent, presented in Fig. 26, confirm the interaction of fluoroalkoxyborane with lithium salts. The effect of complexation is shown by the appearance in the spectra of a new signal, also like in $CDCl_3$ shifted towards the lower field region. Moreover, the signal assigned to the non-complexed form undergoes a shift in the same direction. The boron signal in the $[R_2OBF_2]_2$ spectrum without the addition of salt, presented in Figure 26, is not split, but as can be seen, it is broadened and probably is composed of two signals. This effect is connected with the interaction of the boron compound with the solvent which has donor properties. With an increase in the ability of the added salt anions to interaction with fluoroalkoxyborane, the intensity of the non-complexed boron signal increases in the spectra. As seen in Figure 26, for LiF nearly exclusively the comlexed form is present, the chloride anions slightly weaker complex boron, whereas in the case of triflate as well as imide salt in solution the neat form prevails.

In the ^{11}B NMR spectra of trialkoxyboranes in $CDCl_3$ and DME no effect of the added lithium salt on the chemical shift was noticed. For solutions in chloroform the boron signal occurs at ca. 18 ppm, and in DME only one signal is observed at ca. 23 ppm. Therefore, the

acidic properties of trialkoxyborane derivatives cannot be concluded on the basis of boron resonance.

I.3.3.3. Characterization of electrolytes comprising difluoroalkoxyborane compounds
I.3.3.3.1. Thermal properties

The obtained trialkoxy and difluoroalkoxyborane compounds were applied as additives to solid polymeric electrolytes comprising PEO as polymer matrix and 10 mol. % of lithium salt. In all the cases the electrolytes obtained had the form of flexible membranes with the exception of $LiN(CF_3SO_2)_2$, for which the electrolyte was viscous. In Table 1 are presented the results of DSC measurements of electrolytes obtained involving $[R_2OBF_2]_2$.

Table 1. DSC data of polymer electrolytes based on PEO comprising equimolar ratio of $[CH_3(OCH_2CH_2)_2OBF_2]_2$ and lithium salts[a]

Salt	T_m[b] (C)	% of crystalline PEO[c]	T_g[d] (^{o}C)
LiI	56.4	38.2	−49.0
$LiN(CF_3SO_2)_2$	–	–	−47.7
$LiCF_3SO_3$	59.4	22.9	−43.4
$LiCF_3SO_3$[e]	60.4	40.7	−50.2
$LiBF_4$	57.7	45.7	−38.9
LiF	65.0	79.4	−31.9

[a] Li: EO = 10
[b] determined from I[st] heating cycle
[c] calculated with respect to PEO content in electrolyte
[d] determined from IInd heating cycle
[e] measurement repeated after 30 days.

As can be noticed, the addition of the boron compound does not limit the ability of PEO chains towards crystallization. The polymer crystalline phase content in the electrolytes increases in time, which is indicated by the repeated after 30 days result of measurement carried out for the same sample containing $LiCF_3SO_3$. The measurements performed for samples conditioned for the same period of time indicate that the greatest tendency towards crystallization is characterized by the system involving LiF, for which the crystalline phase content is nearly 80%. It also has the highest glass transition temperature $T_g = −31.9$ °C. The electrolyte comprising $LiN(CF_3SO_2)_2$ is completely amorphous and is characterized by low glass transition temperature of −47.7 °C. At the same time it is characterized by the worse mechanical properties, it is viscous and flows under pressure. The lowest T_g of −49.0 °C was found for the system with LiI, at about 40% of crystalline phase this electrolyte bears good mechanical properties, it is flexible and maintains dimensional stability under moderate pressure.

I.3.3.3.2. Electrochemical properties of electrolytes comprising difluoroalkoxyboranes

The difluoroalkoxyboranes obtained were used as additives for polymer electrolytes containing PEO as polymer matrix, and various lithium salts at an equimolar ratio of the boron compound to salt. The ionic conductivity of these systems was determined by impedance spectroscopy as a function of temperature in a system of blocking steel electrodes. Fig. 27 shows the conductivity of electrolytes involving difluoroalkoxyboranes $[R_nOBF_2]_2$ containing one or two oxyethylene monomeric units ($n = 1, 2$).
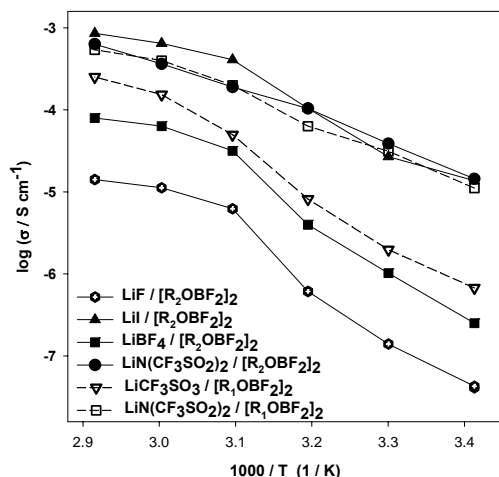
Fig. 27. *Effect of the type of lithium salt on the conductivity of electrolytes based on PEO and difluoroalkoxyboranes $[R_nOBF_2]_2$ containing one or two oxyethylene monomeric units (n = 1, 2). $[R_nOBF_2]_2$: salt molar ratio = 1.*

As seen in Figure 27, the lowest ionic conductivity is shown by the electrolyte containing LiF, for which the σ course as a function of temperature is characteristic of highly crystalline systems. As appears from DSC studies, this system bears nearly 80% of PEO crystalline phase (Table 1). Its ambient temperature conductivity is 4×10^{-8} S cm^{-1}, and above T_m the conductivity clearly increases to values of the order of 10^{-5} S cm^{-1}. A nearly an order higher conductivity is shown by the system containing LiBF$_4$. Considerably higher values were obtained for a fully amorphous system with LiN(CF$_3$SO$_2$)$_2$, in the 10^{-5}–10^{-4} S cm^{-1} range, practically the same for $[R_nOBF_2]_2$ containing 1 or 2 oxyethylene monomeric units. Surprisingly high conductivity values, comparable with electrolytes containing an imide salt were achieved for systems with LiI. The Arrhenius plot for LiCF$_3$SO$_3$ lies in the range between the plots for LiF and the best conducting LiI or imide salt.

For PEO electrolytes containing $[R_2OBF_2]_2$ and two salts: LiF and LiCF$_3$SO$_3$, electrochemical measurements were carried out (in Tel Aviv by the group of Professor Diana Golodnitsky and Professor Emanuel Peled) in a system of lithium electrodes in three cells. The cells were preheated at 55 °C for 2 hours, then cooled to RT and the data were collected on heating every 5 °C up to 110 °C in the frequency range from 1 MHz to 1 mHz. Fig. 28 shows the bulk and grain boundary conductivities and SEI resistance of PEO electrolytes containing $[R_2OBF_2]_2$ and LiF at a 1:1 molar ratio.

As can be seen, the bulk and grain boundary conductivities of the electrolyte containing LiF are between 10^{-8}–10^{-5} S cm^{-1} over the temperature range studied. Moreover, high R_{SEI} in the temperature range below 70 °C is observed; with rising temperature the resistance decreases and stabilizes at the level of $40 - 50$ Ω. These changes are illustrated by exemplary Nyquist plots at low AC frequency presented in Fig. 29 for three temperatures: 55, 70 and 90 °C.

Analogous measurements were carried out for the electrolyte containing LiCF$_3$SO$_3$. Figure 30 presents the Arrhenius plots of the Li-PEO/[R$_2$OBF$_2$]$_2$/CF$_3$SO$_3$Li - Li cells bulk conductivity data. Figure 31 presents a comparison of grain boundary and bulk conductivity. As can be noticed, σ$_{GB}$ conductivity is higher than the bulk one over the whole temperature range. The difference between σ$_{bulk}$ and σ$_{GB}$ increases at a temperature above melting of the PEO crystalline phase.
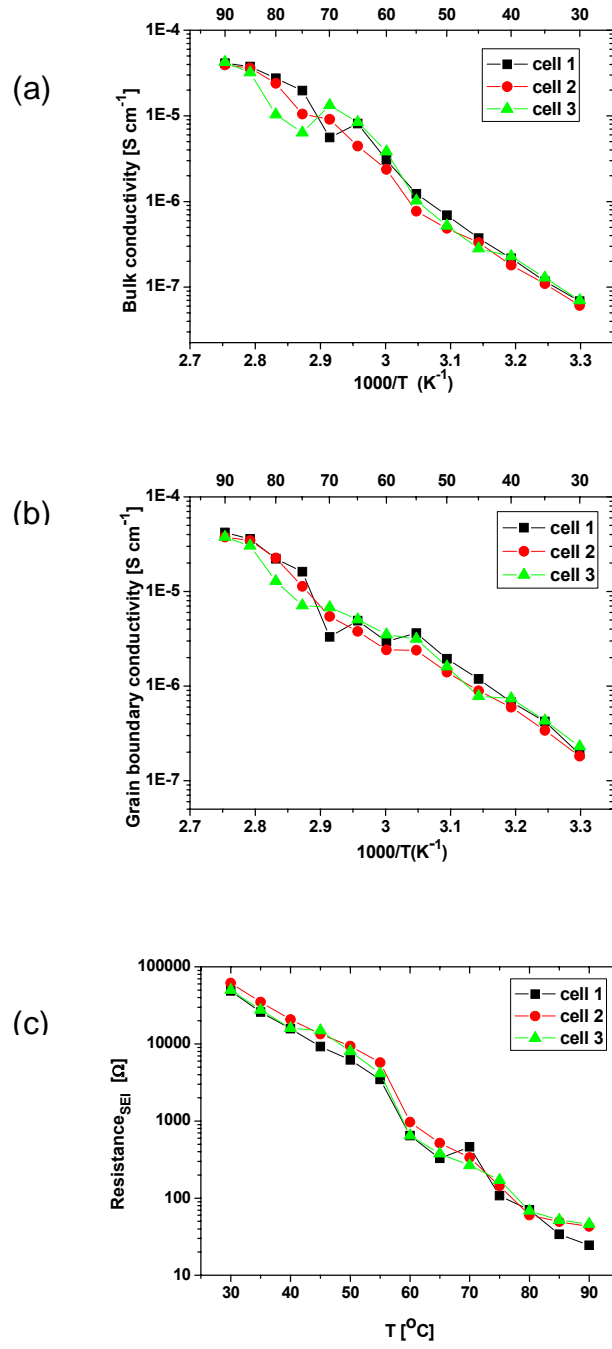
Fig. 28. *Bulk (a), grain boundary (b) conductivity and SEI resistance (c) of PEO electrolytes containing [R$_2$OBF$_2$]$_2$ and LiF at 1:1 molar ratio.*

Nyquist plot at 55ºC.
1MHz-1mHz

Nyquist plot at 70ºC
1MHz-1mHz

Nyquisy plot at 90ºC
1MHz-1mHz
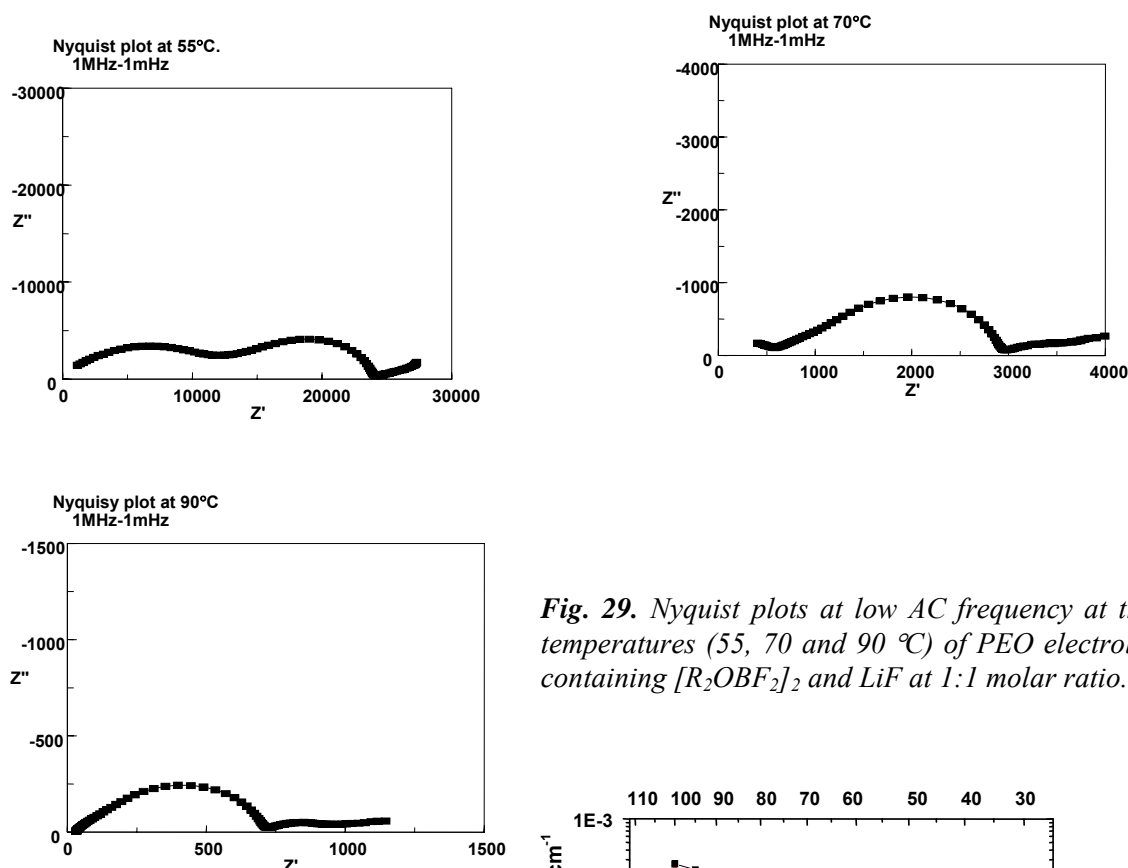
Fig. 29. *Nyquist plots at low AC frequency at three temperatures (55, 70 and 90 ℃) of PEO electrolytes containing [R₂OBF₂]₂ and LiF at 1:1 molar ratio.*
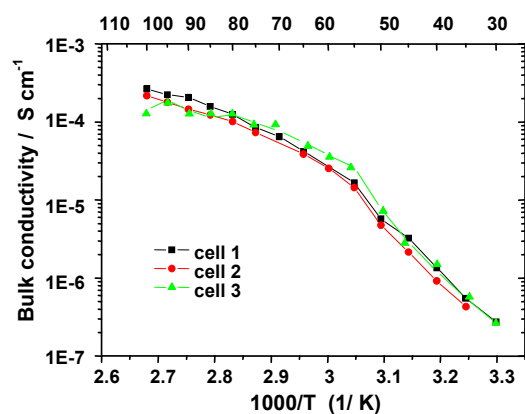
Figure 30. *Bulk conductivity of PEO electrolytes containing [R₂OBF₂]₂ and LiCF₃SO₃ at 1:1 molar ratio.*
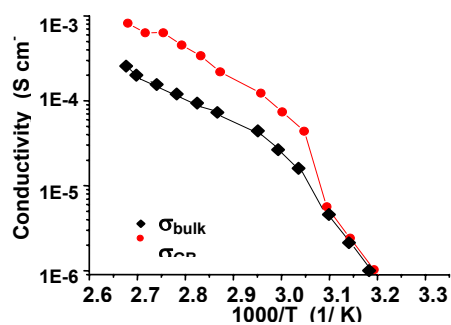
Figure 31. *Grain boundary and bulk conductivity of PEO electrolytes containing [R₂OBF₂]₂ and LiCF₃SO₃ at 1:1 molar ratio.*

The lithium ion transference number values of the polymer electrolyte containing [R₂OBF₂]₂ and LiF or LiCF₃SO₃ determined (in Tel Aviv by the group of Professor Diana

Golodnitsky and Professor Emanuel Peled) by ac-dc polarization experiments are presented in Fig. 32.
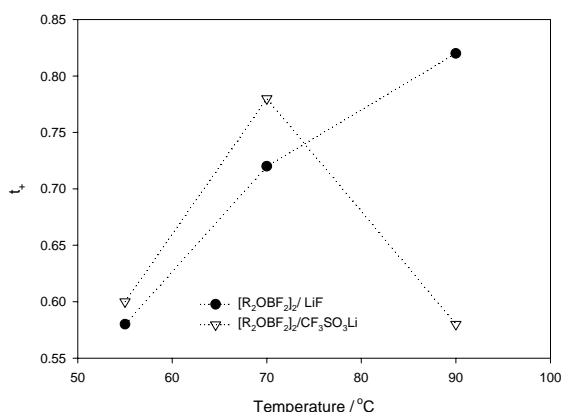
Fig. 32. *Lithium transference numbers vs temperature of polymer electrolytes comprising [R₂OBF₂]₂ and lithium salt LiF (•) and LiCF₃SO₃ (∇) at molar ratio 1:1.*

As can be noticed in the diagram, for the system with LiF with a rise of temperature a rapid increase in t_+ occurs, from the value 0.58 at 55 °C to 0.82 at 90 °C. The increase in the share of lithium cations in the electric charge transport with a rise of temperature indicates a more efficient interaction of fluoride anions with the difluoroalkoxyborane, especially above T_m of the PEO crystalline phase ($T_m = 65$ °C, Table 1). Such high t_+ values show a considerable immobilization of the salt anions, which at relatively high ionic conductivity, σ at 90 °C is 4 × 10^{-5} S cm^{-1}, indicates high mobility of lithium cations in the polymer matrix.

For the system with lithium triflate the lithium transference number varies from 0.6 to 0.78 with a maximum at 70 °C (Fig. 32). It should be mentioned that t_+ on heating and subsequent cooling from 110 °C to room temperature were found to be very similar. In the Nyquist plots (not presented in the report) the diffusion branch is almost absent at 70 °C, while it can be clearly distinguished in the plots at 55 °C and 90 °C. The impedance behavior points to the fact of a much higher t_+ value at 70 °C, than that at other temperatures. This phenomenon is difficult to explain at the present stage of studies. There is probably a complex superimposition of two effects connected with the phase changes in the electrolyte and equilibrium interaction of the salt anion with the applied Lewis acid. In general, the data presented show a considerable decrease in the anion mobility when using difluoroalkoxyborane as the additive, resulting from the Lewis base-acid type interaction.

I.3.4. Conclusions

In the reaction of BF₃ etherate with oligooxyetylene glycols we obtained a new class of boron compounds - difluoroalkoxyboranes [R$_n$OBF₂]₂, which are characterized by Lewis acid properties. These properties are weaker than that of BF₃, but clearly distinguishable in the reaction with the Lewis base used – pyridine, which was not observed for trialkoxyboranes on the basis of NMR analysis. The [R$_n$OBF₂]₂ obtained interact with lithium salts anions, and the strength of this interaction can be compared for different anions in the ^{11}B NMR spectra. It seems that small "hard" fluoride anions should complex boron easier, but probably due to the low degree of dissociation of this salt, they give smaller shifts in ^{11}B NMR than that of iodide ions. The application of [R₂OBF₂]₂ as additives for PEO based solid polymer electrolytes enables to obtain polymer electrolytes characterized by a predominant share of lithium cations in the electric charge conduction; the lithium transference number values for these systems are within the 0.6−08 range. The DSC data indicate that the introduction of [R₂OBF₂]₂ to the system in an

equimolar amount with respect to the salt does not limit the tendency to crystallization of the PEO chains. The ionic conductivity of the electrolytes obtained is, therefore, an outcome of effects connected with the strength of interaction of $[R_2OBF_2]_2$ with the salt, resulting in limiting the anion mobility, degree of salt dissociation and content of the PEO crystalline phase. In our opinion the preliminary results of studies obtained are encouraging for further work in order to optimize the conducting, charge transport, and mechanical properties of electrolytes comprising fluoroalkoxyboranes.

I.3.5. References

[1] B. Scrosati, Applications of Electroactive Polymers, Chapman and Hall, London 1993.
[2] F.M. Gray, Polymer Electrolytes, RSC Monographs, The Royal Society of Chemistry, Cambridge, U.K. 1997.
[3] Y. Ma, M. Doyle, T.F. Fuller, M.M. Doeff, L.C. De Jonghe, J. Newman, J. Electrochem. Soc. 142 (1995) 1859.
[4] F. Croce, G.B. Appetecchi, L. Persi, B. Scrosati, Nature 394 (1998) 456.
[5] F. Croce, R. Curini, A. Martinello, L. Persi, F. Ronci, B. Scrosati, R. Caminiti, J. Phys. Chem. 103 (1999) 10632.
[6] H.Y. Sun, H.J. Sohn, O. Yamamoto, Y. Takeda, N. Imanishi, J. Electrochem. Soc. 146 (1999) 1672.
[7] D. Golodnitsky, G. Ardel, E. Strauss, E. Peled, Y. Lareah, Y. Rosenberg, J. Electrochem. Soc. 144 (1997) 3484.
[8] W. Wieczorek, J.R. Stevens, Z. Florjańczyk, Solid State Ionics 85 (1996) 67.
[9] A. Błażejczyk, W. Wieczorek, R. Kovarsky, D. Golodnitsky, E. Peled, L.G. Scanlon, G.B. Appetecchi, B. Scrosati, J. Electrochem. Soc. 151 (2004) A1762.
[10] A. Błażejczyk, M. Szczupak, P. Cmoch, W. Wieczorek, R. Kovarsky, D. Golodnitsky, E. Peled, L.G. Scanlon, G.B. Appetecchi, B. Scrosati, Chem. Mater. 17 (2005) 1535.
[11] M. Kalita, M. Bukat, M. Ciosek, M. Siekierski, S.H. Chung, T. Rodriguez, S.G. Greenbaum, R. Kovarsky, D. Golodnitsky, E. Peled, D. Zane, B. Scrosati, W. Wieczorek, Electrochim. Acta 50 (2005) 3942.
[12] Z. Florjańczyk, E. Zygadło-Monikowska, W. Bzducha, Electrochim. Acta 45 (2000) 1203.
[13] Z. Florjańczyk, E. Zygadło-Monikowska, E. Rogalska-Jońska, F. Krok, J.R. Dygas, B. Misztal-Faraj, Solid State Ionics 152-153 (2002) 227.
[14] Y. Masuda, M. Seki, M. Nakayama, M. Wakihara, H. Mita, Solid State Ionics 177 (2006) 843.
[15] Y. Kato, Sh. Yokoyama, H. Ikuta, Y. Uchimoto, M. Wakihara, Electrochem. Comm. 3 (2001) 128.
[16] Y. Kato, K. Hasumi, Sh. Yokoyama, T. Yabe, H. Ikuta, Y. Uchimoto, M. Wakihara, Solid State Ionics 150 (2002) 355.
[17] Y. Kato, Sh. Yokoyama, T. Yabe, H. Ikuta, Y. Uchimoto, M. Wakihara, Electrochim. Acta 50 (2004) 281.
[18] I.R.M. Kottegoda, Zh. Bakenov, H. Ikuta, M. Wakihara, J. Electrochem. Soc. 152 (2005) A1533.
[19] (a) M.A. Mehta, T. Fujinami, T. Inoue, J. Power Sources. 81-82 (1999) 724. (b) M.A. Mehta, T. Fujinami, S. Inoue, K. Matushita, T. Inoue, Electrochim. Acta 45 (1999) 1175.
[20] X. Sun, C.A. Angell, Electrochim. Acta 46 (2001) 1467.
[21] P-Y. Pennarun, P. Jannasch, Solid State Ionics 176 (2005) 1103.
[22] H.S. Lee, X.Q. Yang, J. MacBreen, J. Electrochem. Soc. 145 (1998) 2813.
[23] H.S. Lee, X.Q. Yang, X. Sun, J. McBreen, J. Power Sources 97-98 (2001) 566.
[24] J. McBreen, H.S. Lee, X.Q. Yang, X. Sun, J. Power Sources 89 (2000) 163.
[25] M. Marcinek, G.Z. Żukowska, W. Wieczorek, Electrochim. Acta 50 (2005) 3934.
[26] P.G. Bruce, M.T. Hardgrave, C. A. Vincent, Electrochimica Acta 37 (1992) 1517.
[27] G.B. Appetecchi, G. Dautzenberg, B. Scrosati, J. Electrochem. Soc. 143 (1996) 6.

I.4. Studies on the course of the complexation reaction of the poly(2-acrylamido-2-methyl- 1-propanesulfonic acid) lithium salt (PAMPSLi) by means of BF$_3$

The present part of work is devoted to the synthesis and characterization of new polymeric matrix obtained in the reaction of boron trifluoride with polyelectrolytes containing lithium sulfonic groups. The derivatives described until now were low molecular weight compounds and as shown by X-ray studies, in some cases suitable spatial arrangement of the functional groups with respect to each other is required. In this part of the report are presented the results of studies

on the course of reaction of boron trifluoride with ionic groups immobilized *via* chemical bounding with the polymeric matrix in the form of a polyelectrolyte, such as poly(2-acrylamido-2-methyl-1-propanesulfonic acid) (PAMPSA).

I.4.1. Reaction of PAMPSLi with BF₃ etherate

The lithium salt of poly(2-acrylamido-2-methyl-1-propanesulfonic acid) (PAMPSLi) was obtained in a two-step reaction. In the first step the AMPSA monomer in the form of a sulfonic acid was reacted with n-butyllithium, and the salt formed precipitated from the solution in acetonitrile. The isolated salt was washed with acetonitrile and dried. Then, polymerization was carried out in a DMF solution in the presence of a radical initiator (benzoyl peroxide) at 70°C. The polymer precipitated in the form of a white powder.
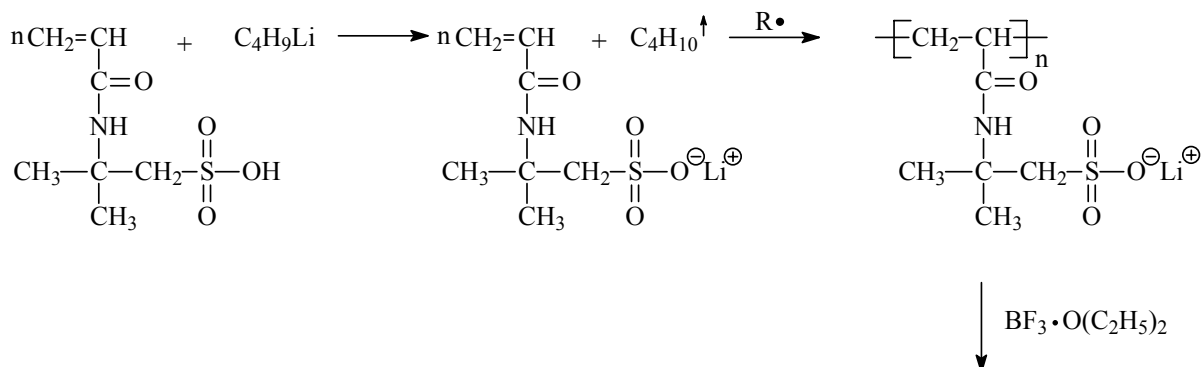
The isolated polymer, PAMPSLi was suspended in acetonitrile and then a three-fold molar excess of BF₃ etherate was dropped in. Gradual dissolution of the polymer was observed until a transparent solution was obtained. Then, the solvent and volatile reaction products were distilled off under reduced pressure.

I.4.2. Analysis of the PAMPSLi and BF₃ etherate reaction products

The isolated reaction product was treated with methylene chloride. Two fractions were obtained: a white precipitate insoluble in methylene chloride and a soluble fraction. Flame analysis of the insoluble product shows the presence of boron and lithium. Figure 33 presents the ^{11}B NMR spectrum of this product.
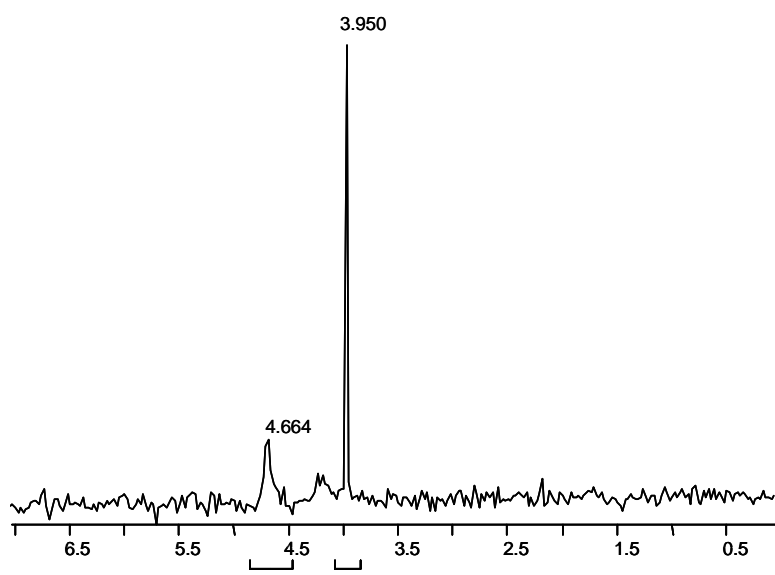
Figure 33. *^{11}B NMR spectrum of the precipitate isolated from the PAMPSLi and BF₃ reaction, fraction insoluble in methylene chloride.*
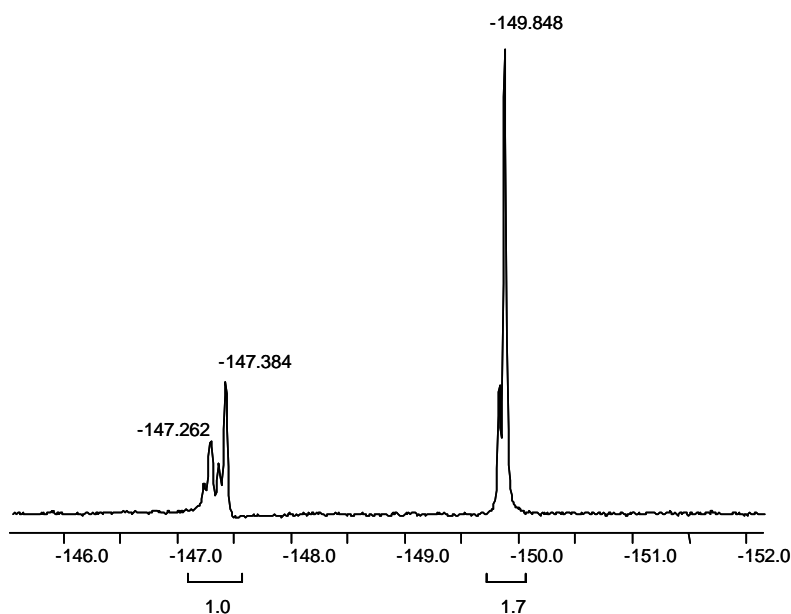
Figure 34. *^{19}F NMR spectrum of the precipitate isolated from the PAMPSLi and BF$_3$ reaction, fraction insoluble in methylene chloride.*

In the spectrum presented in Figure 33, the signal of the greatest intensity has a chemical shift of 3.95 ppm. Moreover, in the spectrum a signal of smaller intensity at 4.7 ppm is present. This is the region characteristic of four-coordinative boron.

The ^{19}F NMR spectrum of this product is presented in Figure 34. In this spectrum the basic signal occurs at a chemical shift of −149.8 ppm and a group of signals of much lower intensity is present in the −147.26 and −147.38 ppm range. The ratio of the basic signal surface to that of the less intensive signal is similar, like in the boron resonance. The presence of lithium in the sample and the spectra presented indicate that the salt LiBF$_4$ is the main component of this product. In order to confirm this interpretation, commercial LiBF$_4$ was added to the solution of the sample and ^{11}B and ^{19}F NMR spectra were recorded. The spectra are presented in Figures 35 and 36, respectively.
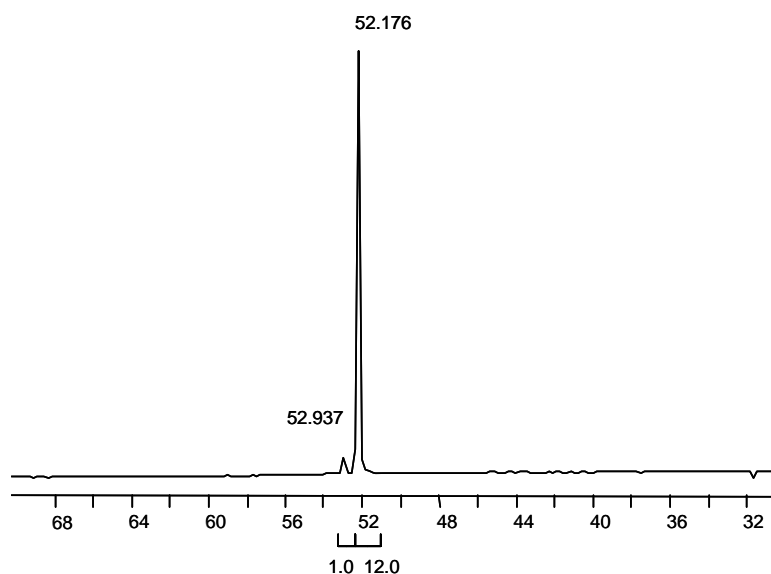
Figure 35. *^{11}B NMR spectrum of the precipitate isolated from the PAMPSLi with BF$_3$ + LiBF$_4$ reaction.*

After LiBF$_4$ addition, the intensity of the main signals undergoes an increase. In the boron resonance spectrum the scale of chemical shifts is changed, but the fluorine resonance confirms the presence of LiBF$_4$ as the main product of the fraction insoluble in methylene chloride.
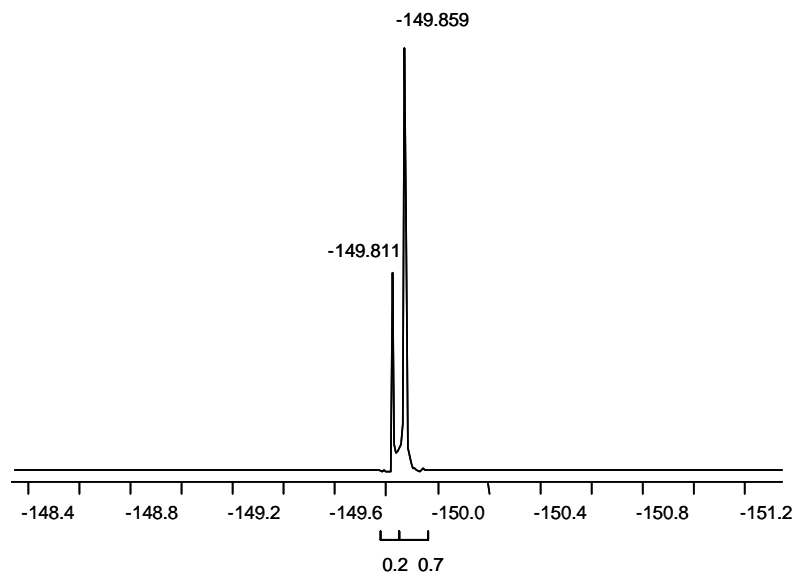
Figure 36. ^{19}*F NMR spectrum of the PAMPSLi and BF$_3$ reaction product soluble in methylene chloride.*

The second fraction, soluble in methylene chloride, does not contain lithium or boron, according to the flame test. The ^{11}B and ^{19}F NMR spectra of this fraction recorded in CDCl$_3$ are shown in spectra 37 and 38.
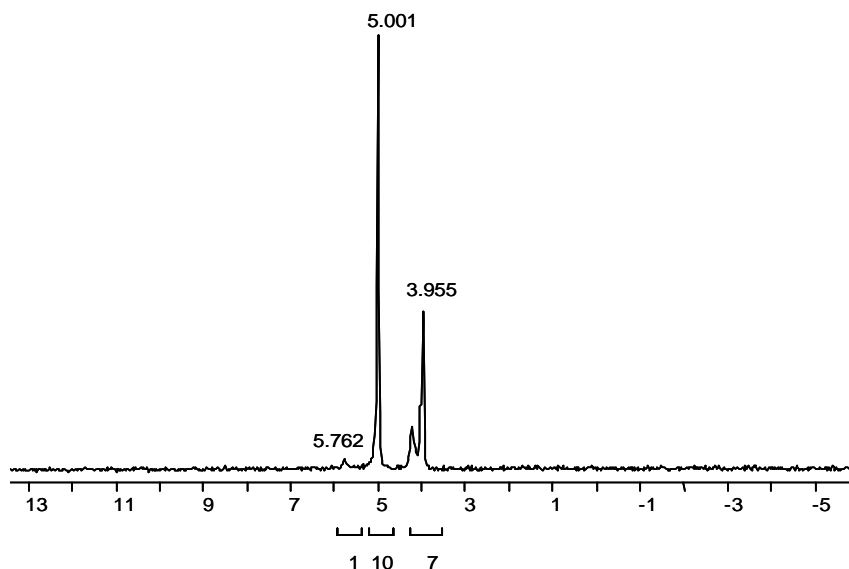
Figure 37. ^{11}*B NMR spectrum of the PAMPSLi and BF$_3$ reaction product soluble in methylene chloride.*

In the ^{11}B NMR spectrum signals are present in the range characteristic of four-coordinative boron. Since the precipitation with methylene chloride was carried out from an acetonitrile solution, the soluble fraction could contain the not completely separated salt LiBF$_4$.
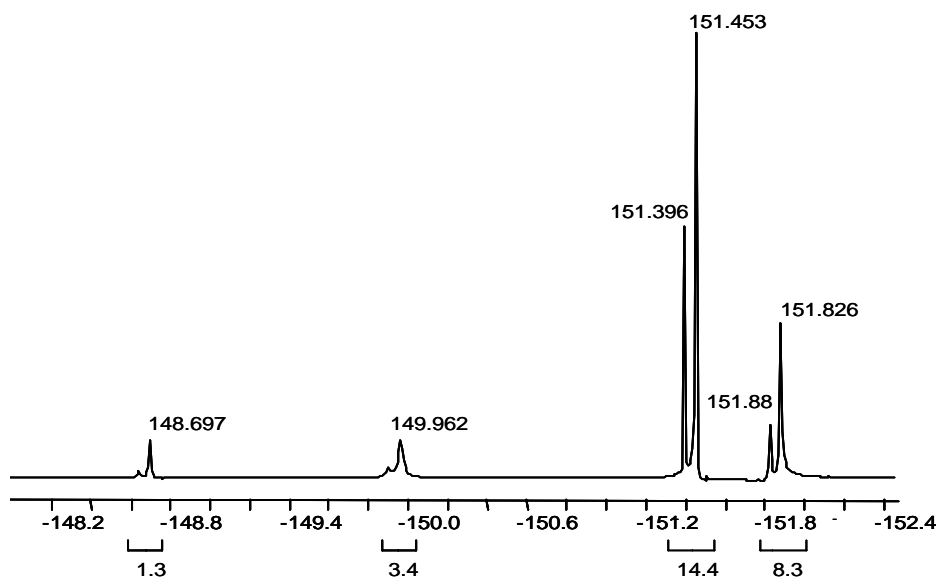
Figure 38. *^{19}F NMR spectrum of the PAMPSLi and BF$_3$ reaction product soluble in methylene chloride.*

For comparison with the signal of the BF$_4^-$ anion, LiBF$_4$ was introduced to the sample and ^{11}B and ^{19}F NMR spectra were again recorded. In the ^{11}B NMR spectrum shown in Figure 39, a clear strengthening of the signal of the chemical shift at 3.955 ppm (Figure 37) is observed, but in this case, due to different scaling, at 52.782 ppm. The signal at 5.001 ppm can be assigned to the main reaction product.
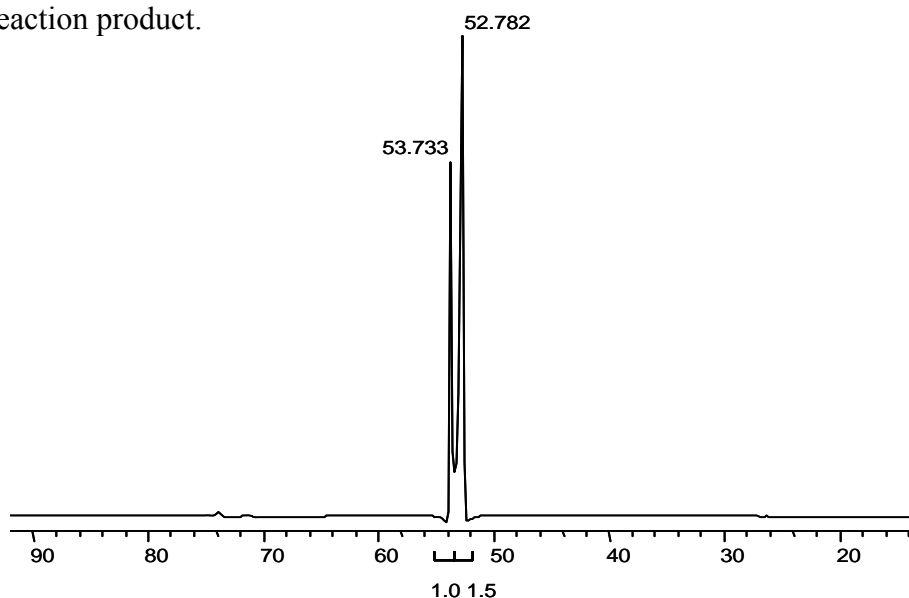
Figure 39. *^{11}B NMR spectrum of the PAMPSLi and BF$_3$ reaction product soluble in CH$_2$Cl$_2$ + LiBF$_4$.*

In the fluorine resonance (Figure 38), the main reaction product occurs at the chemical shift of ca. 151.4 ppm, which is indicated by the experiment with the addition of LiBF$_4$ (Figure 40). Two signals of much smaller intensity of chemical shifts of ca. 149 and 150 ppm are also visible in the spectrum.
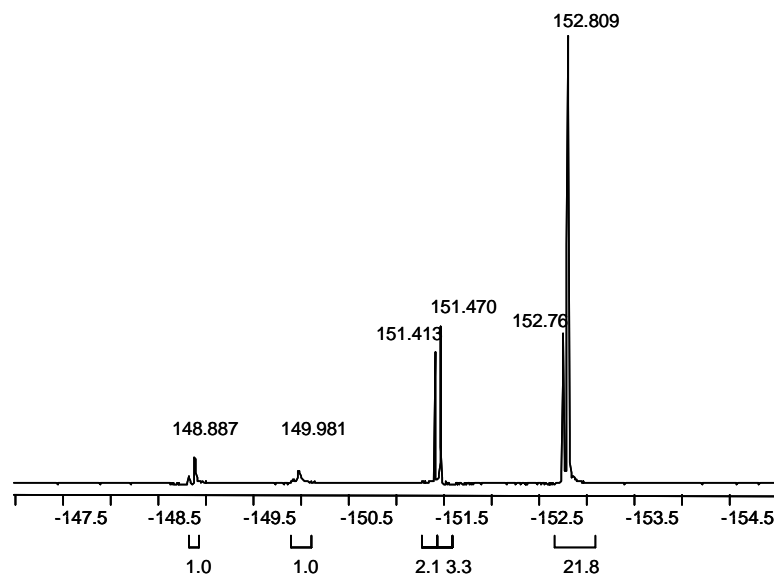
Figure 40. *^{19}F NMR spectrum of the PAMPSLi and BF$_3$ reaction product soluble in CH$_2$Cl$_2$ + LiBF$_4$.*

In Figures 41 and 42 are presented IR spectra of PAMPSLi and the reaction product with BF$_3$ soluble in methylene chloride.
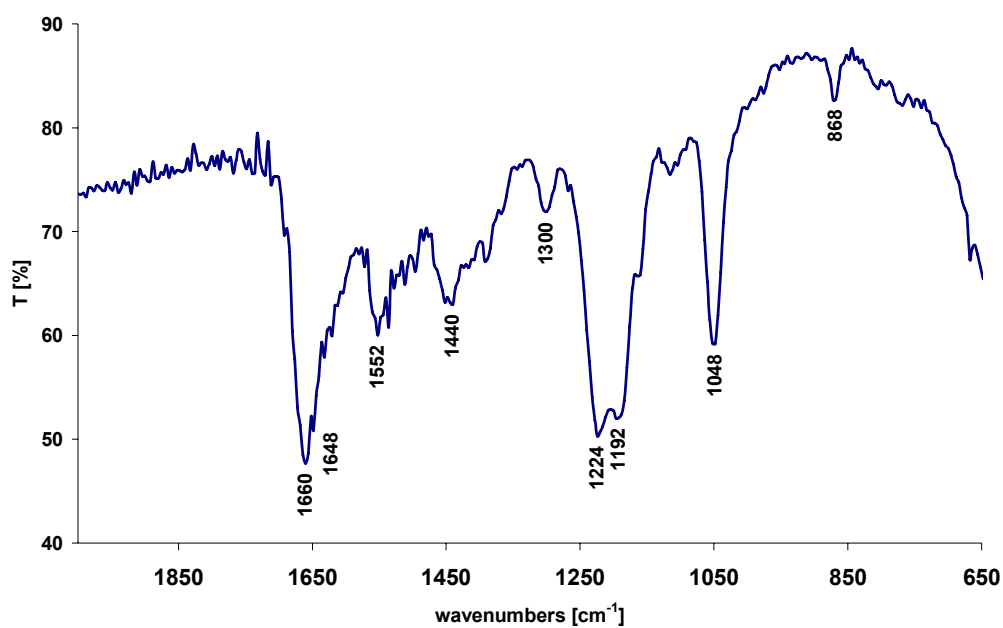
Figure 41. *IR spectrum of PAMPSLi measured in nujol.*
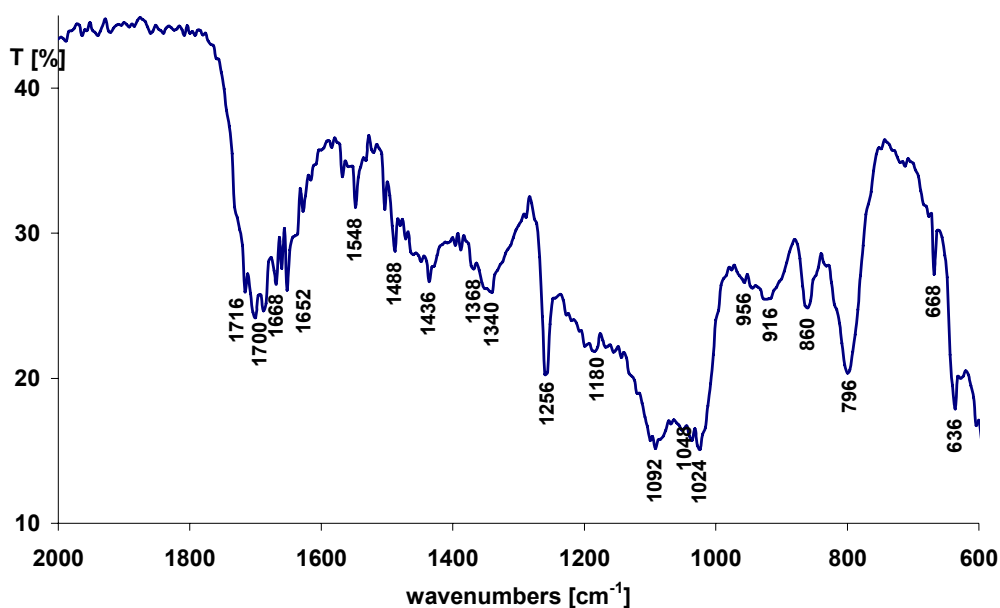
Figure 42. IR spectrum of the PAMPSLi and BF$_3$ reaction product soluble in methylene chloride measured in the form of a thin film.

In the spectrum of the initial PAMPSLi salt, bands characteristic of amides: $\nu_{C=O}$ 1660 cm^{-1} (amide band I), δ_{N-H} 1552 cm^{-1} (amide band II), ν_{C-N} 1300 cm^{-1} (amide band III) and derived from vibrations of sulfonic groups $\nu_{S=O}$ 1048 cm^{-1} are present.

In the spectrum of the reaction with the BF$_3$ product, new bands appear, characteristic of B−F bonds of frequency 1024 and 1092 cm^{-1}, and some bands present for the initial salt are shifted, first of all the $\nu_{C=O}$ band. As can be noticed, in the PAMPSLi salt a signal occurring at ca. 1660 cm^{-1} corresponds to the C=O amide bond, whereas in the product this band undergoes broadening and shifts towards higher frequencies with a maximum at ca. 1700 cm^{-1}.

An analysis of the PAMPSLi and BF$_3$ etherate reaction products shows that the reaction probably starts from the addition of BF$_3$ to the salt anion, and then subsequent reactions take place in the presence of BF$_3$ etherate, leading to the isolation of the LiBF$_4$ salt and formation in the polymer of boron and fluorine containing groups.
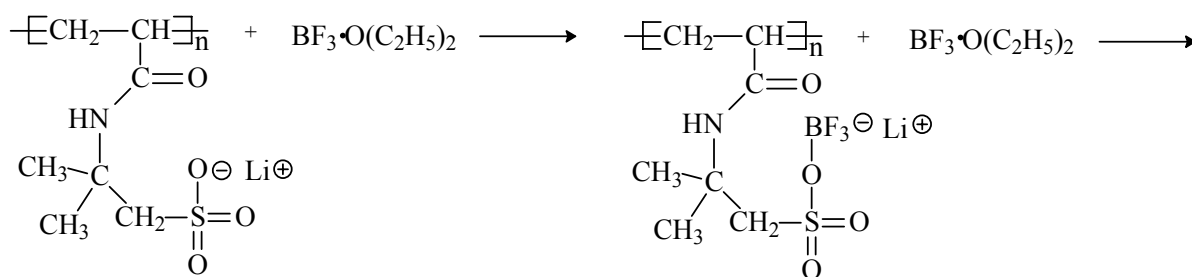
At the present stage of studies, it is difficult to explain the course of the subsequent reactions. Since after the reaction the polymer remains soluble, it can be assumed that the reaction does not proceed between the groups present in different chains. Within one monomeric unit, after BF$_3$ addition a cyclic structure can be formed; in the case when the free electron pair is derived from the carbonyl group oxygen an eight-membered ring can be formed, and when nitrogen is the electron donor, a six-membered ring is formed. The reaction course leading to the formation of a six-membered structure could explain the shift in the IR spectrum of the amide carbonyl group

band towards higher frequencies. In both cases boron is four coordinative. The presence in the fluorine spectrum of signals of smaller intensity (Figures 38 and 40) at ca. 149 and 150 ppm, besides the basic signal, may indicate the occurrence of side reactions. These are probably reactions with moisture leading to the substitution of fluorine atoms with hydroxyl groups.

$$\left[CH_2-CH\right]_n \qquad\qquad \left[CH_2-CH\right]_n$$
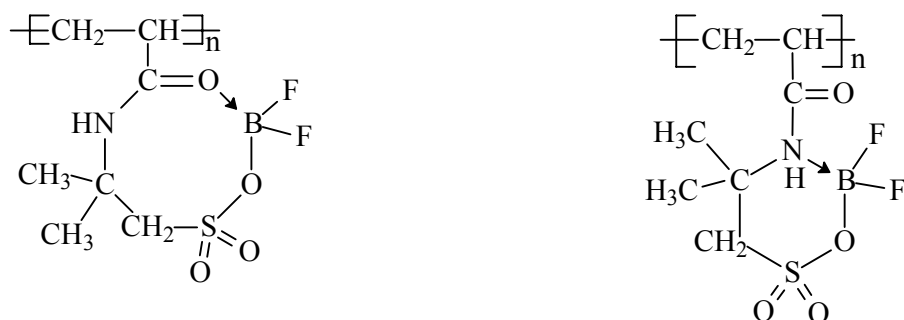
The reaction between the groups present in various monomeric units within one chain cannot be excluded. One of the structures can be formed by the groups occurring in neighboring monomeric units:

$$\left[CH_2-CH\right]_n \;+\; BF_3{\cdot}O(C_2H_5)_2 \;\longrightarrow\; -CH_2-CH-CH_2-CH- \;+\; LiBF_4$$
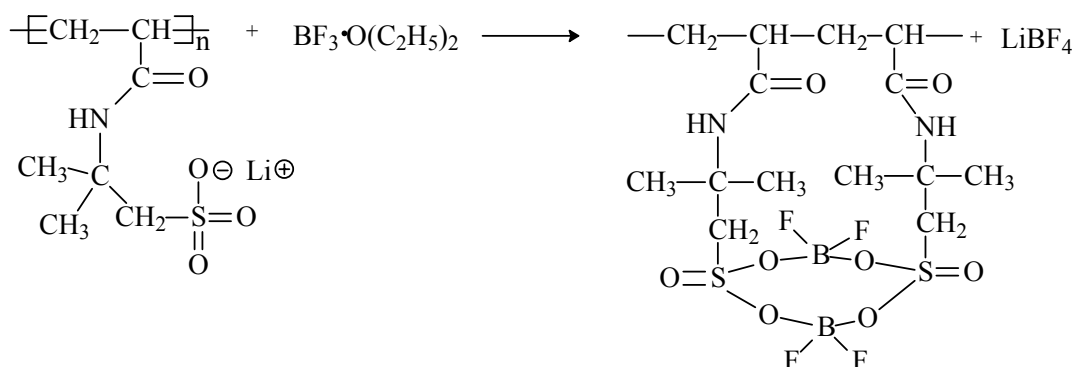
The reaction with traces of moisture may lead to the formation of an oxygen bridge stabilizing the structure by the formation of two six-membered rings:
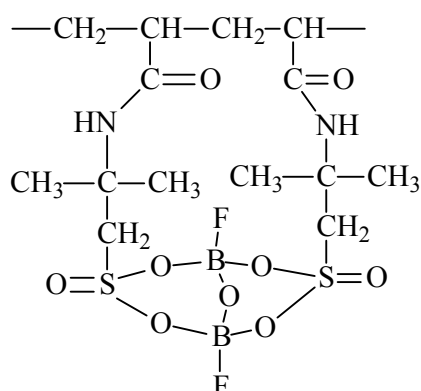
It seems, however, that such a reaction course is less probable due to thermodynamic reasons.

The course of reactions leading to the formation of ionic groups can also be excluded with great probability due to not detecting lithium in the polymeric fraction.
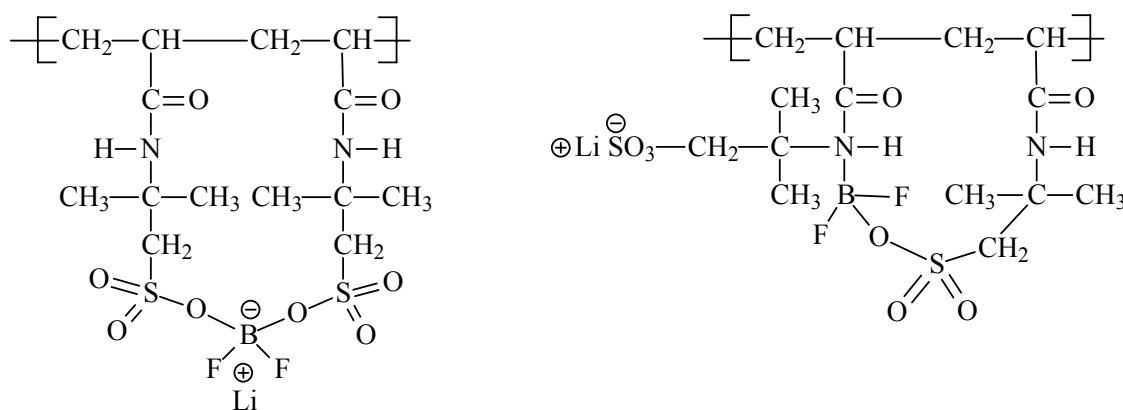
The results presented show that in the reaction of PAMPSLi and BF$_3$ the salt is isolated in the form of LiBF$_4$ and an electrically neutral polymer chain is formed, in which the substituents contain boron atoms bonded with sulfonic groups and fluorine atoms.

I.4.3. Synthesis of a polymer electrolyte involving a new polymer matrix – product of the PAMPSLi and BF$_3$ reaction

Preliminary evaluation of the polymer obtained in the reaction of PAMPSLi and BF$_3$, carried out at an equimolar ratio of reagents, to conduct an electrical charge was carried out. This means that half of the sulfonic groups remain in the form of a lithium salt and half reacted with LiBF$_4$ isolation. Since the polymer does not form membranes of suitable mechanical properties, poly(butyl acrylate), a polymer of low glass transition temperature ($T_g = -55$ °C), was added to the system in the amount of 33 wt. %. The electrolyte was obtained by dissolving poly(butyl acrylate) in chloroform and mixing with a solution of the product of PAMPSLi and BF$_3$ reaction in acetonitrile, followed by evaporation of the solvents under dynamic vacuum. A considerably flexible, but non-transparent membrane was obtained. A change of ionic conductivity as a function of temperature of the thus obtained electrolyte is presented in Figure 43.
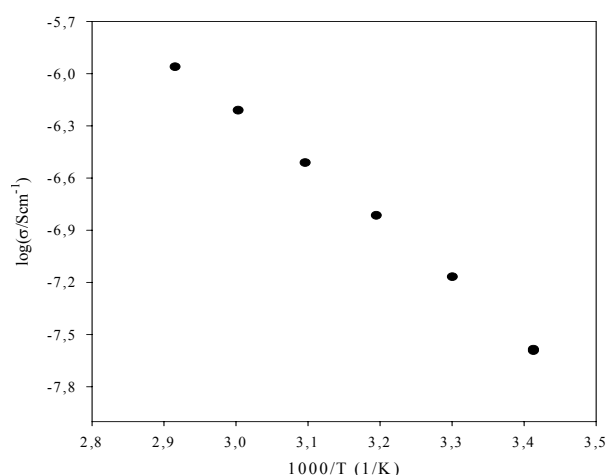
Figure 43. *Conductivity of the electrolyte containing the PAMPSLi and BF$_3$ reaction product and 33 wt. % of poly(butyl acrylate).*

The system obtained shows low ambient temperature ionic conductivity, of the order of 10^{-8} S·cm^{-1}; the conductivity increases with a rise of temperature and reaches a value of the order of 10^{-6} S·cm^{-1} at 70 °C. The preliminary evaluation carried out permits only to state that with respect to the pure PAMPSLi polyelectrolyte, the system modified with BF$_3$ shows much higher ionic conductivity, which probably results from the presence of the LiBF$_4$ salt in the system. The

ions mobility in this system may result from the high polarity of the modified polymer matrix, which facilitates the dissociation of the isolated $LiBF_4$. In order to establish the properties of the polymer formed from PAMPSLi and BF_3, further studies are necessary. First of all the determination of the lithium cation transference number may be helpful in answering the question whether the new polymer matrix possesses the ability to complex the salt anions, and thus affecting the degree of dissociation of lithium salts and lithium cations mobility.

II. COMPOSITE ELECTROLYTES WITH SUPRAMOLECULAR ANION RECEPTORS

II.1.Introduction

In the previous stages of the grant realization the use of calix[4] arene derivatives with various types of active groups in a lover rim was shown to be a very effective way to complex iodide and triflate anions and thus giving lithium transport numbers close to unity. However, this effect was observed for relatively large fractions of the added calix[4]arene, which as a matter of fact affect the ionic conductivity of the studied electrolytes, most probably due to the steric hindrance of the bulky receptor.

To further extend our studies on the use of anionic receptors as well as to overcome some of these limitations, we present a different approach involving calix[6]pyrrole as an anion trapping group. Calix[n]pyrroles have been identified in various reports as being effective in the coordination of different anions.

The ionic conductivity as a function of the fraction of added calix[6]pyrrole, type and concentration of the dopant lithium salt was studied by impedance spectroscopy. Lithium transference numbers were investigated by means of the ac-dc technique in collaboration with the Rome and Tel-Aviv groups.

These studies have been supported by an extensive PFG NMR examination of some of composite systems containing calix[6]pyrrole performed in collaboration with the group of Professor Steve Greenbaum from Hunter College CUNY. The effectiveness of calixpyrrole as an anion trapping agent has been investigated, using NMR techniques. We report multi-nuclear (^{1}H, ^{7}Li, ^{19}F) NMR self-diffusion coefficient measurements in PEO-LiBF$_4$ complexes with and without calixpyrrole at a temperature above the PEO melt temperature. All diffusing species, cation (^{7}Li), anion (^{19}F), and polymer or trapping agent (^{1}H) were measured separately.

We have also decided to continue investigations of an anion trapping agent based on calix[4]arenes characterized with better compatibility (solubility) with the PEO-based matrix than previously synthesized 5,11,17,23-tetra-p-*tert*-butyl-25,27-bis(N-p-nitrophenylureidobutoxy)-26,28-dipropoxycalix[4]arene (Cx2).

In the case of Cx2, modifications in both rims can be applied. However, the modification in the narrow rim can influence the receptor coordination properties negatively. Taking this into account, we focused on the synthesis of a Cx2-like receptor modified with poly(ethylene oxide) chains in the wide rim. The new receptor (Cxg) proposed by us, contains identically located anion coordinating groups as Cx2, but with the wide rim modified with two oligo(ethylene oxide) chains chemically linked to the receptor molecule. This type of changes in the structure of the receptor should improve the properties of the anion receptor-containing composite by the improvement of the matrix- receptor compatibility without any influence on the anion trapping properties of the receptor.

Finally, for the supramolecular receptor giving the most promising effect on properties of polyether electrolytes, the up-scaling of the synthesized amount of the compound has been performed.

II.2. Experimental

II.2.1 Samples preparation

All preparative operations were performed in an argon glove-box with humidity level under 3 ppm. The samples were either closed hermetically in appropriate vessels or left inside with the measurement devices connected into the glove-box.

ACN, CH_2Cl_2 (POCh, for DNA synthesis, water below 50 ppm) and PC (Fluka, puriss, anhydrous, ≥99.0%), were used as is. All salts were dried over 72 hours at temperatures up to 100°C under high vacuum (diffusion pump). For gel fabrication a PVdF-HFP copolymer (courtesy Atofina Poland) was used.

The preparation of the solid electrolyte samples was conducted as follows. The electrolyte was obtained by casting of the mixture of the two separately prepared solutions: salt and PEO in CH_3CN and Cx2 (or Cxg, or C6P) in CH_2Cl_2 and dried using procedure described in [1]. All samples were prepared maintaining ether oxygen to lithium cation molar ratio equal to 20:1. For the Cxg containing ones the oligooxyethylene chains present in the receptor were counted into the total number of the ether oxygens present in the sample. The salt to receptor ratio was always equal to 3:1.

Two methods have been applied to synthesize the gel electrolytes: one-step (casting of the polymer material together with the electrolyte solution) and two-step (preparation of PVdF matrix and soaking-in the electrolyte), giving similar results of ionic conductivity and mechanical strength. The C6P additive did not solve completely in the polymer-solvents solution and in pure polar solvents used in typical organic electrolytes (like PC or ACN). Our gels contained a suspension of C6P in polymer matrix and in the liquid phase.

II.2.2 CV measurements

The electrochemical stability of the electrolytes was studied by means of CV technique. Three electrode cells with Pt working, Ta counter and quasi-reference electrodes have been filled either with liquid solutions or with PVdF gel prepared as soft gel in order to establish good electrical contact. Experiments were performed on PAR 273 (EG&G)– 1255 FRA (Schlumberger) set and the results analyzed with Power Suite (EG&G) software. Symmetric Li/gel electrolyte/Li cells have been assembled for long-time impedance measurements. The ionic conductivity has been measured by means of standard AC impedance technique in cells with stainless steel or titanium blocking electrodes.

II.2.3. Conductivity measurements

The ionic conductivity was determined by means of impedance spectroscopy. The electrolytes were pressed between stainless-steel blocking electrodes. An Atlas 98HI Frequency Response Analyzer was used in 1Hz-100 kHz frequency range. The cell was immersed in a HAAKE DC 50 cryostat to control the measurement temperature in the 293 – 338 K range. The Bernard Boukamp EQ software [2] was used to analyze the obtained impedance data. The thermal dependency of conductivity for all the studied samples was described by the Arrhenius type equation: $\sigma = \sigma_0 \exp(-E_a/RT)$.

II.2.4 NMR spectra

^{1}H and ^{19}F NMR spectra were recorded on a computer-interfaced Varian Gemini 200 NMR spectrometer at 200 MHz and 188 MHz, respectively. All measurements were performed at 25°C. The spectra were analyzed using Mestrec 2.3 software. Procedure of the complex formation constant estimation was presented in [3]. In general, NMR titration is here used where

[1] A. Błażejczyk, W. Wieczorek, M. Kalita, D. Golodnitsky, E. Peled, R. Kovarsky, B. Scrosati, G. Appetecchi, L. Scanlon, "Novel Solid Polymer Electrolytes with Single-Lithium-Ion Transport" US Disclosure and Record of Invention No. OMB 900-0095.

[2] B. A. Boukamp, Solid State Ionics 10 (1986) 31

[3] A. Plewa, M. Kalita, G. Z. Żukowska, A. Sołgała and M. Siekierski, ECS Transactions, 3/12 (2006) 59.

the chemical shift δ is plotted as a function of the guest (e.g. anion) − host (supramolecular receptor) concentration ratio. The observed changes are related to the complexation process. Equilibrium constant value can be found on the basis of non linear least square fit of the obtained data.

II.2.5 SEM images

SEM images were taken using a FEI Quanta 200 microscope with an EDAX EDS analyzer. To preserve the properties and crystalline structure of the tested membranes all operations of the sample preparation were performed in a dry-box and the beam current was minimized to avoid the thermal effect of the beam (sample melting). The low vacuum mode was used for both image gathering and the EDS analysis.

II.2.6 FTIR spectroscopy

Infrared absorption spectra were recorded on a computer interfaced Perkin-Elmer 2000 FT-IR system with a wavenumber resolution of 1 cm^{-1}. The spectra were performed for samples dispersed in KBr pellets or as films using HATR accessory with ZnSe crystal. For KBr pellets, spectra were recorded at 25°C, and for films at 50°C. FTIR spectra were analyzed using a Galactic Grams Research software package using a Gaussian–Lorentzian function [4,5].

II.2.7 Raman spectroscopy

Raman spectra were collected using a Nicolet Almega Raman dispersive spectrometer, equipped with a confocal Raman microscope, a 1800 lines mm^{-1} holographic grating and a CCD camera. A diode laser operating at 780 nm was used as the excitation source and spectral resolution was about $2 cm^{-1}$ for high resolution spectra. In order to avoid contact with air during the measurements, the samples were kept in sealed glass containers. All spectra were recorded at 25°C. For mapping experiments, spectra were recorded using 360 lines mm^{-1} holographic grating and resolution was about 10 cm^{-1}. The exposure time was typically 15 - 20 s for mapping experiments and 60 - 120 s for high resolution spectra.

II.2.8 XRD studies

X-ray powder diffraction patterns were recorded on a Seifert HZG-4 automated diffractometer using Cu Kα radiation (λ=1.5418 Å). The data were collected in the Bragg-Brentano ($\theta/2\theta$) horizontal geometry (flat reflection mode) between 5 and 60° (2θ) in 0.04° steps, at 3 s $step^{-1}$. The optics of the HZG-4 diffractometer was a system of primary Soller slits between the X-ray tube and the fixed aperture slit of 2.0 mm. One scattered-radiation slit of 2 mm was placed after the sample, followed by the detector slit of 0.35 mm. All samples were placed on a glass support and kept sealed during the experiment with a self adhesive tape. The collected data were baseline corrected. The signal intensity was normalized taking into consideration different sample thickness and sweeping velocity.

II.2.9 DSC

DSC data were collected using a Perkin Elmer Pyris 1 DSC at the heating rate of 20°C min^{-1} in $-120\ldots250$°C temperature range. The degree of crystallinity measured by means of DSC was calculated according to the equation $X_c = Q_m Q_{m,PEO}^{-1}$, where Q_m is a latent melting heat for the polyether used and $Q_{m,PEO}$ is latent melting heat found for the crystalline P(EO) phase. According to the literature, Q_{mPEO}=213.7 J g^{-1} [6,7].

[4] C. P. Rhodes, R. Krech, Solid State Ionics 136-137 (2000) 1131.
[5] J. M. Alie, H. G. M. Edwards, Vibrational Spectroscopy 24 (2000) 185.
[6] J. Przyłuski, W. Wieczorek, J. Thermal Analysis 38 (1992) 2229.
[7] X. Li, S. L. Hsu, J. Polym. Sci., Polym. Phys. Ed. 22 (1984) 1331.

II.3. Results and discussion

II.3.1 Synthesis of 1,1,3,3,5,5-meso-hexaphenyl-2,2,4,4,6,6-meso-hexamethyl-calix[6]pyrrole (C6P)

Synthesis in a ¼-technical (semi pilot plant) scale

The main aim to conduct the reaction in a ¼-technical scale was to obtain a sufficient quantity of (1,1,3,3,5,5-*meso*-hexaphenyl-2,2,4,4,6,6-*meso*-hexamethyl-calix[6]pyrrole, C6P) needed for electrochemical investigations (ca. 250 g).

Another aim of this work was the investigation of

- synthesis repeatability
- effect of trifluroacetic acid (CF_3COOH, TFA) quantity on the synthesis - due to the relatively high cost of this reagent,
- effect of the starting material (diphenyldi(2-pyrrole)methane) purity on total yield of calix[6]pyrrole - since during the diphenyldi(2-pyrrole)methane purification, ca. 20% of the starting material is lost.

II.3.1.1 C6P synthesis procedure

C6P was synthesized from diphenyldi(2-pyrrole)methane (synthesis proposed by Eichen *et al.* [8], improved [1] and adapted to a ¼-technical (semi-pilot plant) scale by us as follows:

400 g of di (phenyl)di(pyrrol-2-yl)methane (synthesized by us) and 400 g of trifluoroacetic acid (Fluka) were dissolved in a mixture of 32 kg of 99.5% acetone (Brenntag) and 32 kg of 99.8% ethanol (WIRASET). The reaction mixture was stirred for 5 days at room temperature under argon. Then, the reaction mixture was cooled down to −5°C. After 12 hours the precipitate was filtered off and washed with 1000 ml of cold ethanol, and then dried, yielding 90 g of 1,1,3,3,5,5-meso-hexaphenyl-2,2,4,4,6,6-meso-hexamethylcalix[6]pyrrole.

NMR and MS spectra confirmed obtaining of the correct product.

Before application as an additive, the anion receptor was dried for over 200 hours under high vacuum (diffusion pump) at 80ºC.

II.3.1.2 Results

In the first two runs, we estimated the synthesis repeatability. In both cases, we obtained ca. 90 g of C6P crystallized from the reaction mixture.

In the next synthesis, we tried to conduct the reaction with a smaller (80% of referred) amount of TFA. In this synthesis we obtained about 50 g of C6P. A smaller quantity of TFA afforded a ca. 50% lower yield than that referred. In consequence, from the technological and economical point of view, it is necessary to control the quantity of TFA as the most important factor of high yield in C6P synthesis.

In the last run we conducted the synthesis with diphenyldi(2-pyril)methane with a higher amount of impurities. In this case, we obtained ca. 65 g of the product with a higher amount of impurities. So, also using a non- purified substrate is economically unreasonable.

II.3.2 Synthesis of the receptors being calixarene derivatives

The synthesis and preparation of 5,11,17,23-tetra-p-tert-butyl-25,27-bis(((N-p-nitrophenylureido)butyl) oxy)-26,28-dipropoxycalix[4]arene (Cx2) was conducted as described in [9]. The synthetic route leading to Cxg is depicted in Figures 1 and 2. Calixarenes: C1, 5,11,17,23-tetra-*t*-butyl-25,26,27,28-tetrahydroxy-calix[4]arene, [10,11,12,13], C2, 25,26,27,28-

[8] B. Turner, A. Shterenberg, M. Kapon, K. Suwińska, Y. Eichen, Chem.Commun. 2001, 13-14.

[9] A. Błażejczyk, M. Szczupak, W. Wieczorek, P. Ćmoch, G. B. Appetecchi, B. Scrosati, R. Kovarsky, D. Golodnitsky, E. Peled, Chem. Mat 17 (2005) 1535.

[10] C. D. Gutsche, M. Iqbal, Org. Synth., 68 (1990) 234.

[11] C. D. Gutsche, M. Leonis, D. Steward, Org. Synth., 68 (1990) 238

[12] C. D. Gutsche, J. A. Levine, J. Am. Chem. Soc., 104 (1982) 2652.

tetrahydroxycalix[4]arene, [14], C3, 25,27-dipropoxy-26,28-dihydroxycalix[4]arene, [15], C4, 25,27-dipropoxy-26,28-diallyloxy-calix[4]arene, [15], C5, 5,17-diallyl-25,27-dipropoxy-26,28-dihydroxycalix[4]arene, [16,17] were synthesized according to the literature procedures.
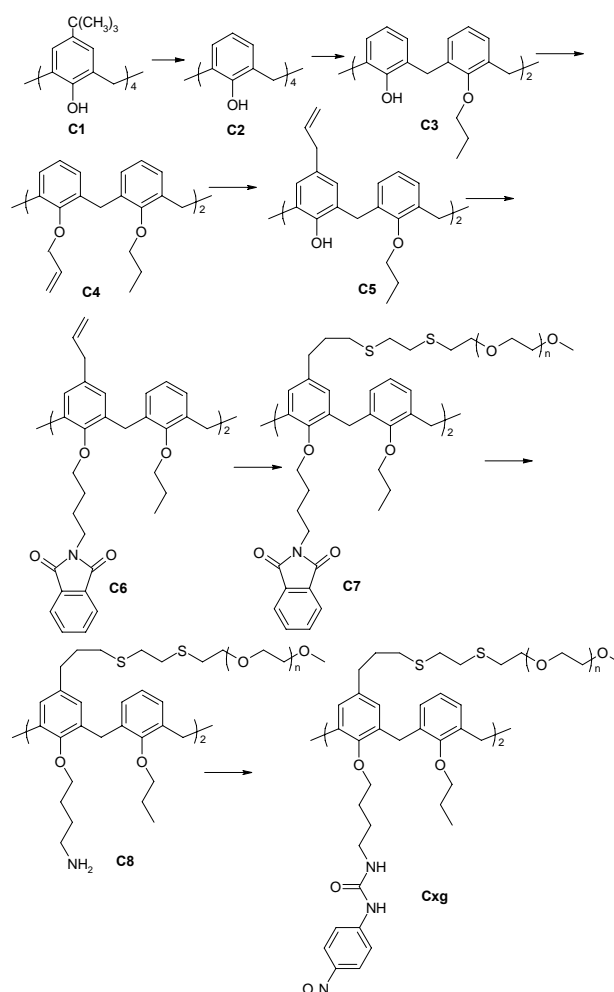
Figure II.1. Cxg synthetic scheme- part 1 – main synthetic route.
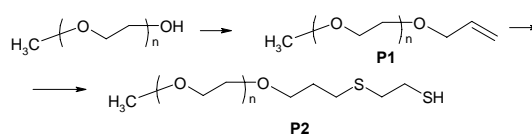
Figure II.2. Cxg synthetic scheme- part 2 –intermediate oligooxyethylene compounds.

The spectral characteristics of the obtained compounds and their melting points match well with the literature data. The next synthetic steps of the calix[4]arene derivatives C6-C9 (see Figure II.1) and the intermediate oligo(ethylene oxide) compounds P1-P2 (see Figure II.2) were originally developed by our group and are described below. All the operations (except of C8 synthesis) were conducted in the atmosphere of nitrogen. The C8 step was realized in open air conditions as one of the reagents (hydrazine hydrate) contains water. All the solvents (benzene,

[13] J. H. Munch, C. D. Gutsche, Org. Synth., 68 (1990) 243.

[14] C. D. Gutsche, L.-G. Lin, Tetrahedron, 42 (1986) 1633.

[15] A. Casnati, A. Pochini, R. Ungaro, F. Ugozzoli, F. Arnaud, S. Fanni, M.-J. Schwing, R. J. M. Egberink, F. de Jong, D. N. Reinhoudt, J. Am. Chem. Soc., 117 (1995) 2767.

[16] G. Arena, A. Casnati, A. Contino, L. Mirone, D. Sciotto, R. Ungaro, Chem. Commun., 1996, 2277.

[17] C. D. Gutsche, J. A. Levine, P. K. Sujeeth, J. Org. Chem. 50 (1985) 5802.

toluene, dimethylformamide (DMF), tetrahydrofurane (THF), ethyl acetate, dichloromethane, hexane fraction from petroleum, all pure), NaOH and MgSO4 (both pure) were supplied by POCH. DMF and THF were dried prior to use. Hydrazine hydrate (reagent grade), N-(4-bromobutyl)phthalimide, 1,2-ethanedithiol (both purum), 1-hydroxycyclohexyl-phenyl ketone (Irgacure 184, 99%), poly(ethylene glycol) methyl ether (MW=350), allyl chloride (99%), 4-nitrophenyl isocyanate (98%) and NaH (95%) were supplied by Aldrich. For UV-induced reactions, a medium-pressure mercury lamp PLK Type 5 (80 W) characterized with the following wavelength ranges: 100-280 nm (maximum 10% absorption), 280-315 nm (minimum 30% absorption), and 315-380 nm (minimum 50% absorption) was used.

II.3.2.1 Synthesis of 5,11-diallyl-25,27-bis[(N-4-phthalimidobutoxy]-26,28-dipropoxy-calix[4]arene (C6)

The solution of 2.4 g (4 mmol) of C5 in 60 cm^3 of the DMF-THF (1:4) mixture and 0.6 g (25 mmol) of NaH was stirred for 1 h at room temperature. After that, 5.8 g (21 mmol) of N-(4-bromobutyl)phthalimide was added. Then, the reaction was carried out for another 24 h at 70°C. The reaction progress was controlled by thin layer chromatography (TLC) (eluent: ethyl acetate/hexane 1:3). After the completion of the reaction 40 cm^3 of water was added and the product was extracted with CH$_2$Cl$_2$. The solution was dried with MgSO$_4$ and evaporated to dryness. The residue was purified using column chromatography (ethyl acetate-hexane 1:3). After removal of the solvents, 2.1 g of C6 were obtained (53%). ^{1}H NMR (400 MHz, CDCl3), δ(ppm): 7.78-7.76 (m, 4H, ArH-Pht), 7.69-7.67(m, 4H, ArH-Pht), 6.56 (s, 4H, ArH), 6.45 (m, 6H, ArH), 5.89-5.83 (m, 2H, CH=CH2), 5,00-4.95 (m, 4H, =CH2), 4.39 (d, 4H, ArCH2Ar, ax, J=13.2 Hz), 3.94 (t, 4H, CH2N, J=7.6Hz), 3.79-3.72 (tt, 4H, OCH2, J=7.6 Hz), 3.12 (m, 4H, ArCH2CH), 3.11 (d, 4H, ArCH2Ar, eq, J=13.2 Hz) 1.98-1.94 (m, 4H, OCH2CH2N), 1.92-1.86 (m, 4H, OCH2CH2CH2), 1.82-1.71 (m, 4H, CH2CH3), 0.98 (t, 6H, CH3, J=7.6 Hz).

II.3.2.2 Synthesis of poly(ethylene glycol) allylmethyl ether (P1)

The solution of 16 g (0.4 mol) of NaOH in a mixture of 40 ml of benzene and 28 g (80 mmol) of poly(ethylene glycol) methyl ether (MW=350) was heated up to 60°C. Then, to this solution 19.5 ml (0.24 mol) of allyl chloride was added dropwise during 1.5 h. The mixture was stirred for 20 minutes at the same temperature. This was followed by the addition of 7g (0.175 mol) of NaOH and 10 ml of benzene. Then, 13 ml (16 mol) of allyl chloride was added dropwise within 0.5 h. After this, the reaction was conducted for another 2 hours at 60°C. The reaction mixture was cooled down to room temperature, filtered, washed with 5% hydrochloric acid and dried over anhydrous MgSO$_4$. Benzene and volatile impurities were distilled off under vacuum yielding 30 g of poly(ethylene glycol) allylmethylether (MW = 390) (93%).

II.3.2.3 Synthesis of P2

1 g (1.7 mmol) of P1 and 0.324 g (3.45 mmol, 0.288 cm^3) of 1,2-ethanedithiol were dissolved in 5 cm^3 of ethyl acetate. Then 0.04 g (0.196 mmol) of photoinitiator Irgacure 184 was added. Then, the reaction mixture was UV irradiated for 20 minutes. After that the solvent was distilled off yielding 1.1 g of P1 (96%). ^{1}H NMR (400 MHz, CDCl3), δ(ppm): 3.65-3.63 (m, 42H, -CH2O-), 3.55-3.52 (m, 2H, CH2OCH3) 3.37 (s, 3H, OCH3), 2.75-2.70 (m, 2H, SCH2CH2), 2.63-2.59 (m, 2H, CH2CH2SH), 1.87-1.83 (m, 2H, CH2CH2CH2O).

II.3.2.4 Synthesis of C7

To 0.3 g (0.303 mmol) of C6 dissolved in 5 ml of ethyl acetate 0.449 g (0.666 mmol) of P2 and 0.023 g (0.113 mmol) of photoinitiator Irgacure 184 were added. Then, the reaction mixture was irradiated by UV for 20 minutes. The removal of the solvent yielded 0.38 g of C7 (76%). ^{1}H NMR (400 MHz, CDCl3), δ(ppm): 7.78-7.76 (m, 4H, ArH-Pht), 7.71-7.68 (m, 4H, ArH-Pht), 6.58-6.36 (m, 10H, ArH), 4.38 (d, 4H, ArCH2Ar, ax, J= 12.8 Hz), 3.96-3.94 (m, 4H, OCH2), 3.75-3.71 (m, 4H, CH2N), 3.66-3.63 (m, 42H, -CH2O-), 3.60-3.52 (m, 4H, OCH2), 3.38 (s, 6H,

OCH3), 3.10 (d, 4H, ArCH2Ar, eq, J=12.8 Hz), 2.85-2.44 (m, 16H, SCH2), 1.98-1.94 (m, 4H, OCH2CH2N), 2.04-1.66 (m, 24H, -CH2-), 0.99 (t, 6H, CH3, J=7.6 Hz).

II.3.2.5 Synthesis of C8

The mixture of 0.3 g (0.18 mmol) of C7 and 2.5 cm^3 (50 mmol) of hydrazine hydrate in 11 cm^3 of ethanol was heated under reflux for 12 h. Then, the product was precipitated with water and extracted with CH$_2$Cl$_2$. The organic layer was washed with water and dried with MgSO$_4$. The solvent was distilled off yielding 0.24 g (94 %) of C8. The product was immediately used in the next reaction. ^{1}H NMR (400 MHz, CDCl$_3$), δ(ppm): 6.87-6.10 (m, 10H, ArH), 4.38 (d, 4H, ArCH$_2$Ar, J= 12.8 Hz), 4.26-3.94 (m, 4H, OCH2), 3.75-3.71 (m, 4H, CH$_2$N), 3.60-3.52 (m, 4H, OCH$_2$), 3.10 (d, 4H, ArCH$_2$Ar, J=12.8 Hz) 1.98-1.94 (m, 4H, OCH$_2$CH$_2$N), 2.86-2.45 (m, H, -CH$_2$-), 2.71 (s, 6H, OCH$_3$) 2.04-1.66 (m, H, -CH$_2$-), 0.99 (t, 6H, CH$_3$, J= 7.6 Hz).

II.3.2.6 Synthesis of Cxg

To the vigorously stirred solution of 0.14 g (0.1 mmol) of calixarene C8 in 12 cm^3 of toluene 0.036 g (0.22 mmol) of 4-nitrophenyl isocyanate was added. The reaction was carried out for 24 h at room temperature. Then the obtained viscous yellow liquid was separated and washed twice with 10 cm^3 of toluene. The residue of solvent was removed by distillation under reduced pressure. The yield of calixarene Cxg was 78% (0.1265 g). ^{1}H NMR (400 MHz, DMSO-d6): δ(ppm): 9.22 (s, 2H, NH), 8.10 (m, 4H, ArH), 7.59 (d, 4H, ArH), 6.59-6.45 (m, 12H, ArH, NH), 4.31 (d, 4H, ArCH2Ar, ax, J=12.4 Hz), 3.85-3.82 (m, 4H, OCH2), 3.72-3.68 (m, 4H, CH2N), 3.49-3.48 (m, 42H, -CH2O-), 3.42-3.40 (m, 4H, OCH2), 3.20 (s, 6H, OCH3), 3.20 (bs, 4H, ArCH2Ar, eq), 2.85-2.44 (m, 16H, SCH2), 1.98-1.94 (m, 4H, OCH2CH2N), 2.04-1.66 (m, 24H, CH2), 0.99 (t, 6H, CH3, J=7.6 Hz).

II.3. 3 Spectroscopic studies on calixpyrrole

II.3.3.1 NMR spectra

To omit problems of deuterated solvents, we decided to perform ^{19}F NMR measurements for solutions of (C$_2$H$_5$)$_4$BF$_4$ and LiBF$_4$ in various solvents. Our aim was to investigate whether the presence of C6P (1 mole per 2 moles of salt) may result in a change of fluorine nuclei chemical shift, which should prove the presence of the anion-receptor interaction. We also tried to estimate the effect of Lewis acidity of the cation. A typical spectrum of ^{19}F NMR for LiBF$_4$ containing sample is shown on Figure 3. The presence of two peaks in the spectra should be explained by different ^{19}F NMR shifts of anions containing two different boron isotopes: ^{10}BF$_4^-$ and ^{11}BF$_4^-$. All the results of maximum of higher peak are shown in Table II.1.
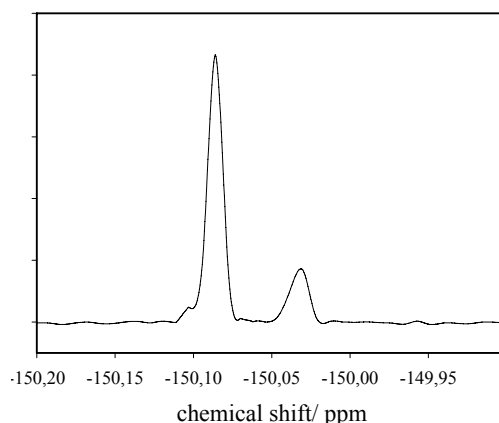
Figure II.3. ^{19}F NMR spectrum of LiBF$_4$ in CH$_2$Cl$_2$/ACN mixture.

Table II.1. ^{19}F NMR chemical shifts (higher) of BF_4^- anion

Solvent	Chemical shift, [ppm]			
	LiBF$_4$		(C$_2$H$_5$)$_4$NBF$_4$	
	No C6P	With C6P	No C6P	With C6P
CH$_2$Cl$_2$/ACN 1:9	-150.08	-149.99	-149.90	-149.91
CH$_2$Cl$_2$/ACN 5:5	-153.23	-152.83	-151.55	-151.56
CH$_2$Cl$_2$/ACN 9:1	-148.89	-150.66	-151.67	-151.69

The greatest change of the chemical shift, 1.77 ppm, is observed for the LiBF$_4$ solution in the least polar solvent mixture (CH$_2$Cl$_2$/ACN 9:1). As expected, the change of chemical shift is lower in solvent mixtures with higher dielectric constant and donor numbers, which both have a significant influence on the salt dissociation and the equilibrium between the solvent-anion and receptor-anion interactions. Surprisingly, in the case of (C$_2$H$_5$)$_4$NBF$_4$, changes in chemical shift are not so significant (this result is in opposition to the results obtained by Eichen for (C$_2$H$_5$)$_4$NBF$_4$ in a mixture of CHCl$_3$ and CH$_3$CN [8]). These results suggest that C6P addition to the LiBF$_4$ solutions improves the salt dissociation. In the case of (C$_2$H$_5$)$_4$NBF$_4$ there was no significant effect on ^{19}F NMR chemical shifts due to better salt dissociation. For samples with high dielectric constant, we suggest that the complexation of the anions by the solvent particles (especially CH$_3$CN) inhibits the anion-receptor interactions.

II.3.3.2 FTIR studies
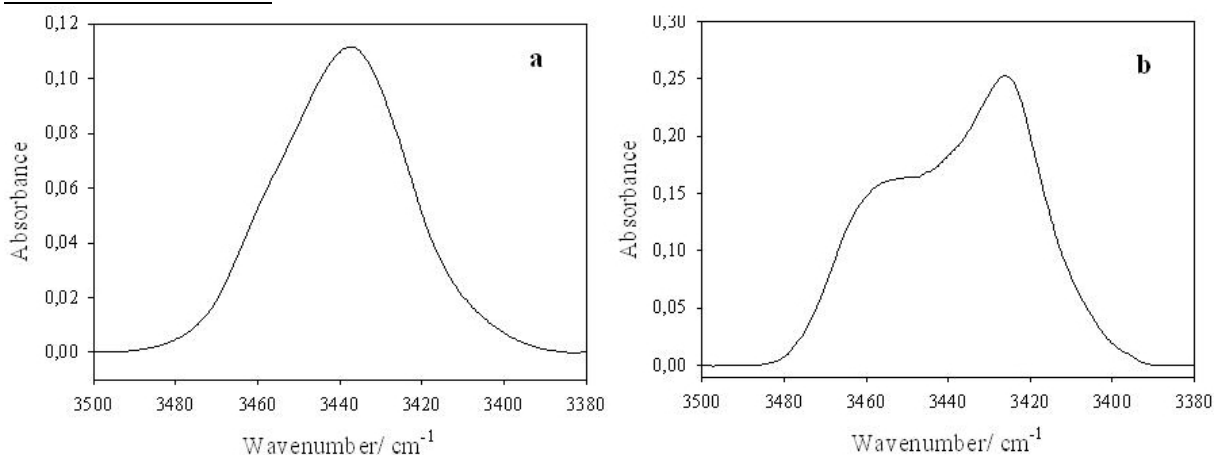
Figure II.4ab. A comparison of FTIR spectra of the C6P solution in CCl$_4$ (2a) and glyme(2b). Concentration of the C6P equal to 20 mmol/kg.

FTIR spectroscopy is widely used to analyze the receptor-ion (e.g. [18,19]), ion-ion (e.g. [20]) or ion-solvent (e.g. [21,22,23]) interactions. In the studied systems, the NH stretching vibration spectral region is of main interest. We compared FTIR spectra of C6P in solvents with various polarity (CHCl$_3$ and glyme) and also spectra of C6P/glyme and C6P/LiTf/glyme with the same C6P concentration (Figure II.4ab). It can be clearly seen that the shape of the NH band differs

[18] J. W. M. Nissink, H. Boerrigter, W. Verboom, D. N. Reinhoudt, J. H. van der Maas, J. Chem. Soc., Perkin Trans. 2 1998, 2541–2546

[19] J. W. M. Nissink, H. Boerrigter, W. Verboom, D. N. Reinhoudt, J. H. van der Maas, J. Chem. Soc., Perkin Trans. 2, 1998, 2623–2630

[20] M. Marcinek, M. Ciosek, G. Zukowska, W. Wieczorek, K. R. Jeffrey, J. R. Stevens, Solid State Ionics 176 (2005) 367

[21] M. Marcinek, M. Ciosek, G. Zukowska, W. Wieczorek, K. R. Jeffrey, J. R. Stevens, Solid State Ionics 171 (2005) 69

[22] P. Johansson, P. Jacobsson, Solid State Ionics 170 (2004) 73

[23] L. Edman, A. Ferry, P. Jacobsson, Macromolecules 32 (1999) 4130

depending on the solvent used. In the C6P/CCl$_4$ solution, we observed a maximum of the peak at 3443 cm^{-1} (Figure II.4a) while in the C6P/glyme solution this band is split into two distinct contributions, with maxima at 3426 and 3260 cm^{-1}. However, these bands are in fact more complex and their deconvolution reveals the presence of at least four peaks, with maxima at 3412, 3424, 3436 and 3459 cm^{-1}.

Additionally, in diglyme solution there are two weaker but broad bands, at 3315 and 3500 cm^{-1}, the former one corresponding to H-bounded NH group, the latter to free NH groups. The same bands, but far less intense (in particular that at 3315 cm^{-1}) were found in the spectrum of C6P/CCl$_4$ solutions. This indicates that in CCl$_4$ solution non-bound NH groups predominate, while in glyme solution part of the NH groups can interact with solvent molecules.

Figure II.5 shows a comparison of the spectra of C6P/ glyme and C6P/LiTf/glyme solutions with the same C6P concentration. As can be seen, the addition of the salt does not influence significantly the NH band shape. The only visible difference is in the slightly lower intensity of the band at 3515 cm^{-1} for the salt containing sample.
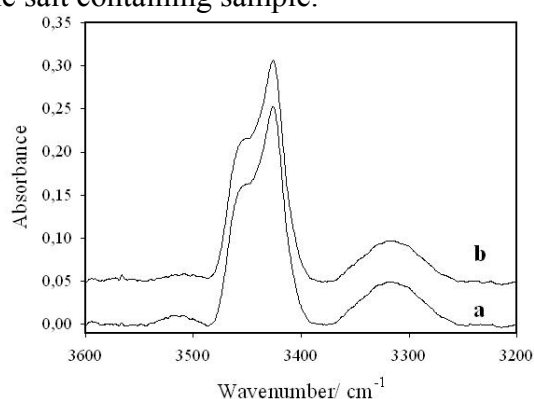
Figure II.5. FTIR spectra of C6P/glyme solution (5a) and C6P/glyme/LiTf solution, C6P: salt molar ratio 1:3 (5b). C6P content was equal to 20 mmol/kg.

II.3.4 Application of C6P to gel systems
II.3.4.1 Conductivity of PVdF- C6P- PC- LiTf gels

Gels prepared by both methods exhibited similar values of ionic conductivity, with Arrhenius type temperature dependence - activation energy of conduction equaled to 10 – 20 kJ/mol, typical for liquid organic electrolytes. The addition of C6P did not afrrect significantly the conduction parameters. The graph (Figure II.6) presents conductivity changes for two-step synthesis of the gel containing LiTf.

Figure II.6. Conductivity of PVdF-based gels (PVdF-PC-LiTf-C6P)

II.3.4.2 Impedance of Li-gel interface

The impedance spectra matched the overall equivalent circuit of serial connection of parallel resonators corresponding to conduction phenomena (HF), interfacial layer (MF) and charge transfer (LF), as shown in idealized impedance spectra depicted in Figure II.7 (upper part).

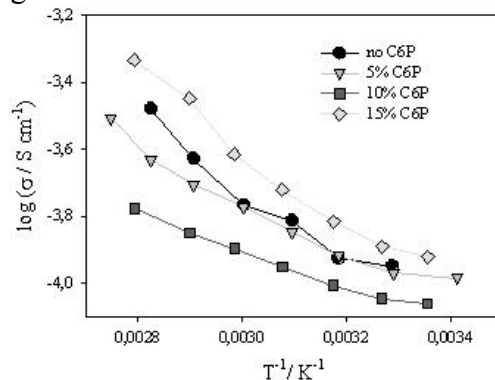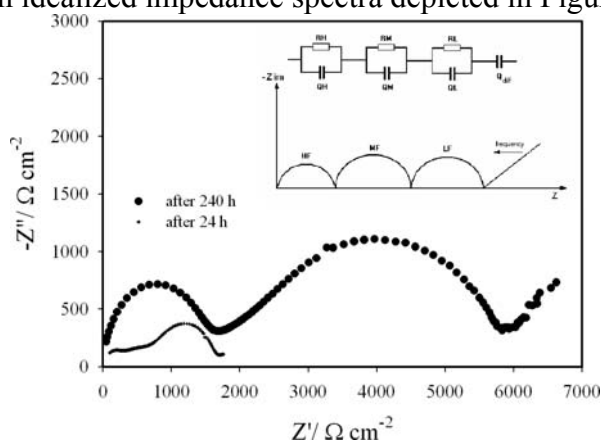**Figure II.7.** Idealized impedance spectrum and corresponding equivalent circuit for Li/gel/Li samples vs. real EIS spectra for PVdF- PC- LiTf- C6P system.
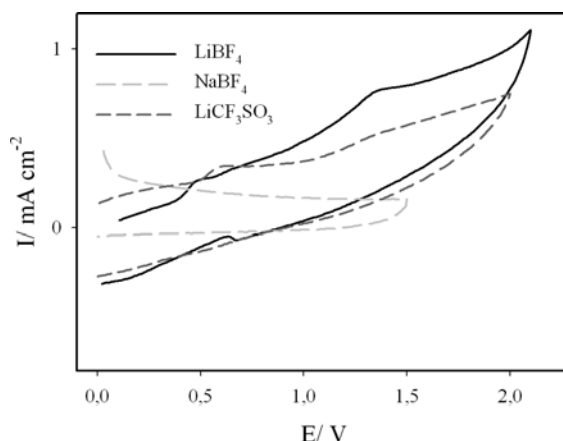
Figure II.8. Comparison of CV characteristics of PVdF/PC gel electrolytes, scan rate 50 mV/s, potential given versus NHE.

Two phenomena are influenced by the C6P addition – the passive layer resistance R(MF) is significantly lower during a prolonged test (up to 350 h) in 5% and 19% C6P containing gels and the charge transfer resistance R(LF) reacts in an opposite way. All impedance results are very irregular – the reason might be structural difference between two sides of a gel separator, as proved by scanning electron microscope analysis. The additive is not completely dissolved in the electrolyte and tends to sedimentate during 3-4 hours curing and hardening of the gel. It is however possible that in suspensions complexes can be formed on the surface of C6P grains.

II.3.7 C6P electrochemical behavior

In presence of C6P an anodic peak appeared at ca. 0.7V/NHE in gel electrolyte (Figure II.8). Further CV-grams were registered in PC solutions (Figures 9-10). The peak, as shown in Figure II.9 is formed only in solutions of lithium salts with anion complexed by C6P macrocyclic ring – $LiBF_4$ and LiTf. Sodium salts, as $NaBF_4$, as well as $(C_2H_5)_4NBF_4$ and $LiClO_4$ do not exhibit anodic waves at these potentials. Because of poor solubility of C6P in PC and other polar solvents more concentrated solutions could not be studied.

Figure II.9. Anodic activity in PC solutions of different salts. Scan rate 50 mV/s, potential given vs. NHE.
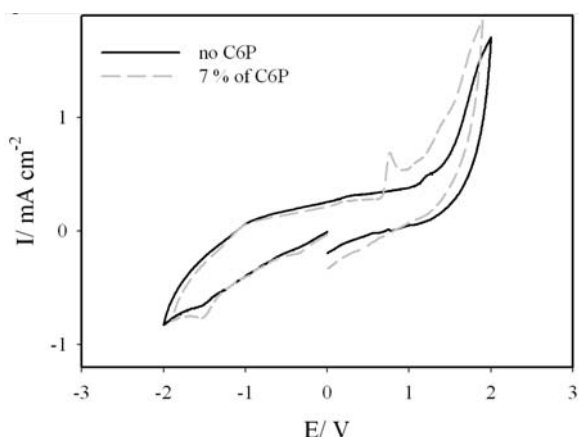
The anodic peaks tend to disappear with time (Figure II.10), suggesting that the equilibrium state of complex formation is reached slowly and does not exhibit further electrochemical activity.
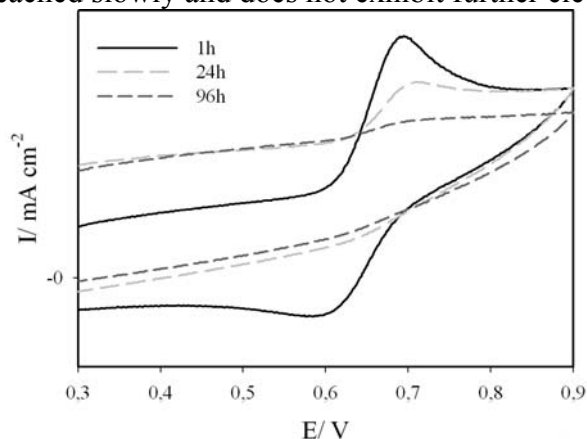

Figure II.10. Anodic oxidation peak dependence on time in Li-triflate/PC solution. Scan rate 50 mV/s, potential given vs. NHE

II.3.5. Spectroscopic studies on Cx2 receptor complexation phenomena with anions and neutral solvent species

II.3.5.1 Introduction

The simplest approach to anion-receptor interaction phenomena omits several problems which occur in real systems. Firstly, in most approaches, full dissociation of salt and receptor is assumed. This assumption, however, is not always fulfilled, especially when systems with high salt and receptor concentrations are studied. Secondly, interaction between solvent species and anion receptors in the system are neglected. We can discuss interaction between anion and anion receptor in particular solutions, however, it is not the case when water (as impurity) is present in the system. Thirdly, the anion receptor can interact with the cation. Indeed, every molecule containing carbonyl (e. g. urea, amide, urethane, ester etc.) or ether group, can interact with a cation. Thus, in our opinion, spectroscopic studies on Cx2 receptor complexation phenomena with anions and neutral solvent species are an interesting point of discussion when the effect of anion receptors as additives is researched.

In the studies presented, we used Raman, FTIR as well as ^{1}H and ^{19}F NMR spectroscopy. Experimental details of preparation of the samples, all spectroscopic techniques used, and methods of complex formation constant estimation as well as estimation of fractions of free ions, ion pairs and ionic triplets from vibrational spectroscopy data are presented in the Experimental section of this work.

II.3.5.2 Results - FTIR studies

FTIR spectroscopy is widely used to analyze the receptor–ion (e.g. [24,25]), ion–ion (e.g. [26]) or ion–solvent (e.g. [27,28,29]) interactions. In the studied systems, the NH stretching vibration spectral region is of main interest. The formation of the hydrogen bonding results in a decrease of the "free NH" stretching band intensity and formation of an additional band. Other changes can be observed in the C=O stretching band in amide **I** spectral region.
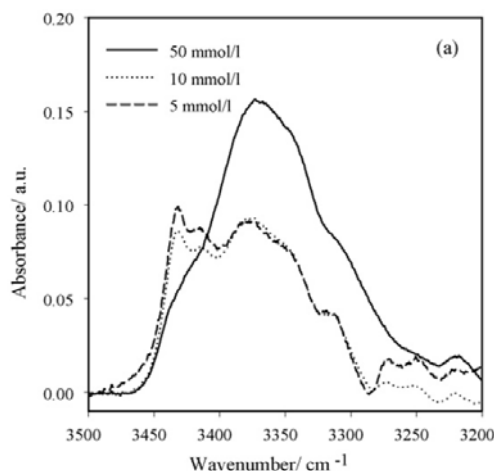

Figure II.11. The Cx2 FTIR spectra- NH stretching band regions for different Cx2 concentrations.

Figure II.11 shows the comparison of spectra of Cx2/CHCl$_3$ solution with various Cx2 concentrations. At the highest (50 mmol/l) Cx2 concentration maximum of the ν_{NH} vibration is found at 3370 cm^{-1} which indicates strong association of Cx2. With a decrease in the Cx2 content the intensity of this band decreases and an increase in intensity of two bands with maxima at 3431 and 3418 cm^{-1}, attributed to "free" N-H stretching vibration respectively of aryl and alkyl NH moiety, are observed. However, for the studied systems, a band of the H-bonded N-H group is still present in spectra with 5 mmol/l Cx2 concentration. Deconvolution of 3500-3200 cm^{-1} spectral region allows distinguishing at least 7 bands. Spectral contributes with maxima at 3377, 3341 and 3310 cm^{-1}correspond to various "bounded" aryl and alkyl NH. Weaker bands below 3300 cm^{-1} are most probably overtones.

In solutions of Cx2-glyme or Cx2-PEODME mixtures in CHCl$_3$ bands attributed to "free" NH groups decrease with an increase in DME/PEODME : Cx2 molar ratio. Figures 12ab show a comparison of the spectral region corresponding to NH stretching vibrations of Cx2. It is noteworthy that for the lower "guest" solvent/Cx2 ratio, spectra of both systems are essentially the same. For the solutions with highest (4:1) "guest" solvent/Cx2 ratio, in the DME (12a) and PEODME (12b) containing solution a maximum of ν_{NH} band is found at 3340 cm^{-1} and 3364 cm^{-1}, respectively. This is the evidence that Cx2 molecules interact stronger with DME than with its oligomeric analogue PEODME.

[24] J. W. M. Nissink, H. Boerrigter, W. Verboom, D. N. Reinhoudt, J.H. van der Maas, J. Chem. Soc., Perkin Trans. 2, 1998, 2541.
[25] J. W. M. Nissink, H. Boerrigter, W. Verboom, D. N. Reinhoudt, J.H. van der Maas, J. Chem. Soc., Perkin Trans. 2, 1998, 2623.
[26] M. Marcinek, M. Ciosek, G. Zukowska, W. Wieczorek, K.R. Jeffrey, J.R. Stevens, Solid State Ionics 176 (2005) 367.
[27] M. Marcinek, M. Ciosek, G. Zukowska, W. Wieczorek, K.R. Jeffrey, J.R. Stevens, Solid State Ionics 171 (2005) 69.
[28] P. Johansson, P. Jacobsson, Solid State Ionics 170 (2004) 73.
[29] L. Edman, A. Ferry, P. Jacobsson, Macromolecules 32 (1999) 4130.
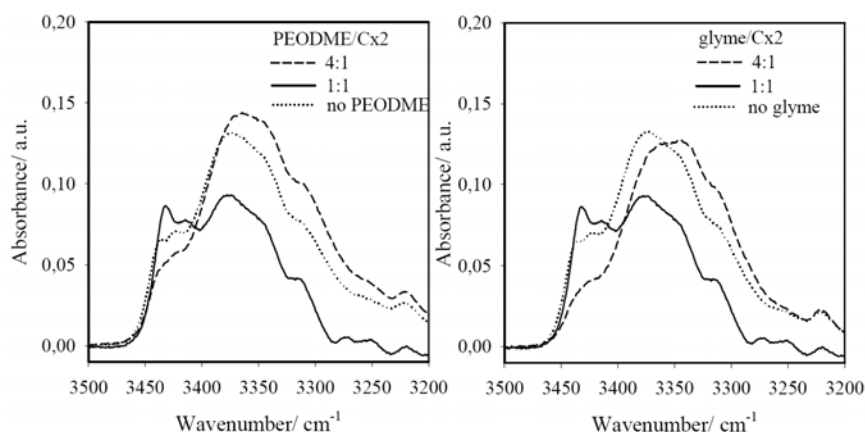
Figure II.12. FTIR spectra (NH stretching band region) of Cx2-CHCl$_3$-PEODME (a) and Cx2-CHCl$_3$-DME (b) systems.
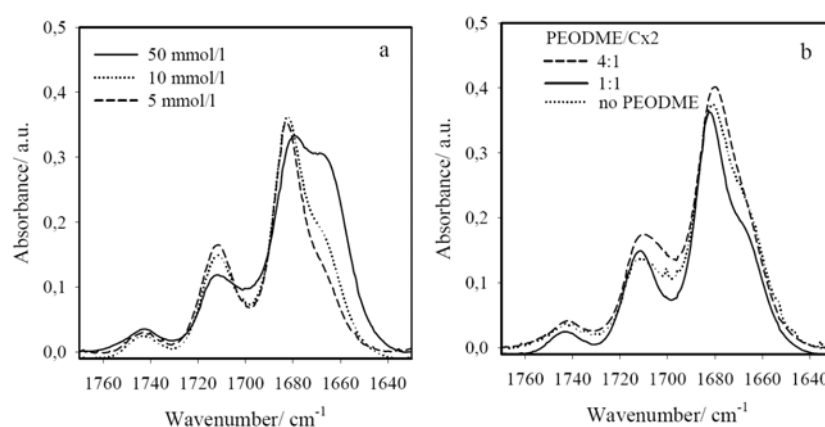
Figure II.13. FTIR spectra (CO stretching band region) of Cx2-CHCl$_3$ (different concentration of Cx2) (a) and Cx2-CHCl$_3$-PEODME (b) systems.

Figure II.13 presents amide **I** spectral region of Cx2-CHCl$_3$ and Cx2-PEODME-CHCl$_3$ solutions. In all spectra of Cx2 in CHCl$_3$ four spectral contributions can be distinguished, with maxima at 1743, 1711, 1682 and 1667 cm^{-1}. The band at 1743 cm^{-1} seem to be independent on Cx2 concentration, whereas 1711 and 1682 cm^{-1} decrease in intensity and that at 1667 cm^{-1} increases with rise in Cx2 content in the studied Cx2 concentration range. Therefore we ascribe bands at 1711 and 1682 cm^{-1} to the "free" carbonyl groups and that at 1667 cm^{-1} to the hydrogen-bounded ones. In spectra containing DME or PEODME mixtures, one may observe am increase of the relative intensity of the band at 1682 cm^{-1} and decrease of that at 1667 cm^{-1}. This effect can be explained as a consequence of the formation of hydrogen bonds mostly between "guest" solvent and Cx2 molecules and, therefore, increase of "free" carbonyl groups as the solvent/Cx2 ratio increases.
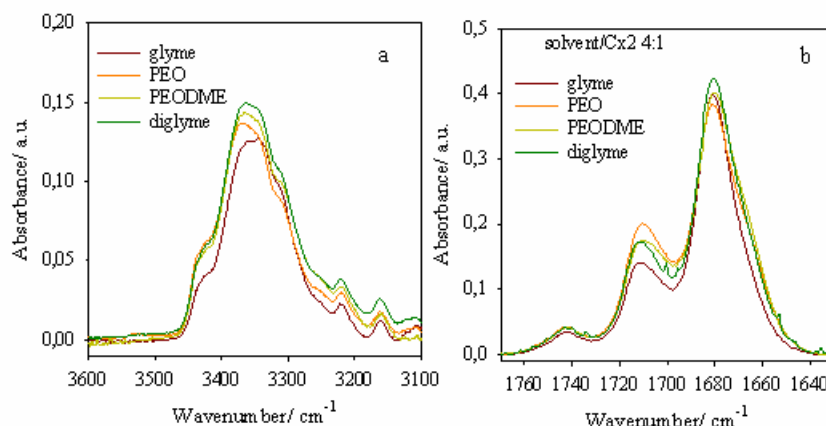
Figure II.14. FTIR spectra of glyme, diglyme, PEODME and PEO– NH (a) and C=O (b) stretching band region.

The chain length strongly influences ether ability to complex formation in the macrocycle containing system. The comparison of FTIR spectra for systems containing –OCH$_2$CH$_2$- units and characterized with different chain length is depicted in Figure II.14. In solutions with the same ether/Cx2 molar ratio, the complexation effect is the strongest for glyme, and the weakest for PEO. In conclusion, in such systems a complex is preferably formed between oxygen of the OCH$_3$ groups of the ether and NH groups of the urea moieties.

To study the phenomenon of complex formation more deeply, 2D-FTIR (correlation spectra) experiments were performed. Figure 15 presents synchronous correlation spectrum of 3200–3500 and 1630–1730 cm^{-1} spectral range for PEO–Cx2 solutions in CHCl$_3$. The negative crosspeaks between bands of the "free" carbonyl groups (at 1711 and 1682 cm^{-1}) and band of the bounded NH groups indicate that hydrogen bonds linking Cx2 molecules disappear at expense of solvent–Cx2 hydrogen bonds as the PEO/Cx2 molar ratio increases.

Figure II.15. Synchronous 2D correlation spectrum of the ν_{NH} and $\nu_{C=O}$ spectral region. FTIR spectra are for Cx2–PEO–CHCl$_3$ solutions. Cx2 concentration is equal to 10 mmol dm^{-3}, CHCl$_3$ and PEO:Cx2 molar ratio was equal to 4, 2, 1, 0.5 and 0.

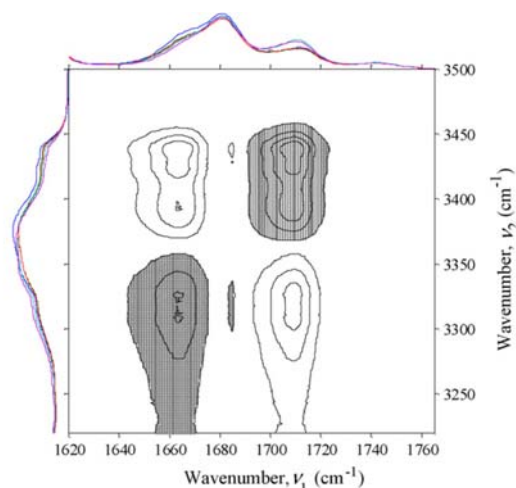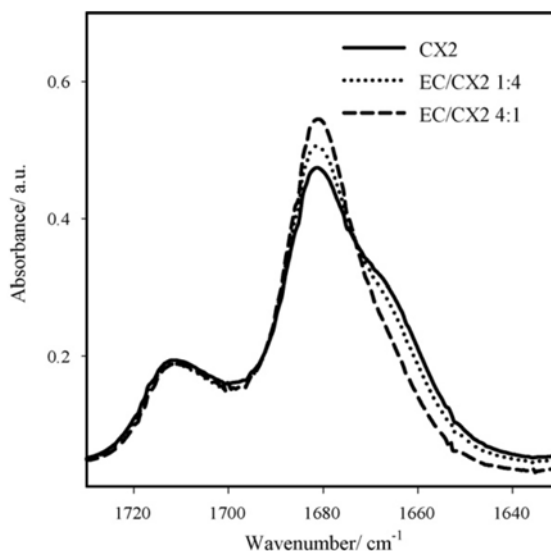**Figure II.16.** FTIR spectra for $\nu_{C=O}$ spectral region of Cx2/EC solutions in CHCl$_3$. Cx2 concentration in EC/Cx2–CHCl$_3$ solutions was equal to 10 mmol dm^{-3}. EC/Cx2 ratio equal to 4:1, 1:1 and 0:1.

In order to compare phenomena of ester- and ether type neutral solvent - Cx2 complex formation, we performed also FTIR studies for dialkyl (or alkene) carbonates - Cx2 complex formation in CHCl$_3$. Figure II.16 presents amide **I** spectral region of Cx2/EC–CHCl$_3$ solutions. It is seen that at the same solvent–Cx2 molar ratio the share of the bound C=O at 1667 cm^{-1} is slightly higher than for the ether containing samples (see Figure 13b). Area ratio of the contributes at 1682 and 1667 cm^{-1} obtained from deconvolution of this band is 3.3:1 for glyme and 2.9:1 for EC. The possible explanation is that the solvent with lower basicity, i.e. EC interacts weaker with the receptor than ethers. This is supported by the fact that even at the highest (4:1) EC-receptor molar ratio we do not observe such an increase of the intensity of the associated NH groups; maximum of this peak was centered at 3372 cm^{-1} for all of the samples. Intensities of peaks with maxima at 3431 and 3418 cm^{-1}, attributed to "free" N–H decrease at higher EC/Cx2 molar ratio, but this peak can be distinguished in spectra of all samples studied.

The most prominent change in the polar solvent spectral pattern is the shift and separation of two strong bands in the EC C=O stretching vibration range. In the spectrum of pure EC we can see a doublet with maxima at 1795 and 1768 cm^{-1}, the first maximum attributed to $\nu_{C=O}$ and the second to an overtone of ν_7 vibration (ring breathing) of EC diluted in CHCl$_3$. Both these bands are shifted to higher frequencies, with maxima at 1810 and 1779 cm^{-1}, respectively. These values are close to that obtained by Fini et al. [30] for diluted EC-benzene solutions. Such an effect was ascribed to the destruction of short-range order responsible for an intermolecular vibrational coupling through transition dipoles. However, we did not find any effect of the EC/Cx2 molar ratio on the position of the peak maxima in the studied samples. Unfortunately, bands ascribed of the EC ring breathing and bending mode, which are more sensitive to complex formation, cannot be analyzed because of their low intensity or overlapping with bands of chloroform.

In spectra of DMC-CHCl$_3$ mixtures (not depicted here) we observed only slight changes, both in the C=O and NH stretching vibration range, up to 4:1 DMC/Cx2 ratio. It is somewhat surprising, considering similar coordination (donor) properties of this solvent (see Table 2).

Also Cx2 solutions in polar solvents, which were taken as guests during studies of the Cx2 complexation phenomena with neutral species, were registered. This was done in order to compare two cases: i) concentration of the polar solvent is in the same level as anion receptor; ii)

[30] G. Fini, P. Mirone, B. Fortunato, J. Chem. Soc., Faraday Trans. 2 (1973) 1243.

polar solvent concentration is more than two orders of magnitude higher than the concentration of anion receptor. When Cx2 was dissolved directly in DMC, maximum of the ν_{NH} band appeared at 3410 cm^{-1}. As shown in Figure 17, for solutions of Cx2 in glyme and dioxane, maximum of this peak is much more shifted towards lower wavenumber. The strongest effect was found for DME, which is characterized by the highest DN (see Table 2). In the spectrum recorded in dioxane, we observed a strong band with maximum at 3340 cm^{-1}, originating from associated NH groups, and almost an equally strong shoulder with maximum at ~3380 cm^{-1}. These results agree with the behavior expected on the basis of donor properties of the solvent (see Table II.2), with exception of DMC.
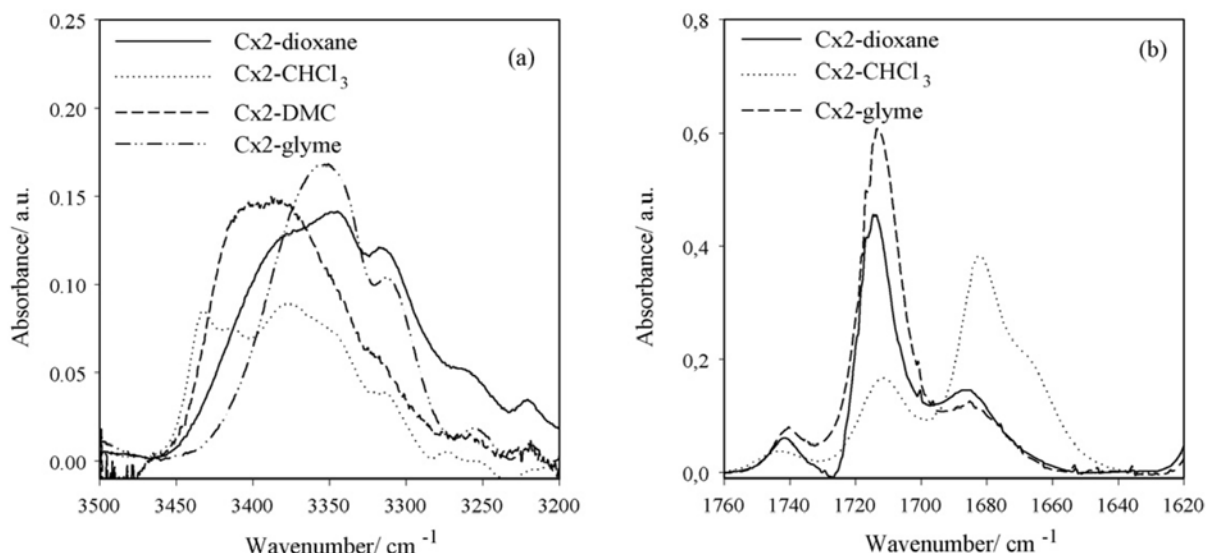

Figure II.17. FTIR spectral range for ν_{NH} (a) and $\nu_{C=O}$ (b) of solutions of Cx2 solutions with Cx2 concentration equal to 10 mmol dm^{-3}.

Table II.2. Properties of the solvents. [a] Data from Ref. [31]. [b]Data from Ref. [32]. [c]Data from Ref. [33].

Solvent	DN	AN
Ethylene carbonate[a]	16.4	-
Dimethyl carbonate[a]	15.1	-
Ethylene glycol dimethyl ether[b]	20	10.2
Diethylene glycol dimethyl ether[b]	24	10.2
Triethylene glycol dimethyl ether[c]	-	10.5
DMF[b]	26.6	16
1,4-Dioxane[b]	14.3	10.3
CHCl$_3$[b]	4	23.1

II.3.5.3 Results - NMR studies and titrations

In previously presented studies, most of the results are qualitative or semi-quantitative and present tendencies (trends) and strength of anion receptor - solvent (matrix) - salt interactions. For quantitative studies, i. e. estimations of complex formation constants, we used techniques taken from the chemistry of anion coordination - NMR titration. In general, this technique bases on the fact that (when the reaction of complex formation is fast enough) the observed chemical shift is the weighted average (with weights equal to the molar fraction of the studied species) of

[31] M. Morita, J. Chem. Soc., Faraday Trans. 94 (1998) 3451.
[32] W. Linert, Y. Fukuda, A. Camard, Coord. Chem. Rev. 218 (2001) 113.
[33] D. Brouillette, G. Perron, J. Desnoyers, J. Sol. Chem. 27 (1998) 151.

all forms present in the system. The details concerning the procedure of estimating the formation constants used are presented in review article [34] as well as in references cited there.
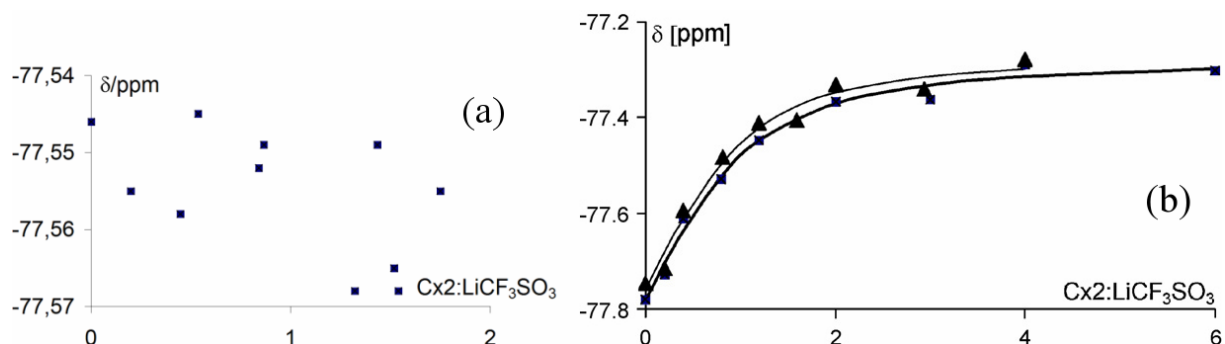

Figure II.18. Figure a: ^{19}F NMR chemical shift of the Tf⁻ as a function of Cx2:LiTf molar ratio in DME (c_{LiTf}=1.15 mmol (kg DME)$^{-1}$). Figure b: ^{19}F NMR chemical shift of the Tf⁻ as a function of Cx2:LiTf molar ratio in dioxane-CH$_3$CN mixtures having ε=5.5 (squares, c_{LiTf}=5.34 mmol (kg of the solvent)$^{-1}$) and ε = 8 (triangles, c_{LiTf}=5.76 mmol (kg of the solvent)$^{-1}$).

In the recorded spectra we observed only a single peak of which the chemical shift is the weighted average of the chemical shifts δ of the complexed $δ_{RA-}$ and non-complexed anions $δ_{A-}$. To simulate the solid polymeric electrolyte, a mixture of dimethoxyethane and dioxane (dielectric constant equal to 5.67) was used (Figure II.18a). Unfortunately, the registered dependency of the chemical shift on the salt:receptor ratio is not representative and cannot be used for the complexation constant estimation. This observation can be related to the phenomenon of the complexation of the supramolecular additive with the solvent species observed by us for C6P- based systems. In contrast to this, the ^{19}F NMR chemical shift for the LiTf and Cx2 in dioxane: acetonitrile mixtures as a function of Cx2:LiTf molar ratio are depicted in Figure 18b. From these data we estimated the complexation constants equal to 650 mol (kg of solvent)$^{-1}$ for solvent having ε = 5.5 and 700 mol (kg of solvent)$^{-1}$ for solvent having ε = 8, respectively.

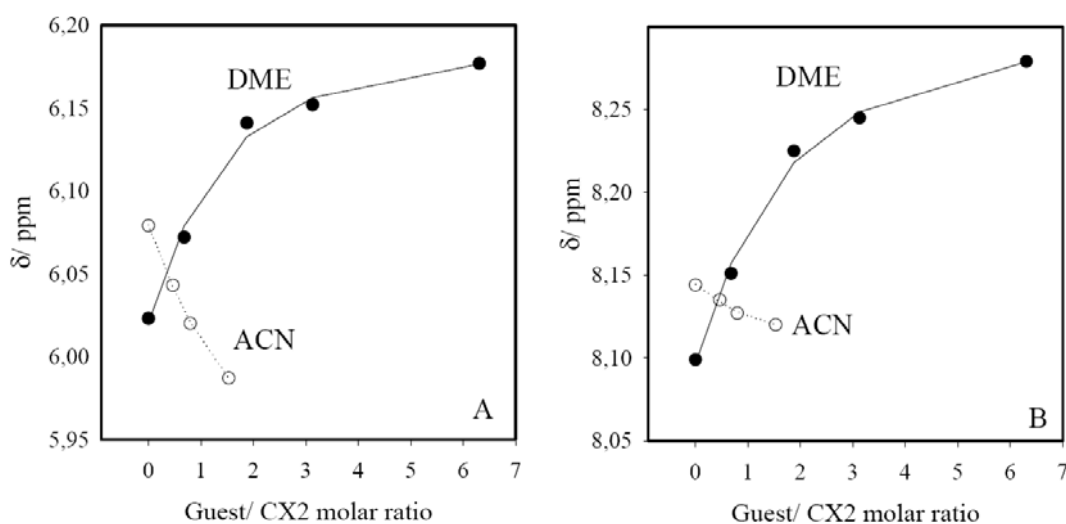**Figure II.19.** The ^{1}H NMR chemical shift of the Cx2 protons of NH connected with aliphatic chain (A) and with aromatic ring (B) after DME (filled) and CH$_3$CN (empty) addition.

Using this technique, studies of complexation phenomena by Cx2 were continued. The changes in the chemical shift of both NH groups were observed with increasing concentration of DME or

[34] L. Fielding, Tetrahedron 56 (2000) 6151.

CH$_3$CN. The obtained curves are depicted in Figure 19. The estimated values of Cx2-CH$_3$CN and Cx2-DME complex formation was between 100 and 300 mol dm^{-3} (more accurate estimation needs at least 12 measurements, i.e. 4 measurements for one estimated value). This result for DME when compared with the Cx2-I$^-$ anion-receptor complex formation constant (about 10^3 mol^{-1} dm^3 in CDCl$_3$, see [35]), at least partially explains the electrochemical behavior of PEO-LiI- Cx2 systems, in which the lithium cation transference number t$_{Li+}$ for the low Cx2 concentration remains the same, and the improvement is only for the high salt: PEO molar ratio (salt: PEO molar ratio should be higher than 1:20).

To confirm this result, we decided to estimate the anion receptor complexation constant in the solution in which solvent (mixture of 1,4-dioxane and acetonitrile) has the same dielectric constant as PEO ($\varepsilon = 5.5$, dioxane:CH$_3$CN mass ratio 12:1) and its liquid oligomeric analogue PEODME ($\varepsilon = 8$, dioxane:CH$_3$CN mass ratio 48:7). The choice of the solvent mixture was a compromise between the coordination properties (represented by the donor number DN related to the solvent–cation affinity and the acceptor number AN which is responsible for the anion–solvent interactions) and the solvent–receptor interactions inhibiting the anion complexation. As is shown later, the ideal mixture of DME and 1,4-dioxane (both solvents have DN and AN almost identical like the PEO matrix) must be replaced with a CH$_3$CN–dioxane mixture being less ideal from the point of view of the physicochemical parameters but not complexing the supramolecular compound (set of parameters for pure solvents was taken from [36] – dielectric constants and [37,38] – AN and DN numbers; see also Table 2). To overcome the problem of chemical shift change as a result of receptor self-complexation and ionic pairs forming, we conducted ^{19}F NMR titration of the anion. A set of solutions was obtained by mixing of the salt (LiTf) and receptor solutions and pure solvent to maintain both constant salt concentration and appropriate host to guest ratio. We emphasize here that this procedure can be applied only for titration of the fluorine atom-containing salts. Thus, it was impossible to apply this procedure to the LiI-containing systems.

II.3.6 Studies of receptor- matrix compatibility in terms of solid membrane microstructure
Introduction
Anion receptor addition should not result in worse (mechanical, chemical or conducting) properties of the membrane. Such problems are present when receptor agglomeration or even precipitation is observed. Thus, compatibility of the receptor with polymer matrix is crucial to omit such problems. Receptor-matrix compatibility results also in simpler synthesis of the membrane.

[35] J. Scheerder, M. Fochi, J. F. J. Engbersen, D. N. Reinhoudt, J. Org. Chem. 59 (1994) 7815 .
[36] W. Linert, Y. Fukuda, A. Camard, Coord. Chem. Rev. 218 (2001) 113.
[37] D. Brouillette, G. Perron, J.E. Desnoyers, J. Solution Chem. 27 (1998) 151.
[38] R.W. Taft, N.J. Pienta, M.J. Kamlet, E.M. Arnett, J. Org. Chem. 46 (1981) 661.
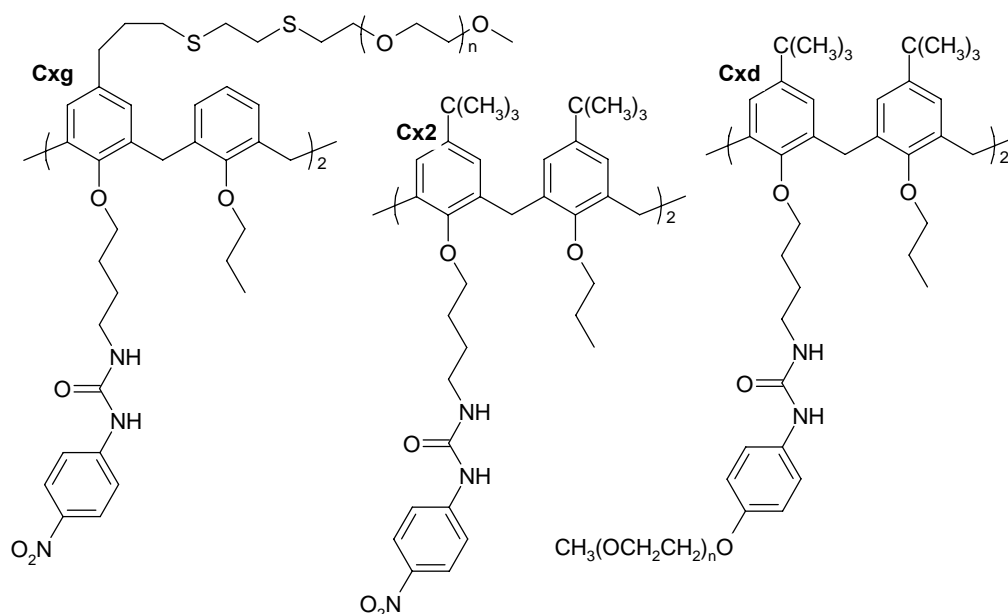
Figure II.20. Structure of Cxg, Cx2 and Cxd.

In our studies, we tried to modify the Cx2 receptor by attaching polyoxyethylene chains to the receptor molecule. In the first approach (receptor Cxd), Cx2 structure was modified by attaching two poly(oxyethylene) chains by replacement of p-OCNC$_6$H$_4$NO$_2$ with p-OCNC$_6$H$_4$(OCH$_2$CH$_2$)$_n$OCH$_3$ in the last step of the synthesis. Unfortunately, this synthetic path failed due to problems with the isolation of p-NH$_2$C$_6$H$_4$(OCH$_2$CH$_2$)$_n$OCH$_3$ (precursor of p-OCNC$_6$H$_4$(OCH$_2$CH$_2$)$_n$OCH$_3$). In another approach, proposed by Rokicki and Parzuchowski, the broad rim of the calixarene ring is modified. This approach, more complicated in synthesis than previously presented, has one important advantage: modification in the broad rim cannot influence the receptor coordination properties negatively [39].

It is worth to note that the receptor-matrix compatibility is also an important factor as it was proved by the McBreen group [40]. His observations for boron-based anion receptors show that the boronate group containing receptors was characterized with better compatibility to liquid matrix due to their lower symmetry in comparison with other boron-based receptors as borate and borane group containing ones. Thus, the boronate group containing receptors was characterized with e. g. higher solubility in the liquid matrix.

3.6.1 Results - Conductivity
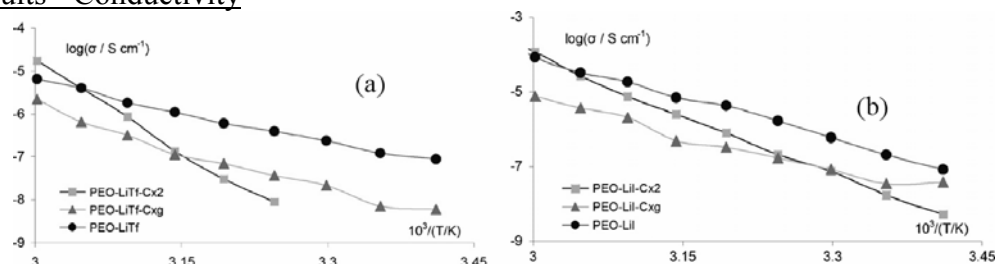
Figure II.21. Thermal dependency on conductivity - systems containing LiTf (a) and LiI (b).

Thermal dependences of conductivities for (PEO)$_{20}$LiTf and (PEO)$_{20}$LiI composites with addition of the anion receptors are depicted in Figures II.21a and II.21b, respectively. In both

[39] P. Parzuchowski, E. Malinowska, G. Rokicki, Z. Brzózka, V. Bohmer, F. Arnaud-Neu, B. Souley, New J. Chem. 23 (1999) 757.

[40] e. g.: H. S. Lee, X. Q. Yang, C. Xiang, J. McBreen, J. H. Callahan, J. H. Choi, J. Electrochem. Soc. 146 (1999) 941.

cases, we observe that the addition of an anion receptor results in the lowering of conductivity for temperatures lower than 50ºC. At higher temperatures, the conductivity of Cx2-containing samples is similar or even higher than that of systems which do not contain an anion receptor. The activation energy (Table 3) of conduction is the highest for systems containing Cx2. For LiI containing samples the lowest value was observed for the system containing Cxg while for LiTf ones the pristine system is characterized with the lowest E_a. Despite of the last fact, the value of the Ea for Cxg-containing samples was always far lower than for the Cx2 ones.

Table II.3. Activation energies of the conductivity.

System	E_a, [kJ mol^{-1}]
PEO-LiI	153
PEO-LiI-Cx2	200
PEO-LiI-Cxg	115
PEO-LiTf	89
PEO-LiTf-Cx2	265
PEO-LiTf-Cxg	118

II.3.6.2 Results - SEM images and EDS analysis

The SEM images of the PEO-LiTf-Cx2 and Cxg composites are depicted in Figures II.22abcd and 23ab, respectively. One can observe that the studied systems reveal different morphology: PEO-LiTf-Cx2 crystallizes forming "sponge-like" structures, PEO-LiTf-Cxg forms large spherulites. In contrast, in the case of LiI-containing systems (Figs. II.22c and d and II.23b) no specific structures separation can be observed with the spherulitic structure still maintained. It can be also observed that the volume of the interspherulitic amorphous phase for Cx2 containing sample is significantly larger than for Cxg containing one. Figure II.24 shows the comparison of the SEM image of the sample with EDS intensity mapping for two elements: carbon characteristic mainly for the receptor and, partially, for the polymer phase and sulfur which is present in the salt.
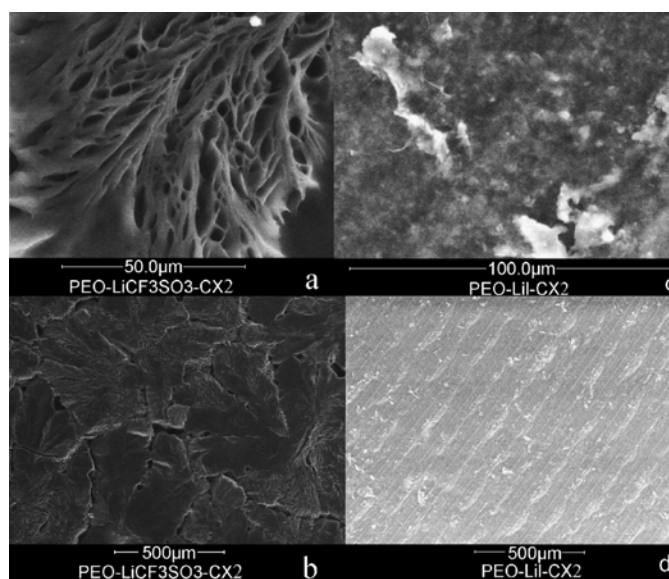

Figure II.22. SEM images- Cx2- containing systems.

Image II.24a shows a well defined boundary between the two spherulites. The carbon line intensity follows exactly the SEM image also revealing the phase boundary (intensity related to the local density of the sample) while the sulfur concentration profile is much more uniform. This observation proves that the salt is located evenly in both spherulites (being heterophase systems themselves) and in the inter-spherulitic amorphous phase, while receptor concentration is significantly higher in the interspherulitic areas than in spherulites.
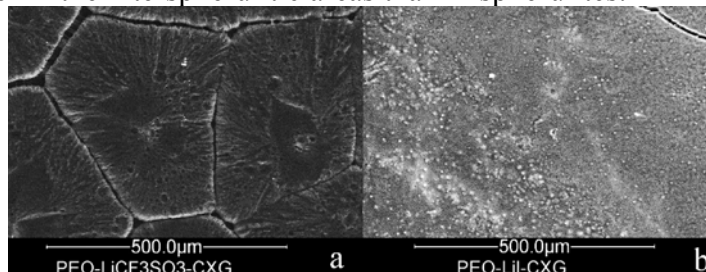

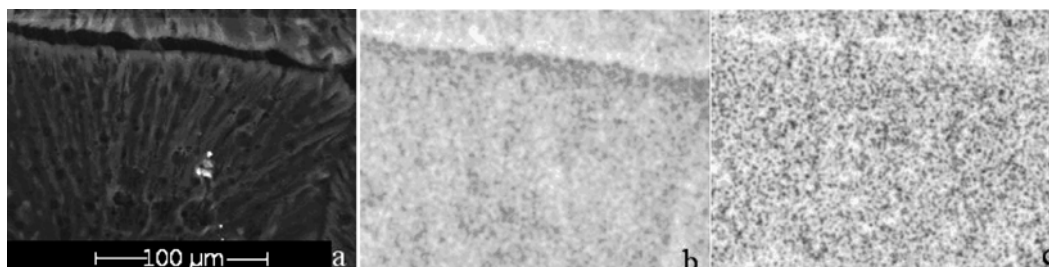**Figure II.23.** SEM images—Cxg-containing systems

Figure 24. EDS images of the PEO-LiTf-Cxg sample. (a) SEM image of the area; (b) carbon K_α line intensity mapping; (c) sulfur K_α line intensity mapping.

II.3.6.3 Results - FTIR spectroscopy

The formation of a complex between calixarene receptors and anions was studied using FT-IR spectroscopy. The hydrogen bond formation between the amide group of the receptor and the anion (or polymer) results in the change of several amide characteristic bands. The most pronounced changes are observed for bands of the C=O stretching vibrations. Figure 25 shows a comparison of the carbonyl stretching region in FT-IR spectra of PEO-Cx2, PEO-Cx2-LiI and PEO-Cx2-LiTf samples. In the spectrum of the PEO-Cx2 sample the band of C=O stretching vibration is split into a doublet with two distinct maxima, at 1710 and 1676 cm^{-1}. The peak at 1710 cm^{-1} corresponds to the free carbonyl group and that at 1676 cm^{-1} can be a superposition of peaks attributed to weakly and strongly associated carbonyl groups, with maxima respectively at ~1680 and 1640 cm^{-1}. In spectra of samples containing lithium salt the maximum of the peak is slightly shifted towards lower wavenumbers (1707 and 1705 cm^{-1} for LiTf and LiI, respectively) and bands of the free and associated carbonyl groups are highly overlapped.
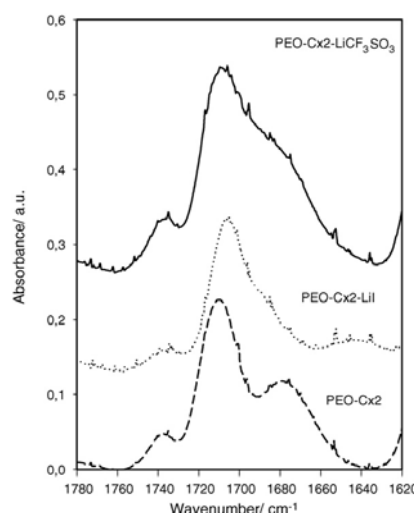
Figure II.25. FT-IR spectra of PEO membranes doped with Cx2.

It should be stressed here that the band is much broader for the PEO-Cx2-LiTf than for PEO-Cx2-LiI sample. Additionally, the low frequency shoulder which appears at ~1675 cm^{-1} for the triflate doped electrolyte shifts to ~1690 cm^{-1} for the iodide containing one. The described effect may indicate that salt addition results in breaking stronger hydrogen bonds linking Cx2 molecules and formation of weaker ones between anions and Cx2. The broadening of the band in spectra of lithium salt-doped membranes may also indicate some interactions between the lithium cation and the carbonyl group of the receptor.

II.3.6.4 Results - Raman spectroscopy, Raman mapping and optical polarized light microscope images

Figure II.26. Polarized light optical microphotograph of the PEO-Cx2 film (distances in mm).

The obtained membranes doped with Cx2 were all heterogeneous and highly crystalline. Optical polarized light microscope images (see Figure II.26) show that the diameter of spherulites is between 50 and 200 μm.

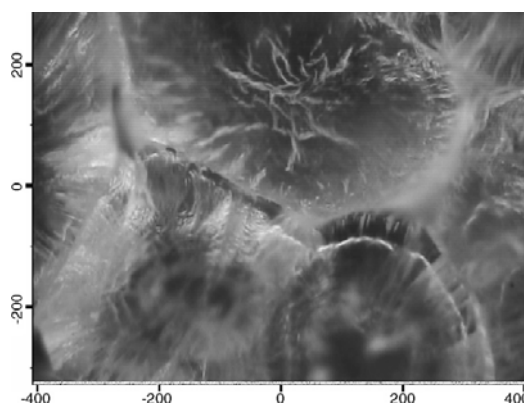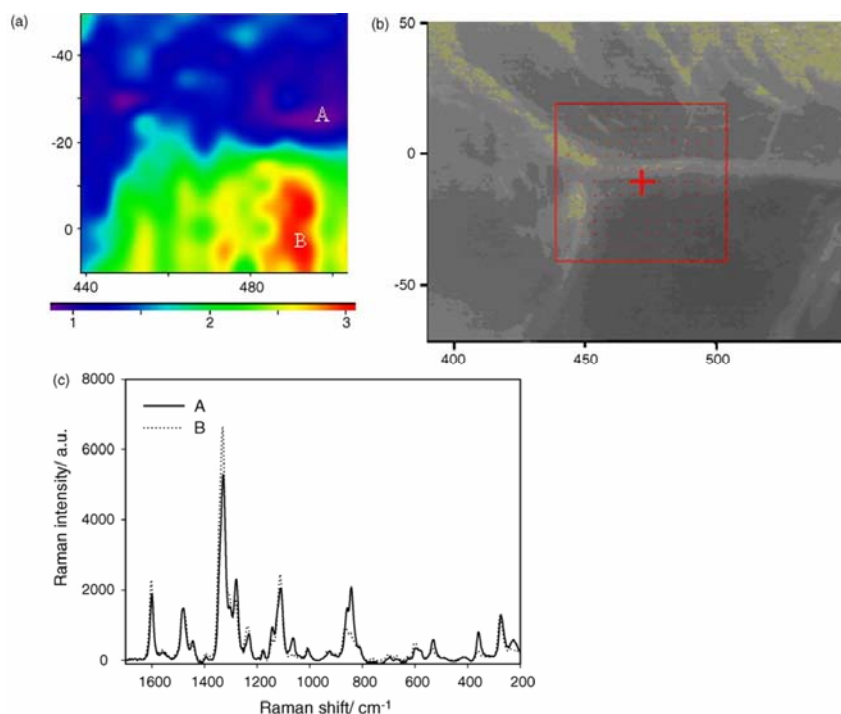**Figure II.27.** (a) Map of intensity ratio of characteristic peaks of Cx2 (ring stretching, 1600 cm^{-1}) and of crystalline phase of PEO (CH$_2$ rocking, 842 cm^{-1}) for PEO- Cx2. (b) Photo of the mapped membrane from CCD camera. (c) Raman spectra recorded in A and B areas. Scale in both maps in μm.

Figure II.27 presents the distribution of calixarene in PEO-Cx2 matrix. It can be seen that the amorphous domains of the membrane are richer in calixarene than the crystalline ones.
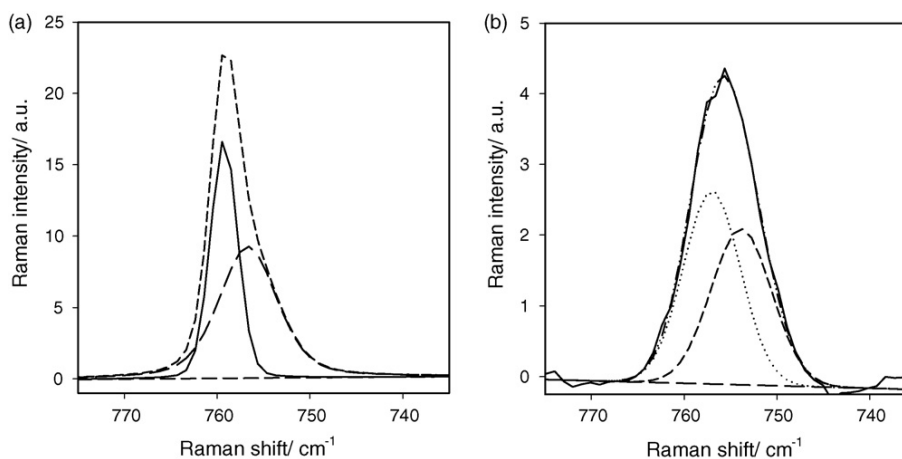
Figure II.28. Deconvolution of the δ_{sCF3} band in Raman spectrum of amorphous (a) and crystalline (b) domains of PEO-LiTf membrane.

In order to study the salt complexation both by calixarene and the polymer matrix, we analyzed Raman spectra recorded in crystalline and amorphous parts of membranes. The band of the δ_{sCF3} vibration of triflate anion is particularly useful to study complex formation. Figure II.28a and b shows deconvolution of the δ_{sCF3} band for the spectrum taken for the crystalline and amorphous parts of the PEO-LiTf membrane. In the crystalline phase the maximum of this band is centered at 755 cm^{-1}, while in the amorphous domains it is shifted to 759 cm^{-1} and has a much stronger intensity. According to the literature, various ionic species should give bands at ~753, ~758 and ~763 cm^{-1}, being ascribed to free anions, ionic pairs and triplets, respectively. In the spectrum

taken in crystalline domains, the peak can be resolved using two contributions, with maxima at 757 and 753 cm^{-1}. The share of the former one is between 50 and 70%. For the amorphous domain, the band was split into contributes - bands at 759 and 756 cm^{-1}. The share of the latter is 58%, and of the former 42%.

Different results were obtained using the band of the ν_{sSO3} vibration. In this case, for the amorphous domain, the deconvolution gives three bands with maxima at 1054 cm^{-1} (triplets, 14%), 1043 cm^{-1} (ionic pairs, 62%) and 1031 cm^{-1} (free ions, 24%). For the crystalline phase, we were able to resolve this band into two contributes with maxima at 1040 cm^{-1} (ionic pairs, 32%) and 1030 cm^{-1} (free ions, 68%). We obtained similar results for the PEO-Cx2-LiTf membranes.
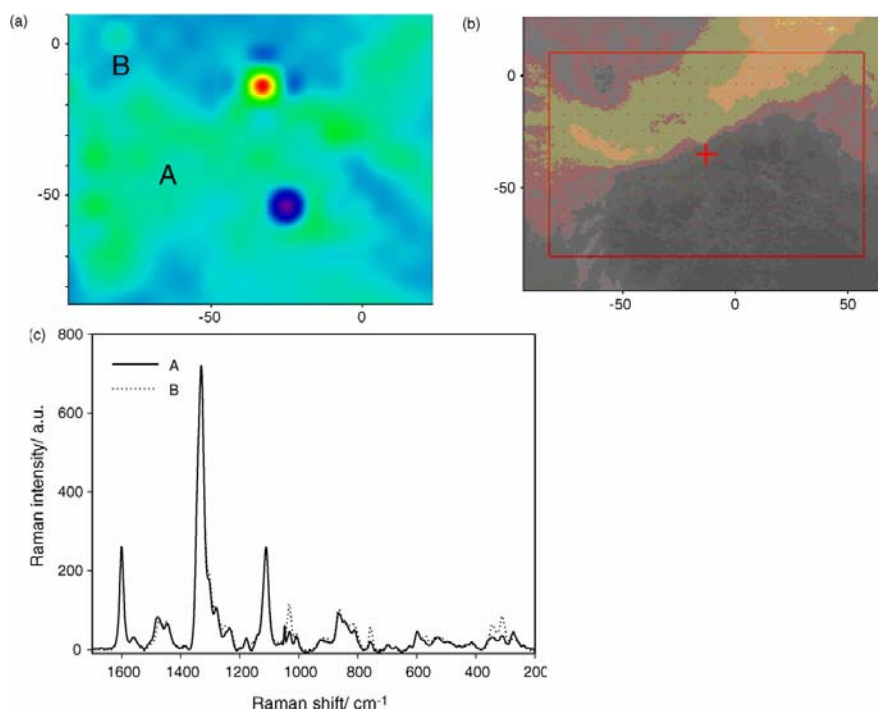

Figure II.29. (a) Map of intensity ratio of characteristic peaks of Cx2 (ring stretching, 1600 cm^{-1}) and of LiTf (δ_{sCF3}, 758 cm^{-1}) for PEO-Cx2- LiTf. (b) Photo of the mapped membrane from CCD camera. (c) Raman spectra recorded in A and B areas. Scale in both maps in micrometers (μm).

Deconvolution of the δ_{sCF3} peak gave 62% of ionic pairs and 38% of free anions for the crystalline phase, and 68%of ionic pairs and 32% of free anions for the amorphous phase. For the band of ν_{sSO3} vibration mode in the amorphous phase we get the same share of ionic pairs (68%) and free anions (32%) as for the membrane without Cx2. In the crystalline phase, the content of free ions was lower than in the PEO-LiTf sample and equal to 60%, while the share of ion pairs was almost the same (34%).

However, we must stress that the studied membranes were heterogeneous and that the estimated values of the ionic species contents are dependent on the crystallinity degree. Comparing the spectra normalized against the intensity of δ_{sCF3} peak of LiTf we also observe that the intensity ratio of ring stretching vibration of Cx2 (maximum at 1598 cm^{-1}) and of δ_{sCF3} is much higher in the amorphous phase. These observations are confirmed by Raman mapping. Figure 29 presents the Raman map for PEO-Cx2-LiTf obtained by comparing intensities of peaks of ring (Cx2) and δ_{sCF3} (salt). The Cx2/salt concentration ratio is higher in the amorphous domains of the sample, and lower in the crystalline ones. These results correspond to those obtained for the PEO-Cx2 membrane (without salt), where, as seen in the Raman map shown in Figure II.27, Cx2 was aggregated in amorphous domains. A similar effect, i.e. relatively higher content of free ions in

the crystalline phase and higher content of calixarene in the amorphous phase was found for membrane containing Cxg.
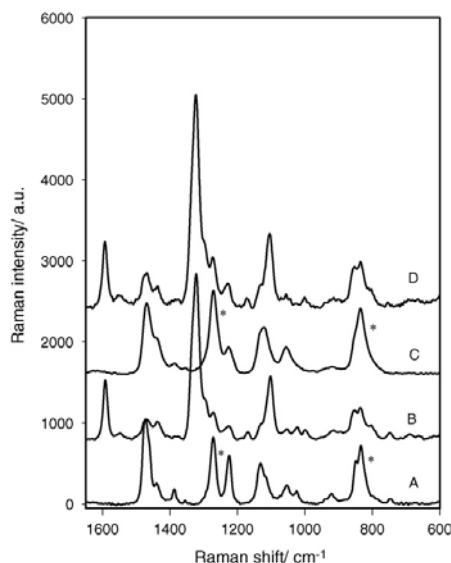

Figure II.30. Raman spectra of (A) PEO-LiTf; (B) PEO-LiTf-Cx2; (C) PEO-LiI; (D) PEO-LiI-Cx2. Bands characteristic for crystalline phase are indicated by asterisks.

Both membranes obtained without the macrocyclic compound addition PEO-LiTf and PEO-LiI were crystalline but the crystallinity was higher for the iodide doped sample. Figure 30 shows a comparison of Raman spectra for PEO-LiTf, PEO-LiI, PEO-LiTf-Cx2 and PEO-LiI-Cx2, recorded in the crystalline areas of samples. It can be seen that the intensity of peaks at 1272 and 835 cm^{-1}, which are characteristic for the crystalline phase, is the strongest for the PEO-LiI sample. The addition of receptors resulted in a decrease of crystallinity for all systems studied but this effect was more pronounced for iodide-doped samples. We found that crystallinity also decreased for the sample without the lithium salt what is consistent with FT-IR data, indicating formation of hydrogen bonds between ether oxygen of PEO and urea moieties of the receptor.
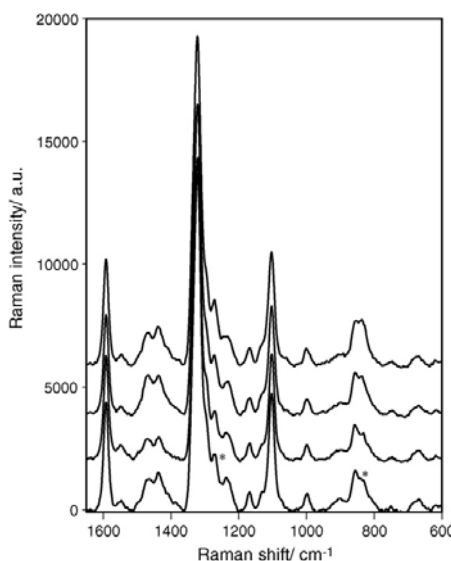

Figure II.31. Raman spectra recorded in different areas PEO-LiI-Cxg membrane. Bands characteristic for crystalline phase are indicated by asterisks.

The application of the substituted calixarene as anion receptor improves the homogeneity of the membrane. Figure II.31 shows a comparison of the Raman spectra extracted from the Raman

map of the PEO-LiI-Cxg membrane. Only slight differences for spectra recorded in various areas of the sample can be found.

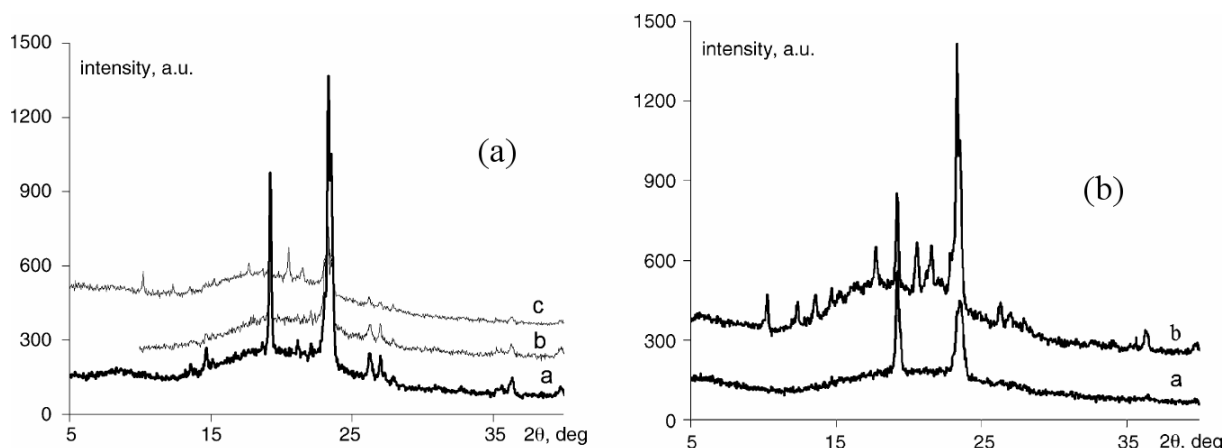## II.3.6.5 Results - XRD diffractography

Figure II.32. Figure a: Diffractograms of the samples containing Cx2: (a) no salt; (b) LiI; (c) LiTf. Figure b: diffractograms of the pristine samples. (a) $(PEO)_{20}LiI$; (b)$(PEO)_{20}LiTf$ (b).

When comparing the plots obtained for all samples containing Cx2 (Figure II.32a) with the diffractogram of the pure supramolecular compound (Figure II.33) one can easily observe that even in the case of the salt free membrane the complete amorphization of the calix[4]arene derivative is observed. This observation proves that even high molecular weight polyether somehow interacts with the receptor.
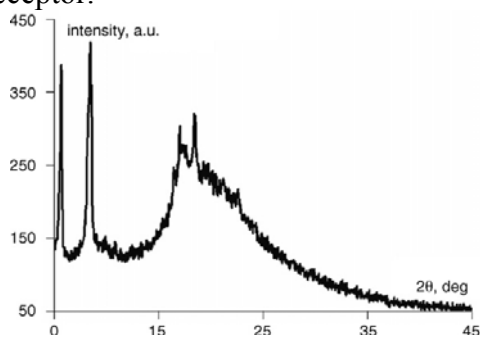
Figure II.33. Diffractogram of Cx2 (powdered compound).

Additionally, a comparison of the plots obtained for the pristine samples (Figure II.32b) with the ones containing the additive (Figure 32a) shows clearly that the modified membranes exhibit a stronger amorphous bump around the PEO reflections. This phenomenon can be also attributed to the polymer-receptor interactions. The distortion effect is stronger for the Cx2 receptor what shows that the negative interactions of the Cxg derivative with the crystalline PEO phase is weaker. Finally, the crystallinity data are gathered in Table II.4. The obtained value was calculated by the integration of the area characteristic for the peak located near $2\theta = 19°$ and is characteristic for the crystalline phase of pure polymer. A $P(EO)_{10}LiI$ sample was used as a reference with crystallinity degree equal to 70%.

The results show that the LiTf containing samples are generally less crystalline than the ones doped with LiI. Additionally, both compounds lead to the amorphization of the triflate containing composites while the crystallinity of iodide complexes remains almost unchanged.

Table II.4. XRD crystallinity data gathered for the studied electrolytes

Sample	Thickness μm	2θ=19° a.u.	2θ=23° a.u.	2θ=19° corrected	2θ=23° corrected	X_c
PEO-Cx2	135	3759	12552	27840	92750	0.79
PEO-LiI	117	2889	4274	24690	36530	0.70
PEO-LiTf	131	1750	9728	13318	74030	0.38
PEO-LiI-Cx2	73	1703	4794	23580	66390	0.67
PEO-LiTf-Cx2	149	623	2965	4158	19790	0.12
PEO-LiI-Cxg	63	1486	3506	23587	55650	0.67
PEO-LiTf-Cxg	55	630	3148	11454	57236	0.33

In the first case the Cx2 compound reveals a stronger amorphization activity in comparison to Cxg. The intensity of the second peak typical for the PEO crystalline phase was also analyzed. The study shows that for some samples the intensity of the peak is much larger than the one which should be predicted on the basis of the crystalline phase content. Additionally, the peak maximum is slightly shifted and/or the peak can be split. This phenomenon is related to the formation of the crystalline polymer salt complex characterized with a much higher specific reflexivity. The intensity of the signal is, thus, a combination of two unequal contributions and cannot be easily interpreted quantitatively.
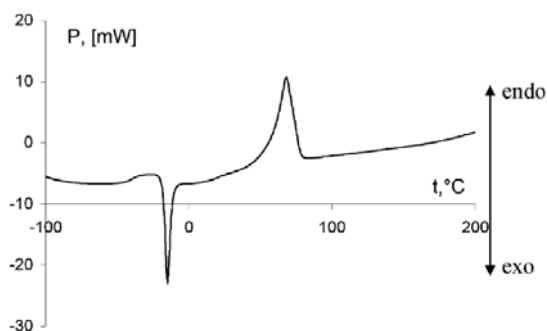
Figure II.34. DSC trace for PEO-LiTf-Cx2 system.

II.3.6.5 Results - DSC

A typical DSC trace for the PEO-lithium salt system presents two effects: the first one (baseline shift) characteristic for the second order transition is observed between −40 and −10°C and can be assigned to the glass transition while the second one (endothermic peak) is located between 60 and 75°C and can be attributed to the melting of the PEO crystalline phase [41,42,43]. The DSC trace for PEO-LiTf-Cx2 systems, which is typical for all samples containing anion receptor as an additive is depicted in Figure 34. In contrast to previous results of our group [44], no heat effect related to the crystalline PEO-salt complex melting was observed. Table II.5 gathers the temperature of the crystalline phase melting, specific enthalpy of melting together with the calculated crystallinity degree. The normalized values are obtained on the basis of pure PEO mass fraction in the studied composition. The comparison of the values obtained for PEO and PEO-Cx2 samples shows that the addition of this supramolecular additive does not prevent the

[41] J.E. Weston, B.C.H. Steele, Solid State Ionics 2 (1981) 347.
[42] Y.W. Kim, W. Lee, B.K. Choi, Electrochim. Acta 45 (2000) 1473.
[43] A. Vallee, S. Besner, J. Prud'Homme, Electrochim. Acta 37 (1992) 1579.
[44]A. Błażejczyk, M. Szczupak, W. Wieczorek, P. Ćmoch, G.B. Appetecchi, B. Scrosati, R.Kovarsky, D. Golodnitsky, E. Peled, Chem. Mater. 17 (2005) 1535.

crystallization of the polymer. In the case of the salt containing samples the Cx2 presence even promotes the matrix crystallization. Remarkably, an important observation can be made for the Cxg composites. Here the normalized crystallinity values are extremely and unreasonably high. This effect clearly shows that the excess heat effect observed must be related with the co-crystallization of the oligooxyethylene chains of the receptor with the PEO matrix. Therefore, a previously mentioned link between these two phases is observed confirming the better polymer-anion trap compatibility. The co-crystallization effect is stronger for LiTf containing samples.

Table II.5. Melting points, enthalpies of melting and DSC-based calculated crystallinites

Sample	T_m, °C	H_m, J g^{-1}	X_c, %	X_c^N, %
PEO	80.1	183	85	85
PEO-Cx2	74.2	121	57	83
PEO-LiI	75.5	114	52	61
PEO-LiTf	72.2	110	51	61
PEO-LiI-Cx2	75.1	98	46	74
PEO-LiTf-Cx2	78.8	99	47	76
PEO-LiI-Cxg	63.5	73	34	84
PEO-LiTf-Cxg	75.5	83	39	98

Glass transition temperatures of the membranes are presented in Table II.6. For both compounds the LiI containing electrolytes are plasticized. This observation is consistent with the previous data obtained by our group [44]. To explain the fact that the plasticization is weaker for the Cxg receptor one must consider, first of all, the stoichiometry of the samples. The salt to ether oxygen atoms ratio was here calculated taking into consideration both polymer and the receptor oligo(ethylene oxide) chains, thus the molar concentration of the salt in respect to the polymer matrix only is almost two times higher. Additionally, this phenomenon can be also related to the stronger physical cross-linking of the polymer matrix observed for the samples containing a receptor with oligo(ethylene oxide) chains which, on one hand, could act as an internal plasticizer but, on the other hand, can play the role of short bridges crosslinking (via lithium cation or ionic aggregate) the polymer matrix with heavy (and thus immobile) receptor molecules.

Table II.6. Temperatures, specific heat of T_g and enthalpy of recrystallization in the composites.

		Glass Transition		Recrystallization	
No.	Sample	T [°C]	Δc_p [J mol^{-1} °C^{-1}]	T [°C]	ΔH [J g^{-1}]
1	PEO	-48.8	0.035	not observed	
2	PEO-LiTf	-46.0	0.058	not observed	
3	PEO-LiI	-12.5	0.210	not observed	
4	PEO-LiTf-Cx2	-38.9	0.396	-8.6	24.2
5	PEO-LiI-Cx2	-38.9	0.343	-18.0	21.7
6	PEO-LiTf-Cxg	-38.4	0.321	-17.1	14.8
7	PEO-LiI-Cxg	-22.8	0.219	16.5	8.0

For samples containing LiTf the effect observed is opposite. The increase of T_g shows that the addition of the supramolecular additive stiffens the polymer matrix. To discuss this phenomenon, first of all, one must consider that for this system the T_g values are generally much lower. A triflate salt addition leads to only a slight increase of this value which can be related to both quasi-plasticizing properties of the trfiluorometanosulfonate molecule and ionic equlibria present in the sample. When studying the glass transition in the PEO based electrolytes one must take into consideration two various effects which can be responsible for the formation of the transient

physical cross-linking and, thus, matrix stiffening. The first type of interaction is related to the lithium cation, which is able to interact with oxygen atoms belonging to different polyether chains. This mechanism is widely observed for various SPE systems and can be partially inhibited by the addition of various modifiers. The additional stiffening interaction is specifically related to the presence of the anion receptor, whose interactions with neutral compounds including PEO and their liquid analogs were already described in our previous papers [45,46]. Therefore, in the case of the iodide anion the general effect is based on the overruling of the second one by the depletion of the very strong first one. Contrary to the triflate anion, the first effect is rather weak and can be easily depressed by the second one.

II.4. Conclusions

From the results obtained during the realization of this part of our joint project it is demonstrated that the addition of even a relatively small amount (molar fraction ~0.25) of calix[6] pyrrole to polyether electrolytes results in a considerable increase in lithium cation transference numbers as revealed from ac-dc polarization, as well as from PFG NMR experiments independently on the type of anion used as a counter ion in lithium salts.

In our groups we focused on the development of the simplified physical model of interactions between receptor-salt and polymer which would explain the observed changes in lithium transference numbers. The increase in the lithium transference numbers which is observed upon the addition of calix[6]pyrrole is usually associated with a decrease in the conductivity of the samples studied. The simplest explanation of this phenomenon relies on the fact of immobilization of mobile anions and thus a decrease in conductivity. This effect is particularly evident for low concentrations of the lithium salt for which high concentration of "free anions" can be expected. However, the behavior observed for high salt concentration for the various types of salt used cannot account on such a simple explanation.

Due to the low dielectric constant of polyethers (which can be assumed as a highly viscous or solid solvent), their complexes with lithium salts can be considered as weak electrolytes. Therefore, for the high salt concentration range (which is the case of most systems under study), the presence of a large fraction of ion pairs and higher aggregates should be expected. The ionic triplets formation constant is lower than that of ion pair formation and lower than the receptor – anion complex formation constants, which according to the literature data are within the range $2\text{-}3\times10^3$ mol^{-1}. Therefore, it can be assumed that it is easier for the receptor to release an anion from a triplet than from the ion-pair. Based on the obtained data, the maximum fraction of anion released is equal to the molar fraction of reacted calixpyrrole equal to 0.25. Since, according to the literature data the positive triplets are preferentially formed, this implies the formation of 0.5 molar fraction of lithium cations, which are free to move. The addition of 0.5 molar fraction of released cations to the lithium transference numbers of pure polymeric electrolytes results roughly in the lithium transference numbers experimentally obtained for composite electrolytes with calixpyrrole receptors. For high salt concentrations the increase in lithium transference number is usually associated with a negligible decrease in conductivity or, as was shown by the group of Tel-Aviv University, even with the increase in conductivity of the studied electrolytes. We have supported these experiments by the studies of the receptor-salt interactions in various mixture of low molecular weight solvent which mimic the polarizability and dielectric permittivity of polyethers. In CH_2Cl_2-CH_3CN mixtures, studies of the ^{19}F NMR chemical shift change show clearly that complexation of anions takes place. The complexation equilibrium is affected by the increasing dielectric constant of the solvent. Surprisingly, the complexation is

[45] A. Plewa, M. Kalita, G. Z. Żukowska, A. Sołgała and M. Siekierski, ECS Transactions, 3/12 (2006) 59.

[46] A. Plewa, F. Chyliński, M. Kalita, M. Bukat, P. Parzuchowski, R. Borkowska, M. Siekierski, G.Z. Żukowska, W. Wieczorek, J. Power Sources 159 (2006) 431.

also affected by the cation type. This phenomenon can be possibly attributed to the changing ion association equilibrium with the cation change.

The results presented for modified calix [4] arene receptor (Cxg) show clearly that a better compatibility between the supramolecular receptor and the PEO polymer matrix can be achieved by the receptor molecule modification through introducing of two polyoxyethylene chains instead of four *tert*-butyl groups in the wide rim. The better compatibility of the Cxg receptor with the polymer host can be attributed to the presence of identical structural units in its molecule leading, in consequence, to co-crystallization with the polymer phase. In this way the agglomeration of the additive particles is overcome by anchoring to the polymer chains. Thus, the electrochemical stability of the newly introduced receptor should be analyzed together with the studies of the conducting properties of the obtained membranes.

Considering the positive effect of the calix[6]pyrrole on the enhancement of lithium transference numbers of a variety of lithium salts we have performed successfully the synthesis of this supramolecular receptor in semi-technological scale. During this synthesis it has been proved that the amount of trifluoroacetic acid and purity of starting materials are the most important factors in C6P synthesis.

III. LIST OF PUBLICATIONS RESULTING FROM WORK CARRIED OUT WITHIN THE PROJECT:

1. E. Zygadło-Monikowska, Z. Florjańczyk, A. Tomaszewska, M. Pawlicka, N. Langwald, R. Kovarsky,, H. Mazor, D. Golodnitsky, E. Peled, *Electrochim. Acta* **2007**, *53*, 1481-1489.
2. M. Pawłowska, G.Z. Żukowska, N. Kalita, A. Sołgała, P. Parzuchowski, M. Siekierski *J. Power Sources* **2007**, *173*, 755-764.
3. M. Kalita, A. Sołgała, M. Siekierski, M. Pawłowska, G. Rokicki, W. Wieczorek *J. Power Sources* **2007**, *173*, 765-773.
4. M. Kalita, M. Bukat, M. Ciosek, M. Siekierski, S.H. Chung, T. Rodriguez, S.G. Greenbaum, R. Kovarsky, D. Golodnitsky, E. Peled, W. Wieczorek, *Electrochim. Acta*, **2005**, *50*, 3942-3948.